University of Dundee

DOCTOR OF PHILOSOPHY

Nonlinear Nonlocal Parabolic-Hyperbolic Coupled Systems for Cancer Cell Movement and Aggregation

Bitsouni, Vasiliki

Award date:
2017

Link to publication

Nonlinear Nonlocal Parabolic-Hyperbolic Coupled Systems for Cancer Cell Movement and Aggregation

By

Vasiliki Bitsouni

A Thesis submitted for the degree of Doctor of Philosophy

Division of Mathematics

University of Dundee

Dundee

August, 2017

Contents

List of figures

List of tables

Acknowledgements

I would first like to thank my supervisors Dr Raluca Eftimie and Professor Mark A. J. Chaplain for giving me the opportunity to carry out my PhD at the University of Dundee. I am very grateful for all their supervision and advice during my research.

I am grateful to my family for the continuous love and support they have given me during my studies. A big thank to Nikos Gialelis, who has helped and supported me, had faith in me and encouraged me constantly during hard times.

I would like to extend my gratitude and appreciation to all the staff members of the Division of Mathematics at the University of Dundee, in particular Nick Dawes, for his great help and mainly for all the interesting discussions we had during my PhD studies.

Declaration

I declare that the following thesis is my own composition and that it has not been submitted before in application for a higher degree.

Vasiliki Bitsouni

Certification

This is to certify that Vasiliki Bitsouni has complied with all the requirements for the submission of this Doctor of Philosophy thesis to the University of Dundee.

Dr. Raluca Eftimie

Professor Mark A. J. Chaplain

Abstract

Cells adhere to each other and to the extracellular matrix (ECM) through protein molecules on the surface of the cells. The breaking and forming of adhesive bonds, a process critical in cancer invasion and metastasis, can be influenced by the mutation of cancer cells. Several molecules have been reported to play a crucial role in cellular adhesion and proliferation, and eventually in cancer progression, with TGF-β being one of the most important.

In this thesis, we propose a general framework to model cancer cells movement and aggregation, in response to nonlocal social interactions (that is, attraction towards neighbours that are far away, repulsion from those that are near by, and alignment with neighbours at intermediate distances), as well as other molecules' effect, e.g., TGF-β. We develop nonlocal mathematical models describing cancer invasion and metastasis as a result of integrin-controlled cell-cell adhesion and cell-matrix adhesion, for two cancer cell populations with different levels of mutation. The models consist of nonlinear partial differential equations, describing the dynamics of cancer cells and TGF-β dynamics, coupled with nonlinear ordinary differential equations describing the ECM and integrins dynamics. We study our models analytically and numerically, and we demostrate a wide range of spatiotemporal patterns. We investigate the effect of mutation and TGF-β concentration on the speed on cancer spread, as well as the effect of nonlocal interactions on cancer cells' speed and turning behaviour.

Chapter 1

Introduction

1.1 Biological background

Normal cells proliferate, divide and die in a highly controlled manner. This proliferation requires mitogenic signals, which are transmitted into the cell by the transmembrane receptors and bind signalling molecules, i.e. diffusible growth factors, extracellular matrix components and cell-cell adhesion molecules (Hanahan and Weinberg, 2000). When a cell divides, its DNA is copied by the two new cells. However, if the DNA is damaged or not copied correctly, the new damaged cells will either die or start to proliferate in an uncontrolled manner, creating a signalling of oncogenes that act by mimicking growth signalling (Hanahan and Weinberg, 2000), eventually leading to an abnormal mass of tissues from cells that differ in clinically important phenotypic features-the tumour (Marusyk et al., 2012). More precisely, tumour formation is a result of clonal expansion driven by somatic mutation, developed by a single precursor (monoclonal) that undergoes genetic and biological changes (Khalique et al., 2007; Nowell, 1976). This transformation of normal cells to cancer cells is a multistep process described via the steps of hyperplasia (i.e., increase in the number of cells in

1

an organ or tissue that appear normal under a microscope), premalignant change (i.e., a state of disordered morphology of cells that is associated with an increased risk of cancer) and dysplasia (i.e., condition marked by abnormal cells that can lead to enlarged tissue or pre-cancerous cells) (Beckmann et al., 1997). Cancer cells lose their ability to regulate genome stability which leads to further genetic changes and tumour development (Khalique et al., 2007). Over the last three decades it has been shown experimentally that tumours consist of heterogeneous populations of cells, which are the result of genetic instability (Stackpole, 1983; Khalique et al., 2007; Loeb and Loeb, 2000; Martelotto et al., 2014). Intra-tumour heterogeneity appears in almost all phenotypic cell features: from cell morphology, to gene expression, motility, proliferation, immunogenicity and metastatic potential (Nicholson, 1984, 1987; Marusyk and Polyak, 2010). It should be mentioned that also normal cells are heterogeneous for various characteristics (e.g., surface antigens). Nevertheless, cellular heterogeneity is more pronounced in malignant neoplasms (Nicholson, 1987). Since the characteristics of the most abundant cell types inside these heterogeneous tumours might not necessarily predict the properties of mixed populations (Marusyk et al., 2012), we need to gain a better understanding of the dynamics of tumours formed of different mutated cell types. In fact, experimental studies have shown complex interactions between clonal sub-populations: from stable coexistence to dominant behaviours (Schuh et al., 2012). For example, some studies have shown the possibility of having competitive exclusion of clonal cancer cell sub-populations in heterogeneous tumours (Leith et al., 1989; Schuh et al., 2012). Other studies have shown that some tumour clones can compete with alternating dominance (Keats et al., 2012). We emphasise that the clonal composition of heterogeneous tumours usually changes over time (Greaves and Maley, 2012), and hence we can expect to see different competition outcomes as time increases (e.g., from transient coexistence of multiple clones to long-term competitive exclusion). Moreover, in some cancer clones there is evidence of contact domination,

i.e., the inhibition of growth in some clones is the result of cell-cell contact between various cell sub-populations (Aabo et al., 1994).

The metastatic and invasive potential of heterogeneous tumours is influenced by the interactions among cells, and the interactions between cells and the extracellular matrix (ECM), via cell surface receptors and various cytokines and chemokines. A major group of cell surface receptors is represented by the integrins, which are involved in both cell-cell adhesion and cell-matrix adhesion (Weitzman et al., 1995). In particular, the successful colonisation of new sites by cancer cells requires changes in integrin expression (Hanahan and Weinberg, 2000). Another group of molecules involved in cell-cell adhesion is represented by the cadherin families (Hanahan and Weinberg, 2000). The processes through which cells bind to each other and to ECM via these surface receptors, are responsible for tissue formation, stability and breakdown (Armstrong et al., 2006). In particular, to detach from the main aggregation/tissue, cells loose cell-cell adhesion and strengthen cell-matrix adhesion, which leads to ECM remodelling and degradation (with the help of enzymes called matrix metalloproteinases; MMPs), thus helping cell migration through the ECM (Friedl and Wolf, 2003).

1.2   Mathematical background

Over the last twenty years, mathematical models have been used intensively to try to gain a better understanding regarding the mechanisms behind cancer invasion and metastasis or the mechanisms behind the aggregation of other types of cells (see, for example, Ambrosi and Preziosi (2002); Andasari and Chaplain (2012); Andasari et al. (2011); Anderson et al. (2000); Armstrong et al. (2006); Byrne and Preziosi (2003); Chaplain et al. (2011); Cristini et al. (2009); Deakin and Chaplain (2013); Domschke et al. (2014); Dyson et al. (2016); Enderling et al. (2006, 2010); Gerisch and Chaplain

(2008); Green et al. (2010); Knútsdóttir et al. (2014); Mogilner and Edelstein-Keshet (1995); Mogilner et al. (1996); Painter et al. (2010); Sherratt et al. (2009); Painter et al. (2015) and many references therein). The early mathematical models were described by local systems of partial differential equations incorporating some generic chemotaxis or haptotaxis mechanisms (Gerisch and Chaplain, 2008; Painter, 2009), or incorporating implicit cell-cell interactions via tumour surface forces (Byrne and Chaplain, 1996). For example, Anderson et al. (2000) developed a local PDE model of parabolic type for the invasion of cancer cells via cell-matrix interactions that lead to ECM degradation. Byrne and Chaplain (1996) modelled phenomenologically the influence of cell adhesion on tumour growth, by considering surface forces on tumour spheroids. As it became more clear that the movement in response to chemical/haptotactic gradients was facilitated by the binding and unbinding of cell surface molecules to other cells and to ECM, new mathematical models of parabolic type have been derived to describe these cell-cell and cell-matrix adhesion processes (Armstrong et al., 2006; Dyson et al., 2016; Gerisch and Chaplain, 2008; Gerish and Painter, 2010; Green et al., 2010; Painter et al., 2015). Since these models incorporate the assumption that cells at position $\mathbf{x}$ bind/unbind to/from other cells at position $\mathbf{x} \pm \mathbf{s}$ (for some $\mathbf{s} > 0$ within cells sensing radius), they are generally nonlocal. For example, Armstrong et al. (2006) focused on cells movement due to cell-cell adhesion, and introduced a nonlocal term that described the nature, the direction, as well as the strength of the adhesive forces between cancer cells. The authors also extended the nonlocal model to two populations that interact via adhesive forces (thus incorporating self-population and cross-population adhesion), and studied the effect of different adhesion strengths on the sorting or the mixing of cell populations. A similar two-population nonlocal model of parabolic type, which incorporated also cell proliferation and cell movement in response to cell "packing", was described and investigated by Painter et al. (2015).

4

The model in Armstrong et al. (2006) was further generalised by Gerisch and Chaplain (2008); Painter et al. (2010); Domschke et al. (2014), to include also cell-matrix interactions. While the majority of these models investigated cell-cell and cell-matrix adhesion in one cell population, a few models considered also multiple interacting cell populations (Domschke et al., 2014). In particular, Domschke et al. (2014) also assumed mutation between different cell populations.

We should emphasise here that all these nonlocal models for cell invasion are variations or generalisations of nonlocal models developed over the last two decades to describe the dynamics of cell populations (Edelstein-Keshet and Ermentrout, 1990) or the dynamics of self-organised animal populations (Mogilner and Edelstein-Keshet, 1999; Topaz et al., 2006; Eftimie et al., 2007; Fetecau and Eftimie, 2010; Carrillo de la Plata et al., 2015; Fetecau, 2011). While the models describing collective cell movement are usually of parabolic type, the latest models for collective animal movement are usually of hyperbolic type.

The malignant feature of cancer leads to an urgent need to study the cancer progression when several cancer cell populations, with different levels of mutation, appear. It is mathematically interesting and biologically realistic to assume two different cancer cell populations, with different movement characteristics, as well as different levels of mutation and proliferation. In general, the more populations we assume, the better the biological approximation of the model. However, this is out of the scope of this thesis, since we are interested in a mathematical approximation of a biological model, which allows us to distill key biological features that can explain observed dynamics.

The main scope of this thesis is to develop mathematical models that will answer questions like: How does the mutation rate affect the behaviour of cancer cells? What type of patterns can we obtain for a model of two cancer cell populations? What is the effect of different molecules, e.g., TGF-β, on those patterns? How do the social interactions,

i.e., attraction towards neighbours that are far away, repulsion from those that are near by, and alignment with neighbours at intermediate distances, lead to different patterns?

To address these questions, in this thesis we develop novel models of nonlocal nonlinear parabolic-hyperbolic partial different equations for collective cancer cell movement and aggregation, that take into account the signals that cells receive from other cells and molecules. Moreover, we present an innovative parabolic-hyperbolic multiscale model of tumour invasion based on multiscale dynamics. We emphasize that there are no analytical results for models that combine all these aspects in the literature.

1.3   Thesis outline

The outline of this thesis is as follows. In Chapter 2, we develop a new nonlocal mathematical model describing cancer cell invasion and movement as a result of integrin-controlled cell-cell adhesion and cell-matrix adhesion, for two cancer cell populations with different levels of mutation. The parabolic-hyperbolic partial differential equations for cell dynamics are coupled with ordinary differential equations describing the extracellular matrix (ECM) degradation and the production and decay of integrins. We perform a linear stability analysis of the model, to investigate the stability of the homogeneous steady states and the possibility of having heterogeneous patterns. Then, we compare these linear stability results with the numerical results showing the type of patterns displayed by the models in the neighbourhoods of steady-state points. In Chapter 3, we incorporate also one more parabolic equation describing the dynamics of TGF-β, a cytokine playing a crucial role in cancer progression. We prove the existence of solutions to our model and we investigate numerically the effect of TGF-β on cell proliferation and adhesion. In Chapter 4 we introduce a two-population model incorporating alignment (i.e., polarisation) into the social forces between cells. The

model assumes density-dependent turning rates and attractive and repulsive speeds. Concluding remarks and directions for future research are given in Chapter 5.

Chapter 2

A mathematical model of two cancer cell sub-populations

2.1 Introduction

In this chapter [1], we will investigate the role of cancer mutation on the possibility of clonal competition with alternating dominance or even competitive exclusion between two cancer cell sub-populations (as discussed before, these types of competition have been observed experimentally (Leith et al., 1989; Keats et al., 2012; Schuh et al., 2012)). To this end, we will introduce a nonlocal model for cell-cell and cell-matrix adhesion for two populations of cells (this model is a generalization of the models in Armstrong et al. (2006); Gerisch and Chaplain (2008); Painter et al. (2015)). However, in contrast to these previous models which are of parabolic type, here we consider a parabolic-hyperbolic model. More precisely, we assume that one early stage cancer

---

[1]A version of this chapter has been submitted for publication.

Bitsouni et al. (2016), Aggregation and travelling wave dynamics in a two-population model of cancer cell growth and invasion

cell population moves both randomly and in a directed manner in response to cell-cell and cell-matrix adhesive forces, while a second late stage cancer cell population (i.e., a mutated clone) moves predominantly in a directed manner following cell-cell interactions (with cells from both populations) and cell-matrix interactions (as suggested by experimental observations in Goswami et al. (2005); Hagemann et al. (2005)). By incorporating this assumption, we aim to bring a more realistic approach to the models since the various intra-tumour cell sub-populations have been shown to be distinct not only in their adhesion capabilities but also in their motility and metastatic potential (Marusyk and Polyak, 2010). Moreover, we are interested in investigating the effect of mutation on the spreading speed of the mutated cancer cells, since the invasion levels of the late stage cancer cells are higher compared to those of early stage cancer cells (Chapman et al., 2014; Wojciechowska and Patton, 2015). Also, while previous non-local models have assumed constant adhesive interactions (see for example Armstrong et al. (2006); Chaplain et al. (2011); Gerisch and Chaplain (2008) and many references therein), here we will assume that these adhesive interactions depend on the level of integrins. We then investigate this nonlocal parabolic-hyperbolic model in terms of pattern formation, with particular attention being paid to the role of mutation rate on the coexistence (or not) of cell sub-populations that form stationary aggregations or travelling wave patterns.

The layout of this chapter is as follows. In Section 2.2 we formulate a model of partial integro-differential equations for the dynamics of two cancer cell populations, coupled with ordinary differential equations describing ECM and integrins dynamics. In Section 2.3 we use linear stability analysis to investigate the ability of the model to form cell aggregations. In Section 2.4 we investigate numerically some types of spatio-temporal patterns exhibited by this nonlocal model. In Section 2.5 we investigate numerically and analytically travelling wave behaviours. We conclude in Section 2.6 with a summary and discussion of the results.

9

2.2 The mathematical model

Cancer invasion is a complex process involving cell-cell interactions, and interactions between cells and non-cellular components (Calvo and Sahai, 2011). To develop our model we consider two populations of cancer cells, an early stage cancer population and a late stage (descendant clone) cancer population, which interact with each other as well as with the ECM via long-range adhesive and repulsive forces (Deman et al., 1976; Geiger, 1991); see Fig. 2.1.
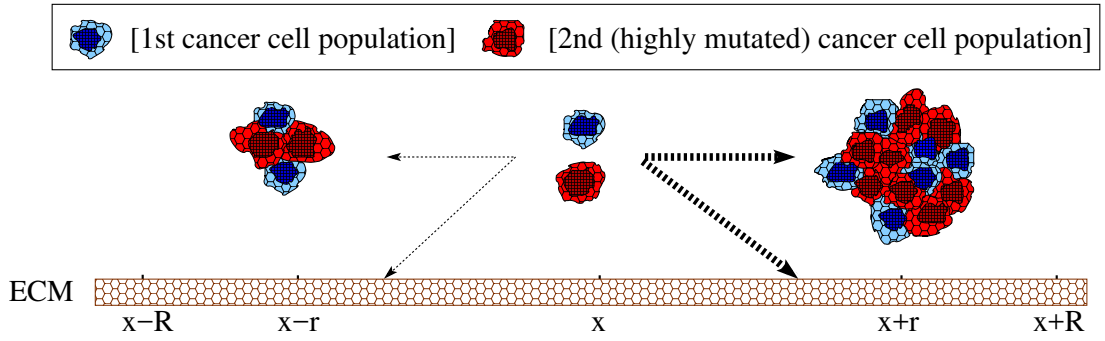
Figure 2.1: A caricature illustration of movement decisions made by cells at x, following interactions with neighbouring cells at $x - r$ and $x + r$, and with the ECM. For very strong attraction (represented here by thicker arrows), cells move towards larger cell aggregations.

Let $\Omega \subset \mathbb{R}^n$ denote a bounded spatial domain with smooth boundary $\partial \Omega$ (here we consider only $n = 1$; for a 2-dimensional version of the model see Section 2.3.2), with periodic boundary conditions. Let $I_T = [0, \infty)$ be the time interval. Denote by $u_1(t, x)$ the density of early stage cancer cells at position x and time t, and by $u_2(t, x)$ the density of late stage cancer cells at position x and time t. We also denote by $f(t, x)$ the ECM density, and by $c(t, x)$ the density of integrin receptors on the surface of cancer cells (receptors involved in cell-cell and cell-matrix interactions). For compact notation, we define the vectors $\underline{u}(t, x) = \left(u_1(t, x), u_2(t, x) \right)^\top$ and $\underline{v}(t, x) = \left(\underline{u}(t, x), f(t, x) \right)^\top$.

Dynamics of cancer cells. Experimental studies (Chapman et al., 2014) have shown that cancer cells can switch from a homogeneous type of invasion to a heterogeneous type of invasion described by invading chains (Chapman et al., 2014; Friedl and Wolf, 2003; Wojciechowska and Patton, 2015). Here, we assume that u_1 cells can mutate into u_2 cells at a constant rate M. We can derive a model for heterogeneous cancer cell populations by considering the equations

$$\frac{\partial u_i}{\partial t} = -\frac{\partial J_i}{\partial x} + (-1)^i M u_1 + G_i(\underline{u}), \; i = 1, 2, \tag{2.1}$$

where J_i, $i = 1, 2$, are the cell fluxes and $G_i(\underline{u})$, $i = 1, 2$, are the growth functions of populations u_i, $i = 1, 2$. The fluxes describe the factors that define cell movement. In this chapter we assume that the movement of the early stage cancer cell population u_1 is governed by random motility (which underlines a homogeneous type of invasion), as well as directed motility in response to cell-cell and cell-matrix adhesive forces (which underlines the heterogeneous type of invasion) (Calvo and Sahai, 2011). In contrast, the late stage u_2 cell population moves only in a directed manner (hence exhibiting a heterogeneous type of invasion) in response to cell-cell and cell-matrix adhesion forces. Biologically, this directed movement of late stage (more invasive) cancer cells can be explained by the increase of macrophage density near highly mutated cancer cells (Lin et al., 2006), which promotes the directed movement and invasion of these cancer cells, and decreases their random movement (Goswami et al., 2005; Hagemann et al., 2005). Therefore, in this chapter we assume that the movement of the u_2 population due to random walk can be considered negligible. In this case, the total fluxes will be

$$J_1 = J_D + J_{a_1} \; \text{and} \; J_2 = J_{a_2}, \tag{2.2}$$

where J_D is the flux due to Fickian diffusion, given by $J_D = -D \partial u_1 / \partial x$, with D to be the diffusion coefficient, and J_{a_i}, $i = 1, 2$, are the adhesive fluxes for cell-cell and

cell-matrix adhesion. In the case of u_2 the diffusion is considered very small and thus we ignore it.

Cell-cell/cell-matrix adhesion-mediated directed cancer cell migration occurs as a result of the social forces, i.e., attraction and repulsion, between cells and between cell and ECM components, when adhesive bonds are formed and broken. Cell-cell adhesion is described as the adhesion between cells of the same population, as well as cross-adhesion between cells of the two sub-populations. The cell-cell/cell-matrix adhesion forces are created through the binding of adhesion molecules, e.g., integrins, at the cell surface. To model these forces, let us define $R_s > 0$ to be the sensing radius of the cells, i.e., the maximum range over which cells can detect other surrounding cells, which biologically represent the extent of the cell protrusions (e.g., filopodia) (Armstrong et al., 2006). Let $g_i\left(\underline{v}(t,x+r),c(t,x)\right)$, $i = 1,2$, describe the nature of the cell-cell and cell-matrix adhesive forces created at x due to signalling with cell/ECM components at $x+r$. These functions increase when the cell density and ECM density increase, and accordingly they decrease when the cell density and ECM density decrease. The functions $g_i, i = 1,2$, are given by

$$
\begin{aligned}
g_1\left(\underline{v}(t,x+r),c(t,x)\right) :=& S_1\left(c(t,x)\right)u_1(t,x+r) + S\left(c(t,x)\right)u_2(t,x+r) \\
& + C_1\left(c(t,x)\right)f(t,x+r),
\end{aligned}
\tag{2.3}
$$

and

$$
\begin{aligned}
g_2\left(\underline{v}(t,x+r),c(t,x)\right) :=& S_2\left(c(t,x)\right)u_2(t,x+r) + S\left(c(t,x)\right)u_1(t,x+r) \\
& + C_2\left(c(t,x)\right)f(t,x+r),
\end{aligned}
\tag{2.4}
$$

where $S_i\left(c(t,x)\right)$ is the cell-cell self-adhesion strength function for populations u_i,

$S\left(c\left(t,x\right)\right)$ is the cell-cell cross-adhesion strength function between the two populations, and $C_i\left(c\left(t,x\right)\right)$ is the adhesion strength function between population u_i and ECM. We should mention here that a similar term was considered before by Chaplain et al. (2011). Other studies (Armstrong et al., 2006; Gerisch and Chaplain, 2008) consider a volume filling effect to avoid unbounded aggregations. While unbounded aggregations are possible in this type of nonlocal models, these have not been observed in our system (at least not for the parameter ranges used in this study).

We define these adhesion strength functions in terms of the integrin density c: the more integrins a cell has, the stronger its adhesion force (Gallant et al., 2005). However, the adhesion strength reaches a plateau for great densities of integrins (Maheshwari et al., 2000). Thus, we require an increasing, bounded function, so that we avoid extreme phenomena for large values of integrin density. A biologically realistic choice is a sigmoid function, as there have been several examples of sigmoid functions describing a biological process in the literature, including cell adhesion and spread (Cutler and García, 2003; Michael et al., 2009; Schakenraad et al., 1986), oxygen saturation (Shiao and Ou, 2007), artificial neural network (Basheer and Hajmeer, 2000), and many other biological processes. Note also that since cell mutation could lead to more integrins (Kidera et al., 2010), we consider strength functions with different integrin levels for each of the two populations. To this end, we choose the adhesion strength functions to be given by:

$$S_1\left(c\right) = s_1{}^*\left(1 + \tanh\left(a_1 c\right)\right), \; S_2\left(c\right) = s_2{}^*\left(1 + \tanh\left(a_2 c\right)\right), \; S\left(c\right) = s^*\left(1 + \tanh\left(dc\right)\right),$$
$$C_1\left(c\right) = c_1{}^*\left(1 + \tanh\left(b_1 c\right)\right), \; C_2\left(c\right) = c_2{}^*\left(1 + \tanh\left(b_2 c\right)\right), \tag{2.5}$$

where $d, a_i, b_i, i = 1, 2$, and $s^*, s_i{}^*, c_i{}^*, i = 1, 2$, are positive real numbers.

Within this sensing radius, let us now define K_{cc} and K_{cm}, the kernels for cell-cell and

cell-matrix adhesion ranges, respectively:

$$K_{cc}(r) = \begin{bmatrix} K_{11}(r) & K_{12}(r) \\ K_{21}(r) & K_{22}(r) \end{bmatrix}, \quad K_{cm}(r) = \begin{bmatrix} K_1(r) \\ K_2(r) \end{bmatrix}.$$

These interaction kernels describe the dependency of the force magnitude on the distance r from x. Here $K_{ij}, i, j = 1, 2$, are the interaction kernels between population i and population j (i.e., cell-cell interactions), and $K_i, i = 1, 2$ are the kernels for cell-matrix interactions (for the two populations). For simplicity, throughout this study we will consider (see also Domschke et al. (2014)):

$$K_{11} = K_{12} = K_1 \text{ and } K_{22} = K_{21} = K_2. \tag{2.6}$$

Moreover, we assume that these kernels are attractive at medium/long ranges (i.e., at the edges of the cell) and repulsive at very short ranges (i.e., over cell surface), and thus can be defined as

$$K_{1,2}(r) := q_a K_a^{1,2}(r) - q_r K_r^{1,2}(r), \tag{2.7}$$

with q_a and q_r describing the magnitudes of attractive and repulsive interactions, and $K_a^{1,2}(r)$ and $K_r^{1,2}(r)$ describing the spatial ranges over which these interactions take place. We will discuss various examples of attractive (K_a) and repulsive (K_r) kernels in Section 2.3, in the context of linear stability analysis.

Therefore, the local cell-cell and cell-matrix adhesion forces will be described by the product of functions g_i and $K_i(r), i = 1, 2$. To describe the nonlocal cell-cell and cell-matrix adhesion and repulsion forces (Deman et al., 1976; Geiger, 1991), we sum all

such forces by integrating over space to obtain the total forces:

$$F_1\left[\underline{u}, f, c\right](t,x) := \frac{1}{R_s}\int_0^{R_s}\sum_{k=0}^1 \eta\left(k\right)K_1\left(r\right)g_1\left(\underline{v}\left(t, x+r\eta\left(k\right)\right), c\left(t,x\right)\right)dr, \qquad (2.8)$$

and

$$F_2\left[\underline{u}, f, c\right](t,x) := \frac{1}{R_s}\int_0^{R_s}\sum_{k=0}^1 \eta\left(k\right)K_2\left(r\right)g_2\left(\underline{v}\left(t, x+r\eta\left(k\right)\right), c\left(t,x\right)\right)dr, \qquad (2.9)$$

where $\eta\left(k\right) = \left(-1\right)^k, k = 0, 1$, is the direction of the forces. Thus, the full nonlocal interaction terms are described by

$$F_1\left[\underline{u}, f, c\right](t,x) = \frac{1}{R_s}\int_0^{R_s}\sum_{k=0}^1 \eta\left(k\right)K_1\left(r\right)\left[S_1\left(c\right)u_1\left(t, x+r\eta\left(k\right)\right) + S\left(c\right)u_2\left(t, x+r\eta\left(k\right)\right)\right]dr$$
$$+ \frac{1}{R_s}\int_0^{R_s}\sum_{k=0}^1 \eta\left(k\right)K_1\left(r\right)C_1\left(c\right)f\left(t, x+r\eta\left(k\right)\right)dr, \qquad (2.10)$$

and

$$F_2\left[\underline{u}, f, c\right](t,x) = \frac{1}{R_s}\int_0^{R_s}\sum_{k=0}^1 \eta\left(k\right)K_2\left(r\right)\left[S_2\left(c\right)u_2\left(t, x+r\eta\left(k\right)\right) + S\left(c\right)u_1\left(t, x+r\eta\left(k\right)\right)\right]dr$$
$$+ \frac{1}{R_s}\int_0^{R_s}\sum_{k=0}^1 \eta\left(k\right)K_2\left(r\right)C_2\left(c\right)f\left(t, x+r\eta\left(k\right)\right)dr. \qquad (2.11)$$

We assume that the adhesive fluxes are proportional to the density of the cells and the nonlocal adhesion forces, F_i, $i = 1, 2$. Thus we obtain the following expressions for the two adhesive fluxes:

$$J_{a_i} = u_i F_i\left[\underline{u}, f, c\right], \ i = 1, 2. \qquad (2.12)$$

Substituting (2.12) into the general mass conservation equations, we have the following

equations describing the dynamics of the two cancer cell populations:

$$\frac{\partial u_1}{\partial t} = D\frac{\partial^2 u_1}{\partial x^2} - \frac{\partial}{\partial x}\left(u_1 F_1\left[\underline{u}, f, c\right]\right) - Mu_1 + G_1\left(\underline{u}\right), \qquad (2.13a)$$

$$\frac{\partial u_2}{\partial t} = -\frac{\partial}{\partial x}\left(u_2 F_2\left[\underline{u}, f, c\right]\right) + Mu_1 + G_2\left(\underline{u}\right). \qquad (2.13b)$$

We assume that both u_1 and u_2 cells can proliferate in a logistic manner (to describe the observed slow-down in tumour growth following the loss of nutrients (Laird, 1964)). Thus, the growth functions are given by

$$G_i\left(\underline{u}\right) = r_i u_i \left(1 - \frac{u_1 + u_2}{k_u}\right), i = 1, 2, \qquad (2.14)$$

where r_1 and r_2 are the growth rates of the u_1 and u_2 populations, respectively, and k_u is the carrying capacity. Note that these growth functions incorporate also the principle of competition between clonal sub-populations in heterogeneous tumours (Leith et al., 1989).

ECM dynamics.   Cancer cell populations degrade the ECM upon contact. Moreover, ECM density is remodelled back to normal levels, at a constant rate of $\delta \geq 0$. Thus, the dynamics of ECM, $f(t, x)$, can be described by:

$$\frac{\partial f}{\partial t} = -\alpha u_1 f - \beta u_2 f + \delta f\left(1 - \frac{f}{f_m}\right), \qquad (2.15)$$

where α and β are the positive rate constants of ECM degradation by u_1 and u_2 cell population, respectively, and f_m is the maximum ECM density at which the ECM fills up all available physical space. Following the approach of Anderson et al. (2000); Gerisch and Chaplain (2008), we choose to ignore the ECM remodelling terms for this model, i.e. we assume here that $\delta = 0$.

16

Integrin dynamics. We assume that the level of integrins depends on cancer cell density. Moreover, we assume that cell mutation changes the density of receptors (since in highly metastatic cancers, the expression of integrins is up-regulated (Kidera et al., 2010)). Therefore, the dynamics of integrins $c(t,x)$ can be described by

$$\frac{\partial c}{\partial t} = p_1 u_1 + p_2 u_2 - qc, \tag{2.16}$$

where q is the decay rate of c, and p_1 and p_2 are the production rates of integrins by u_1 and u_2 cancer cell population, respectively. To model the increase in receptors on highly mutated cancer cells, we assume that $p_2 > p_1$ (see Table 2.2). Note that integrins are produced at the positions where these cells exist, and as cells move to different spatial positions the integrins will be produced at these new positions, too (this can be seen more clearly in Figs. 2.4-2.10). We emphasize here that cell dynamics are described by mean field equations, and equation (2.16) describes the average density of integrins on cells in space. A different direction where the model could be taken is to structure the cells based on integrins (as in Engwer et al. (2015)). In this way the equation describing integrin dynamics would arise as characteristic equation along trajectories. However, this approach is beyond the scope of this study.

We impose the following initial conditions

$$u_i(0,x) = u_{i_0}(x) \geq 0, \ i = 1, 2, \ f(0,x) = f_0(x) \geq 0, \ c(0,x) = c_0(x) \geq 0, \ \text{in } \Omega. \tag{2.17}$$

To complete our model we need to impose boundary conditions. A boundary condition describes the way that the flux through the boundary is connected to the concentration across the boundary (Hadeler, 1999). Throughout this chapter we assume that the cancer cell populations u_1 and u_2 move on a circular finite domain of length L, that is $x \in [0,L]$, where they leave the domain at one end and enter it again at the other end.

The periodic boundary conditions that model this movement are the following

$$u_1(t,0) = u_1(t,L) \text{ and } u_2(t,0) = u_2(t,L). \tag{2.18}$$

2.2.1 Non-dimensionalisation of the model

To non-dimensionalise system (2.13) and equations (2.15)-(2.16), we define the following quantities:

$$\tilde{t} = \frac{t}{\tau}, \quad \tilde{x} = \frac{x}{L_0}, \quad \tilde{u}_1 = \frac{u_1}{k_u}, \quad \tilde{u}_2 = \frac{u_2}{k_u}, \quad \tilde{f} = \frac{f}{f_m}, \quad \tilde{c} = \frac{c}{c_m}, \quad \tilde{R}_s = \frac{R_s}{L_0}, \quad \tilde{r} = \frac{r}{L_0},$$

$$\tilde{S}(\tilde{c}) = \frac{\tau k_u}{L_0^2} S(c_m \tilde{c}), \quad \tilde{S}_i(\tilde{c}) = \frac{\tau k_u}{L_0^2} S_i(c_m \tilde{c}), \quad \tilde{C}_i(\tilde{c}) = \frac{\tau f_m}{L_0^2} C_i(c_m \tilde{c}), \quad i = 1,2. \tag{2.19}$$

Here L_0 is a length scale, defined as the maximum invasion distance of the cancer cells at the early stage of invasion (Anderson et al., 2000). Usually L_0 is in the range of 0.1-1cm. We rescale time with $\tau := L_0^2/D_\tau$, where D_τ is the characteristic diffusion coefficient ($\sim 10^{-6} \text{cm}^2 \text{s}^{-1}$). In addition, we rescale the cancer cells, the ECM and the integrins with k_u, f_m and c_m, respectively. Here k_u is the carrying capacity of the cancer cell populations and it is taken to be $\sim 6.7 \cdot 10^7 \text{cell/volume}$, and f_m is the maximum ECM density at which the ECM fills up all available physical space and it is taken to be equal to $4 \, mg/\text{volume}$, as in Domschke et al. (2014). Finally, c_m is the maximum integrin density and it is taken to be $5 \cdot 10^4$ integrins per cell (as in Benedetto et al. (2006)). For the kernels $K_i(r), i = 1,2$, we choose (as in Domschke et al. (2014)) the dimensionless functions $\tilde{K}_i(\tilde{r}), i = 1,2$, given by

$$\tilde{K}_i(\tilde{r}) := L_0 K_i(L_0 \tilde{r}) = L_0 K_i(r), i = 1,2.$$

We define the dimensionless functions $\tilde{g}_i\left(\underline{\tilde{u}}, \tilde{f}, \tilde{c}\right), i = 1, 2$, by

$$\tilde{g}_i\left(\underline{\tilde{u}}, \tilde{f}, \tilde{c}\right) := \frac{\tau}{L_0^2} g_i\left(\underline{u}, f, c\right), i = 1, 2.$$

Therefore we have for the nonlocal terms $F_i\left[\underline{u}, f, c\right], i = 1, 2$, that

$$\tilde{F}_i\left[\underline{\tilde{u}}, \tilde{f}, \tilde{c}\right] := \frac{\tau}{L_0} F_i\left[\underline{u}, f, c\right], i = 1, 2.$$

Finally, we obtain the dimensionless parameters:

$$\tilde{D} = \frac{D}{D_\tau}, \ \tilde{M} = \tau M, \ \tilde{\alpha} = \tau \alpha k_u, \ \tilde{\beta} = \tau \beta k_u, \ \tilde{q} = \tau q, \ \tilde{r}_i = \tau r_i, \ \tilde{p}_i = \frac{\tau p_i k_u}{c_m}, \ i = 1, 2. \tag{2.20}$$

After dropping the tildes for notational convenience, we obtain the following non-dimensionalised system:

$$\frac{\partial u_1}{\partial t} = D\frac{\partial^2 u_1}{\partial x^2} - \frac{\partial}{\partial x}\left(u_1 F_1\left[\underline{u}, f, c\right]\right) - Mu_1 + r_1 u_1\left(1 - u_1 - u_2\right), \tag{2.21a}$$

$$\frac{\partial u_2}{\partial t} = -\frac{\partial}{\partial x}\left(u_2 F_2\left[\underline{u}, f, c\right]\right) + Mu_1 + r_2 u_2\left(1 - u_1 - u_2\right), \tag{2.21b}$$

$$\frac{\partial f}{\partial t} = -\alpha u_1 f - \beta u_2 f, \tag{2.21c}$$

$$\frac{\partial c}{\partial t} = p_1 u_1 + p_2 u_2 - qc. \tag{2.21d}$$

From now on, we will always refer to the non-dimensional quantities in this chapter.

2.3 Linear stability analysis of the model

Next, we investigate the conditions under which the two populations of cancer cells form aggregations. We first calculate the spatially homogeneous steady states of the model, and then apply standard linear stability analysis to investigate the conditions (for parameter values) under which the two cancer cell populations can form aggregations.

To start, we look for the homogeneous steady states of the ODE model associated to system (2.21), that describes the growth and mutation of the two cancer cell populations and the temporal dynamics of ECM and integrins (i.e., no spatial movement):

$$\frac{\partial u_1}{\partial t} = -Mu_1 + r_1 u_1 (1 - u_1 - u_2) = 0, \tag{2.22a}$$

$$\frac{\partial u_2}{\partial t} = Mu_1 + r_2 u_2 (1 - u_1 - u_2) = 0, \tag{2.22b}$$

$$\frac{\partial f}{\partial t} = -\alpha u_1 f - \beta u_2 f = 0, \tag{2.22c}$$

$$\frac{\partial c}{\partial t} = p_1 u_1 + p_2 u_2 - qc = 0, \tag{2.22d}$$

which has the following steady state solutions $\left(u_1^*, u_2^*, f^*, c^*\right)$:

$$\left(0, 0, f^*, 0\right) \text{ and } \left(0, 1, 0, \frac{p_2}{q}\right), \tag{2.23}$$

with $f^* \geq 0$. Here we consider only the non-negative solutions, since we require biological realism. Note that all these homogeneous steady states have $u_1 = 0$ (so the more invasive population u_2 persists longer). However, as we will see in Section 2.4, the model can exhibit non-homogeneous steady states with $u_1 (t, x) \neq 0$.

We now investigate the stability of the steady states for the spatially homogeneous and

spatially heterogeneous systems to see if the introduction of spatial dynamics (i.e., cell movement and cell-cell/cell-matrix adhesion) can lead to instabilities. First, we substitute the steady states (2.23) into the Jacobian matrix of the spatially homogeneous system (2.22) and calculate the four eigenvalues corresponding to each steady state. Thus, for the steady state $\left(u_1^*, u_2^*, f^*, c^*\right) = (0, 0, f^*, 0)$ we have the eigenvalues

$$\lambda_1 = 0, \ \lambda_2 = -M + r_1, \ \lambda_3 = r_2 > 0 \ \text{and} \ \lambda_4 = -q < 0. \quad (2.24)$$

Since $\lambda_3 > 0$, this state is unstable. For the steady state $\left(u_1^*, u_2^*, f^*, c^*\right) = \left(0, 1, 0, p_2/q\right)$ we obtain the eigenvalues

$$\lambda_1 = -\beta < 0, \ \lambda_2 = -M < 0, \ \lambda_3 = -r_2 < 0 \ \text{and} \ \lambda_4 = -q < 0. \quad (2.25)$$

Since all eigenvalues are negative, the state $\left(0, 1, 0, p_2/q\right)$ is always linearly stable to homogeneous perturbations.

Next, we investigate the linear stability analysis of the spatial system (2.21). To this end, we apply small spatial perturbations to the previous homogeneous steady states: $u_i(t, x) = u_i^* + \bar{u}_i(t, x), i = 1, 2, \ f(t, x) = f^* + \bar{f}(t, x), c(t, x) = c^* + \bar{c}(t, x)$, where $\bar{u}_1, \bar{u}_2, \bar{f}$ and $\bar{c}$ denote the small perturbations. (Note that, to avoid negative solutions when we perturb the zero steady states, we consider $\bar{u}_1(t, x), \bar{u}_2(t, x), \bar{f}(t, x), \bar{c}(t, x) \geq 0$.) Substituting these into the system (2.21) (after the adhesion strength functions

$S_i(c)$, $S(c)$, $C_i(c), i = 1, 2$, have been expanded in Taylor series), and ignoring non-linear terms, leads to the following linearised system:

$$\frac{\partial \bar{u}_1}{\partial t} = D\frac{\partial^2 \bar{u}_1}{\partial x^2} - \frac{u_1^*}{R_s}\frac{\partial}{\partial x}\left\{\int_0^{R_s} K_1(r)\left[S_1(c^*)(\bar{u}_1(t, x+r) - \bar{u}_1(t, x-r)) + \right.\right.$$

$$\left.\left. + S(c^*)(\bar{u}_2(t, x+r) - \bar{u}_2(t, x-r)) + C_1(c^*)(\bar{f}(t, x+r) - \bar{f}(t, x-r))\right]dr\right\}$$

$$- M\bar{u}_1 + r_1\bar{u}_1\left(1 - 2u_1^* - u_2^*\right) - r_1u_1^*\bar{u}_2, \tag{2.26a}$$

$$\frac{\partial \bar{u}_2}{\partial t} = -\frac{u_2^*}{R_s}\frac{\partial}{\partial x}\left\{\int_0^{R_s} K_2(r)\left[S_2(c^*)(\bar{u}_2(t, x+r) - \bar{u}_2(t, x-r)) + \right.\right.$$

$$\left.\left. + S(c^*)(\bar{u}_1(t, x+r) - \bar{u}_1(t, x-r)) + C_2(c^*)(\bar{f}(t, x+r) - \bar{f}(t, x-r))\right]dr\right\}$$

$$+ M\bar{u}_1 + r_2\bar{u}_2\left(1 - u_1^* - 2u_2^*\right) - r_2u_2^*\bar{u}_1, \tag{2.26b}$$

$$\frac{\partial \bar{f}}{\partial t} = -\alpha\left(\bar{u}_1 f^* + u_1^*\bar{f}\right) - \beta\left(\bar{u}_2 f^* + u_2^*\bar{f}\right), \tag{2.26c}$$

$$\frac{\partial \bar{c}}{\partial t} = p_1\bar{u}_1 + p_2\bar{u}_2 - q\bar{c}. \tag{2.26d}$$

We look for solutions of the form $A_{u_1}e^{ikx+\lambda t}$, $A_{u_2}e^{ikx+\lambda t}$, $A_f e^{ikx+\lambda t}$ and $A_c e^{ikx+\lambda t}$ with $|A_{u_1}|$, $|A_{u_2}|$, $|A_f|$, $|A_c| \ll 1$, where k and λ are the wave number and frequency, respectively. Then system (2.26) reduces to

$$\lambda A_{u_1} = -k^2 DA_{u_1} + \frac{2ku_1^*}{R_s}\left[S_1(c^*)A_{u_1} + S(c^*)A_{u_2} + C_1(c^*)A_f\right]\hat{K}_1^s(k) - MA_{u_1}$$

$$+ r_1 A_{u_1}\left(1 - 2u_1^* - u_2^*\right) - r_1 u_1^* A_{u_2}, \tag{2.27a}$$

$$\lambda A_{u_2} = \frac{2ku_2^*}{R_s}\left[S_2(c^*)A_{u_2} + S(c^*)A_{u_1} + C_2(c^*)A_f\right]\hat{K}_2^s(k) + MA_{u_1}$$

$$+ r_2 A_{u_2}\left(1 - u_1^* - 2u_2^*\right) - r_2 u_2^* A_{u_1}, \tag{2.27b}$$

$$\lambda A_f = -\alpha\left(A_{u_1} f^* + u_1^* A_f\right) - \beta\left(A_{u_2} f^* + u_2^* A_f\right), \tag{2.27c}$$

$$\lambda A_c = p_1 A_{u_1} + p_2 A_{u_2} - qA_c, \tag{2.27d}$$

where $\hat{K}_{1,2}^s(k) = \int_0^{R_s} K_{1,2}(r)\sin(kr)dr$ are the Fourier sine transforms of the kernels

$K_{1,2}(r)$. For simplicity, throughout the rest of this chapter, we will assume that $K_1(r) = K_2(r) =: K(r)$ and thus $\hat{K}_1^s(k) = \hat{K}_2^s(k) =: \hat{K}^s(k)$.

Cellular aggregations form when the steady states (u_1^*, u_2^*, f^*, c^*) are unstable to spatial perturbations, and for this to happen we require the maximum real part of eigenvalues of the Jacobian matrix of system (2.27) to be positive, for at least one discrete value of $k > 0$.

- For the state $(u_1^*, u_2^*, f^*, c^*) = (0, 0, f^*, 0)$ we obtain the eigenvalues

$$\lambda_1 = 0, \quad \lambda_2 = -k^2 D - M + r_1, \quad \lambda_3 = r_2 > 0, \quad \lambda_4 = -q < 0. \tag{2.28}$$

Thus the steady state $(u_1^*, u_2^*, f^*, c^*) = (0, 0, f^*, 0)$ is unstable.

- For the state $(u_1^*, u_2^*, f^*, c^*) = (0, 1, 0, p_2/q)$ we obtain the eigenvalues

$$\lambda_1 = -\beta < 0, \ \lambda_2 = -k^2 D - M < 0, \ \lambda_3 = S_2(c^*) Y(k) - r_2, \ \lambda_4 = -q < 0, \tag{2.29}$$

where $Y(k) = \dfrac{2k}{R_s} \hat{K}^s(k)$. Recall that in the absence of diffusion and advection, the steady state $(u_1^*, u_2^*, f^*, c^*) = (0, 1, 0, p_2/q)$ is linearly stable. Thus, for aggregation to form, we require this state to be unstable to spatially inhomogeneous perturbations (Benson et al., 1993), i.e. the maximum real part of the eigenvalues to be greater than zero. Since $\lambda_1, \lambda_2, \lambda_4 < 0$, the steady state $(0, 1, 0, p_2/q)$ is unstable if the following dispersion relation holds:

$$Re(\lambda_3(k)) = Re\left(-r_2 + \frac{2ks_2^*}{R_s} \left(1 + \tanh\left(a_2 \frac{p_2}{q} \right) \right) \hat{K}^s(k) \right) > 0. \tag{2.30}$$

We notice that this dispersion relation, and therefore the possibility of cell aggregations

to form, depends on the choice of the interaction kernel. Mogilner and Edelstein-Keshet (1999) showed that the type of kernel affects the possibility of movement and/or aggregation. Throughout the rest of this chapter, we will consider translated Gaussian attraction and repulsion kernels (as in Eftimie et al. (2007); Carrillo de la Plata et al. (2015)):

$$K(x) = \frac{q_a}{\sqrt{2\pi m_a^2}} e^{-\frac{(x-s_a)^2}{2m_a^2}} - \frac{q_r}{\sqrt{2\pi m_r^2}} e^{-\frac{(x-s_r)^2}{2m_r^2}}, \tag{2.31}$$

where s_a and s_r represent half of the length of attraction and repulsion ranges, respectively, with $s_r < s_a$. Also, $m_j = s_j/8, j = a, r$, represent the width of the attractive and the repulsive interaction ranges. (The constants $m_j, j = a, r$, are chosen such that the support of more than 98% of the mass of the kernels is inside the interval $[0, \infty)$ (Eftimie et al., 2007).) In Section 2.3.1 we will investigate how different types of kernels lead to different dispersion relations.
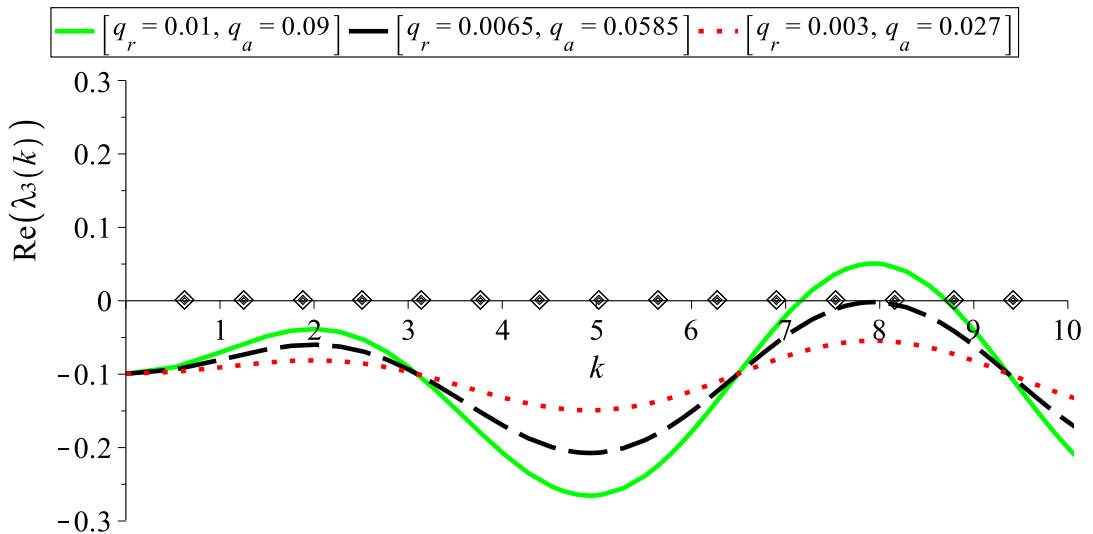
Figure 2.2: Plot of the dispersion relation (2.33) for the steady state $(0, 1, 0, p_2/q)$. The curves represent $Re(\lambda_3(k))$ for: (a) $q_r = 0.01, q_a = 0.09$ (solid green curve); (b) $q_r = 0.0065, q_a = 0.0585$ (dashed black curve); (c) $q_r = 0.003, q_a = 0.027$ (dotted red curve); the rest of the model parameters are given in Table 2.2. The diamonds on the x-axis represent the discrete wave numbers $k_j = 2\pi j/L, j = 1, 2, \ldots$. The two critical wave numbers that become unstable at the same time (giving rise to steady-state/steady-state mode interactions) are k_{12} and k_{13}.

The Fourier sine transform of kernel (2.31) is given by

$$\hat{K}^s(k) = \int_{-\infty}^{\infty} K(r)\sin(kr)\,\mathrm{d}r = q_a e^{-\frac{(km_a)^2}{2}}\sin(ks_a) - q_r e^{-\frac{(km_r)^2}{2}}\sin(ks_r). \qquad (2.32)$$

Therefore relation (2.30) becomes

$$-r_2 + \frac{2ks_2^*}{R_s}\left(1+\tanh\left(a_2\frac{p_2}{q}\right)\right)\left(q_a e^{-\frac{(km_a)^2}{2}}\sin(ks_a) - q_r e^{-\frac{(km_r)^2}{2}}\sin(ks_r)\right) > 0,$$

$$(2.33)$$

where the imaginary part of the eigenvalue $\lambda_3(k)$ will be zero.

An example of such dispersion relation is shown in Figure 2.2. Note the Steady-state/Steady-state mode interaction that occurs when we increase the parameters q_a and q_r (i.e., the strength of attractive and repulsive cell-cell interactions). There is a range of $k-$values for which $Re\left(\lambda_3(k)\right)$ is positive, and thus aggregations can arise from spatial perturbations of the steady state $\left(u_1^*, u_2^*, f^*, c^*\right) = \left(0,1,0,p_2/q\right)$. This means that the steady state $\left(0,1,0,p_2/q\right)$, which is linearly stable for the homogeneous system, is destabilised due to the spatial dynamics (diffusion and advection). Setting diffusion coefficient zero we observe that there is still a range of $k-$values for which $Re\left(\lambda_3(k)\right) > 0$, implying the adhesion-driven instability.

Remark 2.3.1. *Note that model (2.21) does not exhibit Hopf bifurcations (that is $Re\left(\lambda(k)\right) = 0, Im\left(\lambda(k)\right) \neq 0$). Therefore, although aggregations will develop, there will be no traveling patterns that arise via Hopf bifurcations.*

2.3.1 Aggregation with different types of kernel

In Mogilner and Edelstein-Keshet (1999) it was shown that even kernels give rise to group drift, while odd kernels have a greater effect in regions where the distribution of the density is uneven (e.g. the edges of the population), leading to stationary groups.

Considering the importance of the symmetry of the interaction kernels, we next discuss the cases of even and odd kernels, and compare these results with our previous results where we used a translated Gaussian kernel (see equation (2.31)), to investigate the possibility of cell aggregations to form from spatial perturbation of the steady state $(u_1^*, u_2^*, f^*, c^*) = (0, 1, 0, p_2/q)$.

- Aggregation with even kernel

  We consider the situation that the interaction kernel is an even function with respect to the y-axis. We choose the following Gaussian kernel (Mogilner and Edelstein-Keshet, 1999):

  $$K(x) := \frac{q_a}{\sqrt{2\pi m_a^2}} \exp\left(-x^2/2m_a^2\right) - \frac{q_r}{\sqrt{2\pi m_r^2}} \exp\left(-x^2/2m_r^2\right), \qquad (2.34)$$

  where q_a, q_r, m_a and m_r have the same meaning as in equation (2.31). The Fourier sine transform of the above even kernel is zero: $\hat{K}^s(k) = 0$. We know (see equation (2.29)) that the Jacobian matrix of system (2.27) has three negative eigenvalues $\lambda_{1,2,4} < 0$. For the even kernel considered here we also have

  $$\lambda_3(k) = -r_2 < 0. \qquad (2.35)$$

  Therefore, the steady state $(u_1^*, u_2^*, f^*, c^*) = (0, 1, 0, p_2/q)$ is stable, and no aggregations will form.

- Aggregation with an odd kernel

  We investigate now the stability of $(u_1^*, u_2^*, f^*, c^*) = (0, 1, 0, p_2/q)$ when we consider an odd kernel with respect to the origin. To this end, we choose

  $$K(x) := \frac{q_a x}{\sqrt{2\pi m_a^2}} exp\left(-x^2/2m_a^2\right) - \frac{q_r x}{\sqrt{2\pi m_r^2}} exp\left(-x^2/2m_r^2\right), \qquad (2.36)$$

26

where q_a, q_r, m_a and m_r have the same meaning as in equation (2.31). Then the Fourier sine transform of the kernel (2.36) is

$$\hat{K}^s(k) = q_a k m_a^2 exp(-(km_a)^2/2) - q_r k m_r^2 exp(-(km_r)^2/2). \qquad (2.37)$$

As before, the Jacobian matrix of system (2.27) has three negative eigenvalues: $\lambda_{1,2,4} < 0$. The stability of the state $(0,1,0,p_2/q)$ is given by the sign of

$$Re(\lambda_3(k)) = -r_2 + \frac{2k^2 s_2^*}{R_s} \left(1 + \tanh\left(a_2 \frac{p_2}{q}\right)\right) \left(q_a m_a^2 e^{-\frac{(km_a)^2}{2}} - q_r m_r^2 e^{-\frac{(km_r)^2}{2}}\right).$$
$$(2.38)$$
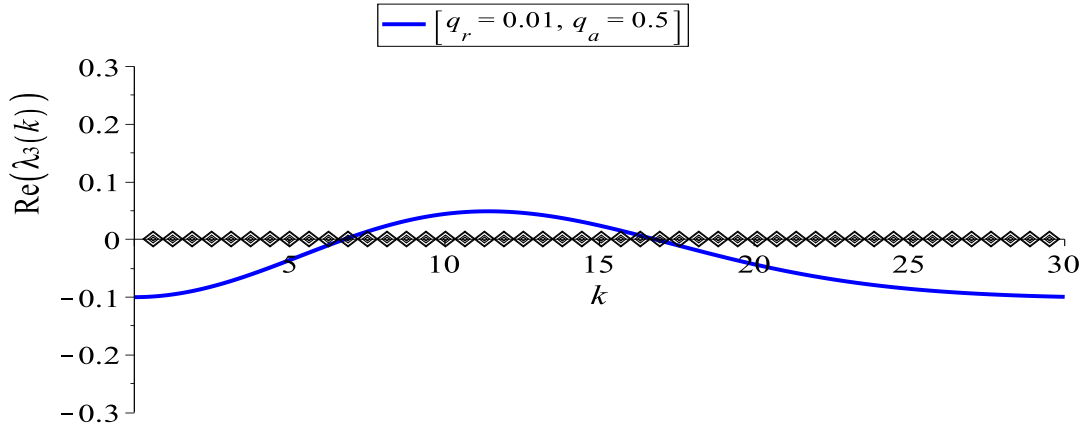
Figure 2.3: Plot of the dispersion relation (2.38) for the steady state $(u_1^*, u_2^*, f^*, c^*) = (0,1,0,p_2/q)$. Here $q_a = 0.5$. The rest of the model parameters are given in Table 2.2. The solid curve represents the real part of λ_3, while the diamonds represent the discrete wave numbers $k_j = 2\pi \frac{j}{L}, j = 0,1,2,\ldots$.

In Figure 2.3 we plot $Re(\lambda_3(k))$ against the wave number k for this steady state. We observe that for values of q_a greater than those in the translated Gaussian case (see Fig. 2.2), there is a range of $k-$values for which $Re(\lambda_3(k))$ is positive, thus the steady state $(0,1,0,p_2/q)$ can become unstable, and spatial aggregations could arise.

27

2.3.2 Extension of the model to two dimensions

The derivation of the model in two dimensions is a straightforward extension of the methods used in Section 2.2.1. Let $\Omega \subset \mathbb{R}^2$ denote again the bounded spatial domain and $I_T = [0, +\infty)$ be the time interval. We only consider a rectangle with periodic boundary conditions. We denote again by $\underline{u}(t,\underline{x}) = \left(u_1(t,\underline{x}), u_2(t,\underline{x})\right)^\top$ the vector-valued cancer cell density of the two populations, by $f(t,\underline{x})$ the ECM density and by $c(t,\underline{x})$ the integrin density. Our two-dimensional system, obtained after non-dimensionalization, is given by

$$\frac{\partial u_1}{\partial t} = D\Delta u_1 - \nabla \cdot \left(u_1 \underline{F_1}[\underline{u}, f, c]\right) - Mu_1 + r_1 u_1 (1 - u_1 - u_2), \tag{2.39a}$$

$$\frac{\partial u_2}{\partial t} = -\nabla \cdot \left(u_2 \underline{F_2}[\underline{u}, f, c]\right) + Mu_1 + r_2 u_2 (1 - u_1 - u_2), \tag{2.39b}$$

$$\frac{\partial f}{\partial t} = -\alpha u_1 f - \beta u_2 f, \tag{2.39c}$$

$$\frac{\partial c}{\partial t} = p_1 u_1 + p_2 u_2 - qc. \tag{2.39d}$$

We now assume that cells interact with each other within a circle of sensing radius $R_s > 0$. Therefore, the nonlocal terms, $\underline{F_i}[\underline{u}, f, c], i = 1, 2$, are given as in Gerisch and Chaplain (2008) by the following relations

$$\underline{F_i}[\underline{u}, f, c](t, \underline{x}) := \frac{1}{R_s} \int_0^{R_s} \int_0^{2\pi} \underline{\eta}(\theta) K_i(r) g_i\left(\underline{v}\left(t, \underline{x} + r\underline{\eta}(\theta)\right), c(t, \underline{x})\right) r \, d\theta \, dr,$$

$$\tag{2.40}$$

where $\underline{\eta}(\theta) := (\cos\theta, \sin\theta)^\top$ is the unit outer normal vector corresponding to angle θ. The functions $g_i, i = 1, 2$, are given by

$$g_i\left(\underline{u}(t,\underline{x}), f(t,\underline{x}), c(t,\underline{x})\right) = S_i(c) u_i(t,\underline{x}) + S(c) u_j(t,\underline{x}) + C_i(c) f(t,\underline{x}), i, j = 1, 2, i \neq j$$

$$\tag{2.41}$$

Linear stability analysis for the two dimensional model. Following the same approach as in the one-dimensional case (see Section 2.3), we analyse the stability of the steady states given by the relation (2.23). To this end, we let

$$u_1(t,\underline{x}) = u_1^* + A_{u_1} e^{i\underline{k}\,\underline{x} + \lambda t}, \; u_2(t,\underline{x}) = u_2^* + A_{u_2} e^{i\underline{k}\,\underline{x} + \lambda t}, \; f(t,\underline{x}) = f^* + A_f e^{i\underline{k}\,\underline{x} + \lambda t},$$

$$c(t,\underline{x}) = c^* + A_c e^{i\underline{k}\,\underline{x} + \lambda t}, \; \text{with } |A_{u_1}|, |A_{u_2}|, |A_f|, |A_c| \ll 1.$$

Here $\underline{k} = (k_1, k_2)$ is a perturbation wave vector and λ is the linear growth rate. Substituting these expressions into model (2.39) we obtain the following linearised system:

$$\lambda A_{u_1} = -|\underline{k}|^2 D A_{u_1} - \frac{iku_1^*}{R_s} \left[S_1\left(c^*\right) A_{u_1} + S\left(c^*\right) A_{u_2} + C_1\left(c^*\right) A_f \right] \underline{\hat{K}}(\underline{k}) - M A_{u_1}$$

$$+ r_1 A_{u_1} \left(1 - 2u_1^* - u_2^*\right) - r_1 u_1^* A_{u_2},$$

$$\lambda A_{u_2} = - \frac{iku_2^*}{R_s} \left[S_2\left(c^*\right) A_{u_2} + S\left(c^*\right) A_{u_1} + C_2\left(c^*\right) A_f \right] \underline{\hat{K}}(\underline{k}) + M A_{u_1}$$

$$+ r_2 A_{u_2} \left(1 - u_1^* - 2u_2^*\right) - r_2 u_2^* A_{u_1},$$

$$\lambda A_f = -\alpha \left(A_{u_1} f^* + u_1^* A_f \right) - \beta \left(A_{u_2} f^* + u_2^* A_f \right),$$

$$\lambda A_c = p_1 A_{u_1} + p_2 A_{u_2} - q A_c,$$

where $\underline{\hat{K}}(\underline{k}) = \int_0^{R_s} \int_0^{2\pi} \underline{\eta}(\theta) K(r) e^{i\underline{k}\,r\underline{\eta}(\theta)} r \mathrm{d}\theta \mathrm{d}r$ is the Fourier transform of the kernel $K(\underline{x})$. Note that $\hat{K}(\underline{k})$ corresponds to the 1D Fourier sine transform (see Section 2.3), since $\hat{K}^s(k) = \int_0^{R_s} K(r) \sin(kr) \mathrm{d}r = \frac{1}{2i} \int_0^{R_s} K(r) \left(e^{ikr} - e^{-ikr} \right) \mathrm{d}r.$

As in one dimensional case, for the steady state $(0, 0, f^*, 0), f^* \geq 0$, we obtain the eigenvalues

$$\lambda_1 = 0, \; \lambda_2 = -|\underline{k}|^2 D - M + r_1, \; \lambda_3 = r_2 > 0 \text{ and } \lambda_4 = -q < 0. \tag{2.42}$$

For the steady state $(0, 1, 0, p_2/q)$ we obtain the eigenvalues

$$\lambda_1 = -\beta < 0, \quad \lambda_2 = -|\underline{k}|^2 D - M < 0, \quad \lambda_3 = -S_2\left(c^*\right) Y\left(\underline{k}\right) - r_2 \text{ and } \lambda_4 = -q < 0,$$

(2.43)

where $Y\left(\underline{k}\right) = \dfrac{i\underline{k}}{R_s} \hat{\underline{K}}\left(\underline{k}\right)$, with $K\left(\underline{x}\right) := q_a K_a\left(\underline{x}\right) - q_r K_r\left(\underline{x}\right)$. Here K_a and K_r are the attraction and repulsion kernels, and q_a and q_r are the constants representing the magnitudes of the attraction and repulsion interactions, respectively. For simplicity we choose the following 2D interaction kernel

$$K\left(\underline{x}\right) = \frac{q_a |\underline{x}|}{2\pi m_a^2} \exp\left(-|\underline{x}|^2 / \left(2m_a^2\right)\right) - \frac{q_r |\underline{x}|}{2\pi m_r^2} \exp\left(-|\underline{x}|^2 / \left(2m_r^2\right)\right),$$

(2.44)

which corresponds to the 1D kernel (2.36). The Fourier transform of the above kernel is given by the following relation

$$\hat{\underline{K}}\left(\underline{k}\right) = \left(q_a i m_a^2 k_1 e^{-\frac{m_a^2 |\underline{k}|^2}{2}} - q_r i m_r^2 k_1 e^{-\frac{m_r^2 |\underline{k}|^2}{2}}, q_a i m_a^2 k_2 e^{-\frac{m_a^2 |\underline{k}|^2}{2}} - q_r i m_r^2 k_2 e^{-\frac{m_r^2 |\underline{k}|^2}{2}}\right).$$

(2.45)

Therefore, the steady state $(0, 1, 0, p_2/q)$ is unstable provided that the real part of the eigenvalue λ_3 satisfies

$$Re\left(\lambda_3\left(\underline{k}\right)\right) = -r_2 + \frac{|\underline{k}|^2 s_2^*}{R_s}\left(1 + \tanh\left(a_2 \frac{p_2}{q}\right)\right)\left(q_a m_a^2 e^{-\frac{m_a^2 |\underline{k}|^2}{2}} - q_r m_r^2 e^{-\frac{m_r^2 |\underline{k}|^2}{2}}\right) > 0.$$

(2.46)

This expression is similar to the one obtained in the 1D case (see equation (2.38)). Therefore we deduce that there is a range of $\underline{k}$−values for which $Re\left(\lambda_3\left(\underline{k}\right)\right)$ is positive, and thus spatial aggregations could develop also for the 2D model (2.39) when applying small spatial perturbations of the steady state $(0, 1, 0, p_2/q)$.

2.4   Numerical results

In this Section we investigate numerically the stability of model (2.21). To discretise our model we use a time-splitting approach, i.e., we split up the equations into their terms and deal with each term separately. The advantage of the time spliting approach is that we can use numerical schemes (either explicit or implicit) that can best approximate each term. More precisely, let us define $\mathbf{A}(\underline{u}, f, c) = (A_1, A_2, 0, 0)(\underline{u}, f, c) = (-u_1 F_1[\underline{u}, f, c], -u_2 F_2[\underline{u}, f, c], 0, 0)^\top$, the flux term of the model, and $\mathbf{R}(\underline{u}, f, c) = (R_1, R_2, R_3, R_4)(\underline{u}, f, c) = (-Mu_1 + r_1 u_1 (1 - u_1 - u_2), Mu_1 + r_2 u_2 (1 - u_1 - u_2), -\alpha u_1 f - \beta u_2 f, p_1 u_1 + p_2 u_2 - qc)^\top$, the reaction term of the model. We then rewrite the system (2.21) as

$$\frac{\partial u_1}{\partial t} = D \frac{\partial^2 u_1}{\partial x^2} + \frac{\partial}{\partial x} A_1 (\underline{u}, f, c) + R_1 (\underline{u}), \tag{2.47a}$$

$$\frac{\partial u_2}{\partial t} = \frac{\partial}{\partial x} A_2 (\underline{u}, f, c) + R_2 (\underline{u}), \tag{2.47b}$$

$$\frac{\partial f}{\partial t} = R_3 (\underline{u}, f), \tag{2.47c}$$

$$\frac{\partial c}{\partial t} = R_4 (\underline{u}, c). \tag{2.47d}$$

We discretize the space-time plane choosing a time step $\Delta t = k$ (throughout the simulations we use the time step $k = 0.001$), and a space step $\Delta x = h$, and we define the discrete mesh points $(t_n, x_j) = (nk, jh), k \in \mathbb{N}$ and $j = 0, \ldots, N-1$ (where $N - 1 = \dfrac{L}{h}$ is the number of the mesh points). The solution $\left(u_{1_j}^n, u_{2_j}^n, f_j^n, c_j^n\right)$ is seen as approximation of the cell averages of $(u_1, u_2, f, c)(t_n, x)$:

$$u_{i_j}^n = \frac{1}{h} \int_{x_{j-1/2}}^{x_{j+1/2}} u_i(t_n, x) \, dx, \; i = 1, 2, \; f_j^n = \frac{1}{h} \int_{x_{j-1/2}}^{x_{j+1/2}} f(t_n, x) \, dx, \; c_j^n = \frac{1}{h} \int_{x_{j-1/2}}^{x_{j+1/2}} c(t_n, x) \, dx.$$

We define the discrete advection terms $A_j^n = \mathbf{A}\left(\underline{u}_j^n, f_j^n, c_j^n\right)$ and the discrete reaction terms $R_j^n = \mathbf{R}\left(\underline{u}_j^n, f_j^n, c_j^n\right)$. First, we focus on the reaction terms and we solve the

31

ordinary differential equations:

$$\left(\frac{\partial u_1}{\partial t}, \frac{\partial u_2}{\partial t}, \frac{\partial f}{\partial t}, \frac{\partial c}{\partial t} \right)^\top = \mathbf{R}\left(\underline{u}, f, c \right). \tag{2.48}$$

Let L_R be the solution operator of this system. Thus, we can write the solution as $\left(\bar{u}_1(t,x), \bar{u}_2(t,x), \bar{f}(t,x), \bar{c}(t,x) \right)^\top = L_R \left(\bar{u}_1(0,x), \bar{u}_2(0,x), \bar{f}(0,x), \bar{c}(0,x) \right)^\top$. Then, we use this solution as the initial condition for the advection term

$$\left(\frac{\partial u_1}{\partial t}, \frac{\partial u_2}{\partial t}, \frac{\partial f}{\partial t}, \frac{\partial c}{\partial t} \right)^\top = \left(\mathbf{A}\left(\underline{u}, f, c \right) \right)_x. \tag{2.49}$$

Similarly, let L_A be the solution operator of this system. Then, we use this solution as the initial condition for the diffusion term

$$\left(\frac{\partial u_1}{\partial t}, \frac{\partial u_2}{\partial t}, \frac{\partial f}{\partial t}, \frac{\partial c}{\partial t} \right)^\top = (Du_1, 0, 0, 0)_{xx}^\top, \tag{2.50}$$

and in a similar way we denote by L_D the solution operator of this system. Therefore, the final solution of the model (2.21) can be given by

$$\left(\bar{u}_1(t,x), \bar{u}_2(t,x), \bar{f}(t,x), \bar{c}(t,x) \right)^\top = L_D L_A L_R \left(\bar{u}_1(0,x), \bar{u}_2(0,x), \bar{f}(0,x), \bar{c}(0,x) \right)^\top.$$

This approach for the numerical method can be achieved by replacing the solution operators L_R, L_A and L_D with numerical schemes. Then we have (LeVeque, 2007):

$$\left(u_1^*, u_2^*, f^*, c^* \right)^\top = \mathscr{N}_R \left(k, u_1^n, u_2^n, f^n, c^n \right),$$
$$\left(u_1^{**}, u_2^{**}, f^{**}, c^{**} \right)^\top = \mathscr{N}_A \left(k, u_1^*, u_2^*, f^*, c^* \right),$$
$$\left(u_1^{n+1}, u_2^{n+1}, f^{n+1}, c^{n+1} \right)^\top = \mathscr{N}_D \left(k, u_1^{**}, u_2^{**}, f^{**}, c^{**} \right),$$

where $\mathcal{N}_R\left(k,u_1^n,u_2^n,f^n,c^n\right)$ represents some one-step numerical method that solves (2.48) over a time step of length k with starting data $\left(u_1^n,u_2^n,f^n,c^n\right)$. Similarly, $\mathcal{N}_A(k,u_1^*, u_2^*,f^*,c^*)$ represents some one-step numerical method that solves (2.49) over a time step of length k with starting data $\left(u_1^*,u_2^*,f^*,c^*\right)$, and $\mathcal{N}_D(k,u_1^{**},u_2^{**},f^{**},c^{**})$ represents some one-step numerical method that solves (2.50) over a time step of length k with starting data $\left(u_1^{**},u_2^{**},f^{**},c^{**}\right)$. Thus the numerical solution at the next time step will be

$$\left(u_1^{n+1},u_2^{n+1},f^{n+1},c^{n+1}\right)^\top = \mathcal{N}_D\mathcal{N}_A\mathcal{N}_R\left(u_1^n,u_2^n,f^n,c^n\right)^\top.$$

For the time-propagation of the reaction terms (see relation (2.48)) we use a classical forth order Runge-Kutta algorithm (LeVeque, 2007; Press et al., 2007), where the integrals are further discretized using the Simpson's rule.

To solve the advection equations (see relation (2.49)), we use a high-resolution method introduced by Nessyahu-Tadmor (Nessyahu and Tadmor, 1990). In this case the solutions $u_{1_j}^n$ and $u_{2_j}^n$ are seen as approximations over of the cells $\left[x_j,x_{j+1}\right]$:

$$u_{i_{j+1/2}}^n = \frac{1}{h}\int_{x_j}^{x_{j+1}} u_i\left(t_n,x\right)\mathrm{d}x,\ i = 1,2.$$

Let $u_j^n = \left(u_{1_j}^n,u_{2_j}^n\right)$. Then the numerical scheme is described by the equations:

$$u_j^{n+1/2} = u_j^n - \frac{k}{2}\left(A_j^n\right)',$$
$$u_{j+1/2}^{n+1} = \frac{1}{2}\left(u_j^n + u_{j+1}^n\right) + \frac{h}{8}\left(\left(u_j^n\right)' + \left(u_{j+1}^n\right)'\right) - \frac{k}{h}\left(\left(A_{j+1}^{n+1/2}\right) - \left(A_j^{n+1/2}\right)\right),$$

where $\left(A_j^n\right)' = \left(\left(A_{1_j}^n\right)',\left(A_{2_j}^n\right)'\right)^\top$ approximates the derivatives of the flux, and $\left(u_j^n\right)'$ approximates the slopes $\underline{u}_x$.

To calculate these derivatives, we use the min-mod limiter:

$$\left(u_j^n\right)' = minmod\left(\frac{u_j^n - u_{j-1}^n}{h}, \frac{u_{j+1}^n - u_j^n}{h}\right),$$

$$\left(F_j^n\right)' = minmod\left(\frac{F_j^n - F_{j-1}^n}{h}, \frac{F_{j+1}^n - F_j^n}{h}\right),$$

where

$$minmod(a,b) = \frac{1}{2}\left(sgn(a) + sgn(b)\right)min(|a|, |b|).$$

Since Runge-Kutta scheme computes the solution at (t_n, x_j), and Nessyahu-Tadmor (NT) scheme computes the solution at an intermediate point $\left(t_n, x_{j+1/2}\right)$, we have to apply NT scheme twice to obtain the solution at (t_n, x_j).

Finally, we use a Crank-Nicolson scheme (LeVeque, 2007) to propagate the solution of the diffusion term (see relation 2.50). This one step method can be written as

$$u_{1_j}^{n+1} = u_{1_j}^n + \frac{k}{2h^2}\left(u_{1_{j-1}}^n - 2u_{1_j}^n + u_{1_{j+1}}^n + u_{1_{j-1}}^{n+1} - 2u_{1_j}^{n+1} + u_{1_{j+1}}^{n+1}\right). \qquad (2.51)$$

This is an implicit method and gives a tridiagonal system of equations to solve for all the values of $u_{1_j}^{n+1}$. It is as sufficient as an explicit method and it is considered as a very efficient method for the diffusion equation, which is "stiff" (LeVeque, 2007).

All simulations are performed on a domain of length $L = 10$ with periodic boundary conditions, and for time up to $t = 500$. The initial conditions for the cancer cell populations are either small random perturbations of spatially homogeneous steady states

$$
\begin{aligned}
u_i(0,x) &= u_i^* + rand(0, 10^{-4}), \ i = 1,2, \\
f(0,x) &= f^* + rand(0, 10^{-4}), \\
c(0,x) &= c^* + rand(0, 10^{-4}),
\end{aligned}
$$

or small random perturbations of rectangular-shaped aggregations located in the middle of the domain

$$u_i(0,x) = \begin{cases} u_i^c + rand(0, 10^{-4}), & x \in (L/2 - 1, L/2 + 1) \\ \\ 0, & \text{everywhere else} \end{cases} \quad (2.52)$$

with $u_1^c = 0$ and u_2^c as specified in the caption of the figures. For the ECM, we assume that the tumour has already degraded some of its surrounding tissues:

$$f(0,x) = 1 - 0.5u_1(0,x) - 0.5u_2(0,x). \quad (2.53)$$

Finally, the integrin density, c, is proportional to the initial tumour cell density

$$c(0,x) = 0.5u_1(0,x) + 0.5u_2(0,x). \quad (2.54)$$

Stationary aggregation patterns. To check the validity of our results obtained via linear stability analysis (see Fig. 2.2), we first run simulations for small random perturbations of the spatially homogeneous steady state $\left(u_1^*, u_2^*, f^*, c^*\right) = \left(0, 1, 0, p_2/q\right)$, and for $q_a = 0.09$ and $q_r = 0.01$. The results, presented in Fig. 2.4, show 12-13 stationary pulses (corresponding to critical wave numbers $k_{12} - k_{13}$). The spread of cancer cells over the whole domain (panels (a),(b)) leads to the degradation of ECM (panel (c)). The integrin density (panel(d)) follows the patterns in the density of cancer cells. We observe here a coexistence between a low u_1 population and a high u_2 population.

To check the effect of initial data on model dynamics, in Fig. 2.5 we investigate the behaviour of model (2.21) when we change the initial conditions to a rectangular pulse describing an initial aggregation of tumour cells. The magnitudes of attractive-repulsive interactions (and all other parameter values) are the same as in Fig. 2.4. The short-term results in Fig. 2.5(a)-(d) show a travelling pulse behaviour exhibited

by the u_2 population that moves away from population u_1 (which is mostly stationary - although even this population spreads a bit). This faster spreading of the u_2 cells compared to the u_1 cells is consistent with experimental observations (Chapman et al., 2014; Wojciechowska and Patton, 2015). The movement of u_2 population eventually stops near the boundary (due to the periodic boundary conditions, the left-moving and right-moving subgroups can sense each other across the boundary). The fast-moving u_2 cells degrade the ECM (panel (c)). We also note the high density of integrins associated with the u_1 population (panel (d)). The long-term results in Fig. 2.5(a')-(d') show the
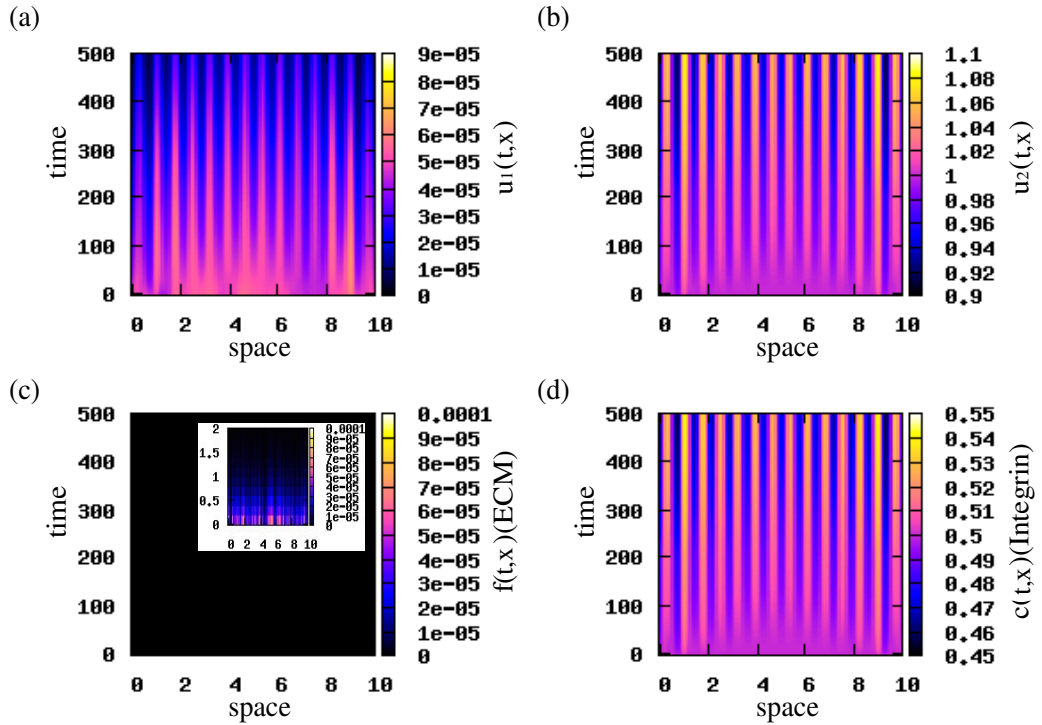
Figure 2.4: Patterns exhibited by model (2.21) for small random perturbations of the steady state $(0, 1, 0, p_2/q)$, corresponding to the dispersion shown in Fig. 2.2. Here, we use the cell-cell interaction kernel given by relation (2.31), and the model parameters given in Table 2.2. (a) Density of u_1 cell population; (b) Density of u_2 (highly mutated) cell population; (c) ECM density f; (d) Integrin density c. Note the formation of 12 or 13 peaks (if counting separately the peaks on the periodic boundaries) of high cell density corresponding to critical wave numbers k_{12}/k_{13}.

36
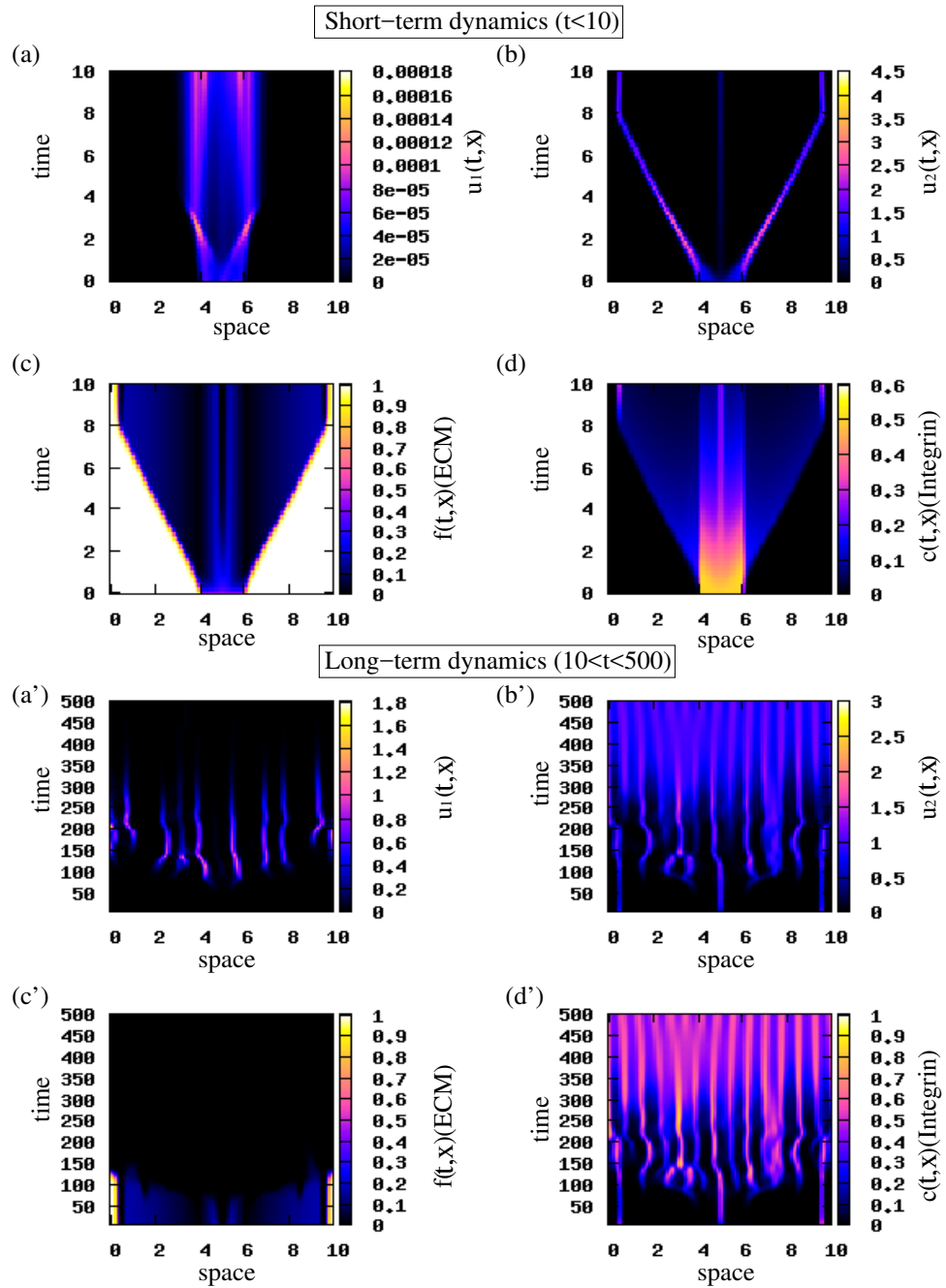
Figure 2.5: Short-term and long-term patterns exhibited by model (2.21). The initial conditions for the two cancer cell populations are described by a rectangular pulse (see (2.52)) with $u_2^c = 1.0$. We use the interaction kernel given by (2.31), and the model parameters given in Table 2.2. (a),(a') Density of u_1 population; (b),(b') Density of u_2 (highly mutated) population; (c),(c') ECM density f; (d),(d') Integrin density c.

37

formation of new aggregations of cells at distant positions in space. For $t \in (100, 250)$, the two tumour populations coexist. For $t > 250$, population u_1 is slowly eliminated and population u_2 dominates the dynamics of model (2.21). We also note that despite some chaotic-like dynamics exhibited by the u_1 and u_2 populations for $t < 300$, in the long term the system approaches stationary pulses defined by 13 peaks (corresponding to unstable wave number k_{13}).

In Figs. 2.6 and 2.7 we investigate the effect of various mutation rates on the dynamics of the u_1 and u_2 populations. In Fig. 2.6 we choose $M = 0.001$ (see Table 2.2), and observe that population u_2 vanishes for $t > 400$, while population u_1 persists and
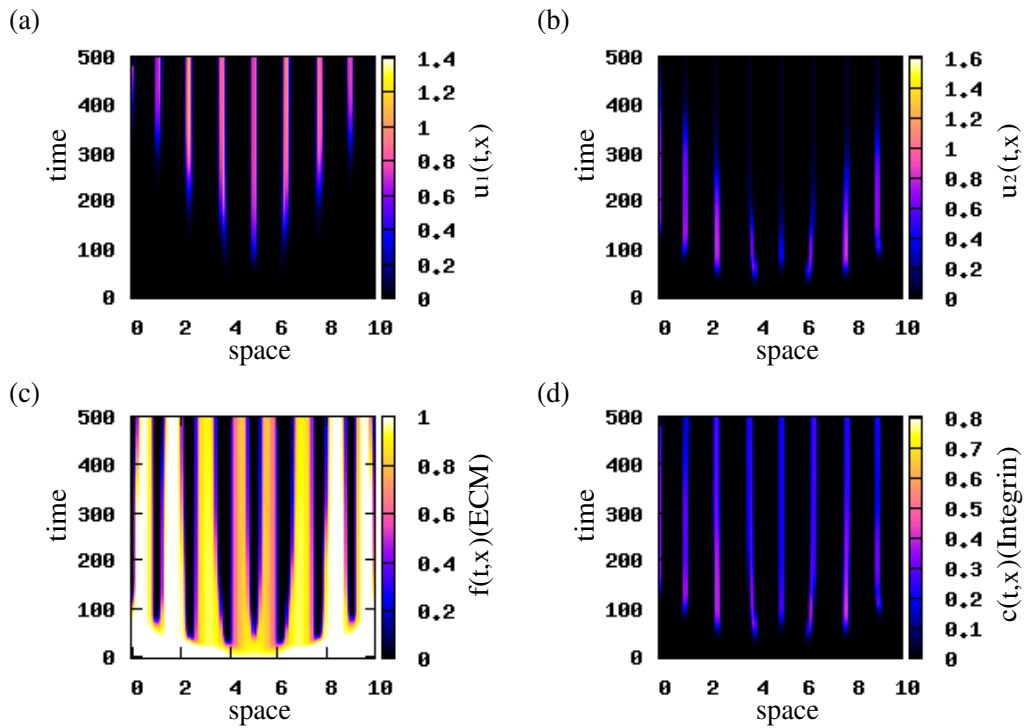
Figure 2.6: Patterns exhibited by model (2.21). Here, we use the interaction kernel given by (2.31). The initial conditions for the cancer cell populations consist of a rectangular pulse (see (2.52)) with $u_2^c = 0.001$. The mutation rate is $M = 0.001$. The rest of model parameters are given in Table 2.2. (a) Density of u_1 population; (b) Density of u_2 population; (c) ECM density f; (d) Integrin density c.
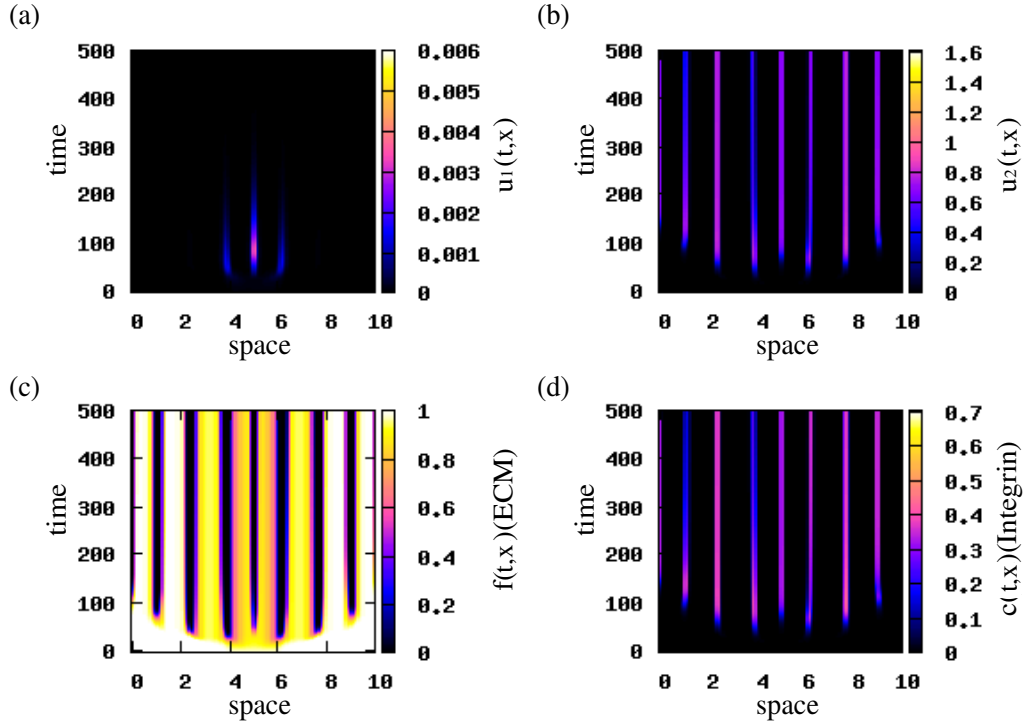
Figure 2.7: Patterns exhibited by model (2.21). Here, we use the interaction kernel given by (2.31). The initial conditions for the cancer cell populations consist of a rectangular pulse (see (2.52)) with $u_2^c = 0.001$. The mutation rate in $M = 0.05$. The rest of model parameters are given in Table 2.2. (a) Density of u_1 population; (b) Density of u_2 population; (c) ECM density f; (d) Integrin density c.

forms small high-density aggregations of cells. This unexpected behaviour might be explained by the combined effect of three factors: (i) the mutation rate ($M = 0.001$) that is much smaller than the growth rates ($r_{1,2} = 0.1$) of the two cancer cell populations; (ii) The lack of diffusion for u_2, and (iii) the competition for nutrients between the two cell populations (which is modelled implicitly by the logistic terms $G_{1,2}$; see equations (2.14)). This eventually leads to an overall increase in the first population, u_1, and a decrease in the second (highly mutated) population, u_2. In Fig. 2.7 we increase the mutation rate to $M = 0.05$, while chosing the growth rates fixed at $r_1 = r_2 = 0.1$. We observe that faster mutation rates lead to a decrease and eventual elimination of the u_1 population. The u_2 population increases and dominates the long-term dynamics of

39

model (2.21).

Travelling wave patterns. Choosing again rectangular pulse initial conditions, we reduce the magnitudes of cell-cell attractive and repulsive interactions to $q_a = 0.00025$ and $q_r = 0.0005$. The numerical simulations in Fig. 2.8 show travelling waves that propagate in opposite directions at a constant speed. Similar behaviour is obtained for $q_a > q_r$. The evolution of the travelling waves is shown in Fig. 2.9 for $t = 25j$, $j = 1,\dots,9$. We observe that the waves connect the unstable steady states $(0,1,0,p_2/q)$, with $p_2/q = 0.5$, and $(0,0,f^*,0)$, with $f^* = 1$.
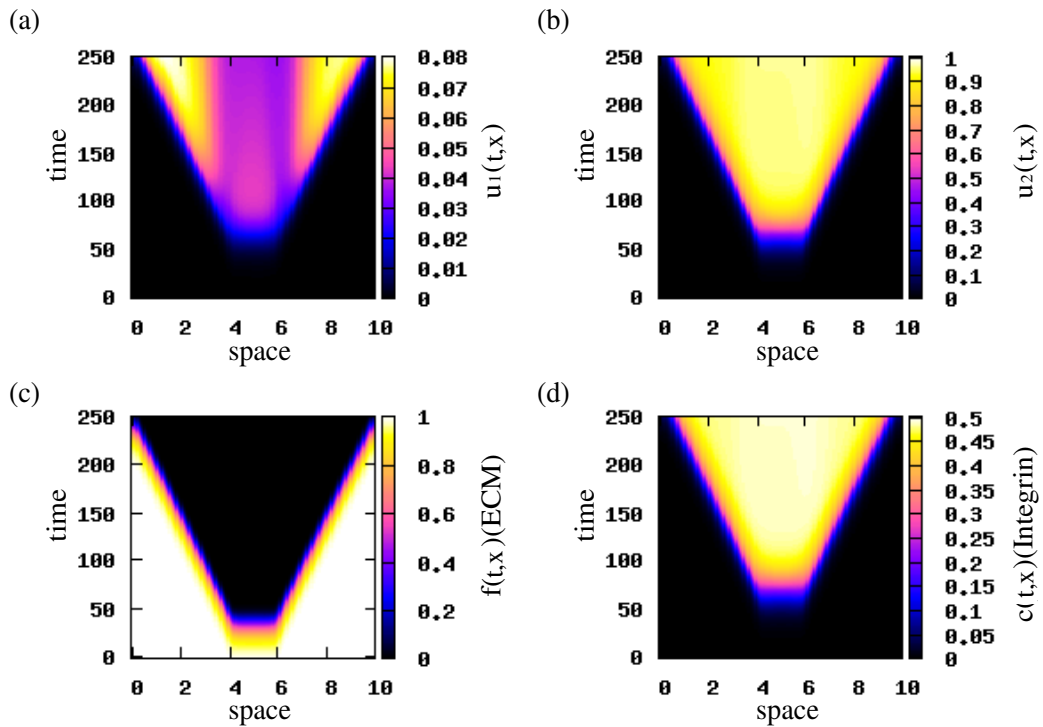
Figure 2.8: Patterns exhibited by model (2.21) for initial conditions for the two cancer cell populations consisting of a rectangular pulse with $u_2^c = 0.001$. Here, $q_r = 0.0005, q_a = 0.00025$, and the rest of the model parameters are given in Table 2.2. We use the interaction kernel given by (2.31). (a) Cell density for u_1 population; (b) Cell density for u_2 population; (c) ECM density f; (d) Integrin density c. Travelling waves are obtained for the translated Gaussian kernel given by relation (2.31).
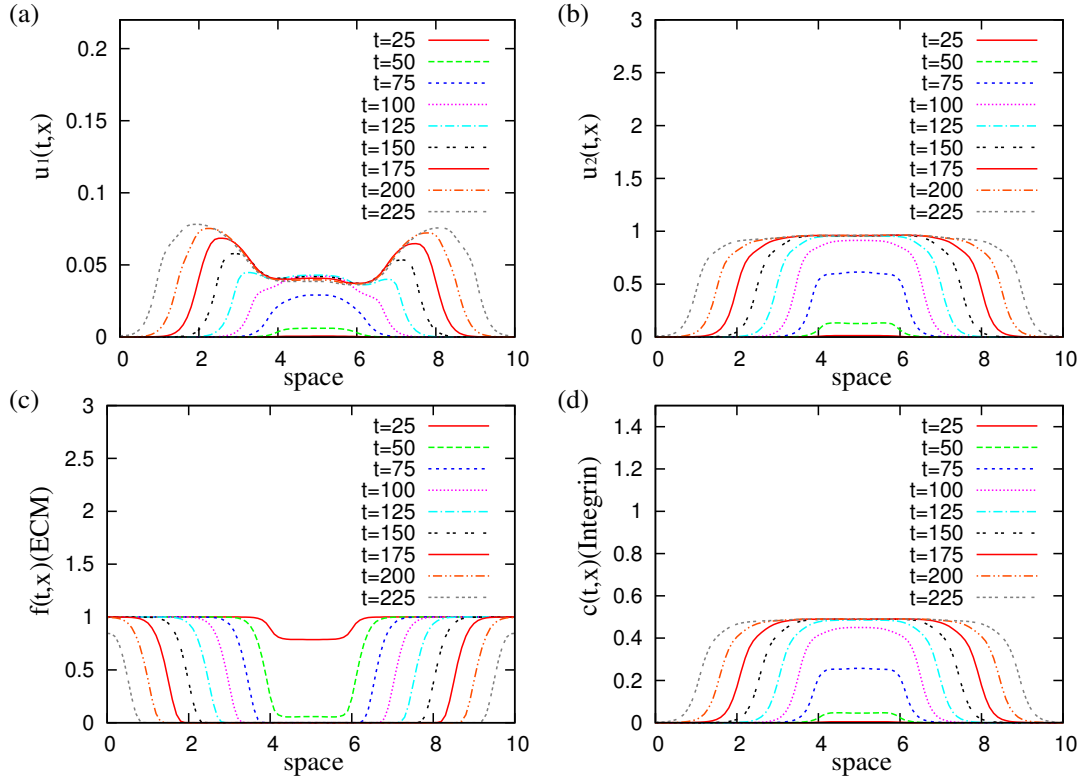
Figure 2.9: The evolution of the travelling waves under small perturbations for $q_r = 0.0005, q_a = 0.00025$, and the rest of the model parameters given in Table 2.2, of (a) Cancer cell density u_1 of the first (early stage) population; (b) Cancer cell density u_2 of the second (late stage) population; (c) ECM density f; (d) Integrin density c.

Finally, we check the effect that an increase in the mutation rate M has on the travelling wave behaviour exhibited by model (2.21). Fig. 2.10 shows that for high mutation rates ($M = 0.05$) the first population still exhibits a travelling wave before vanishing.

Remark 2.4.1. *To understand the long-term behaviour of model (2.21) with odd kernels, we also ran numerical simulations using the interaction kernel given by (2.36). The spatial patterns obtained in this case were similar to the patterns obtained for the translated Gaussian kernel (see relation (2.31)).*

2.4.1 Summary of model variables and parameters

Here we present two tables with the model variables and parameters. In Table 2.1 we list the model variables with their units. In Table 2.2 we list the parameters of our model and their corresponding units and non-dimensional values used in the simulations.

Parameter estimation.
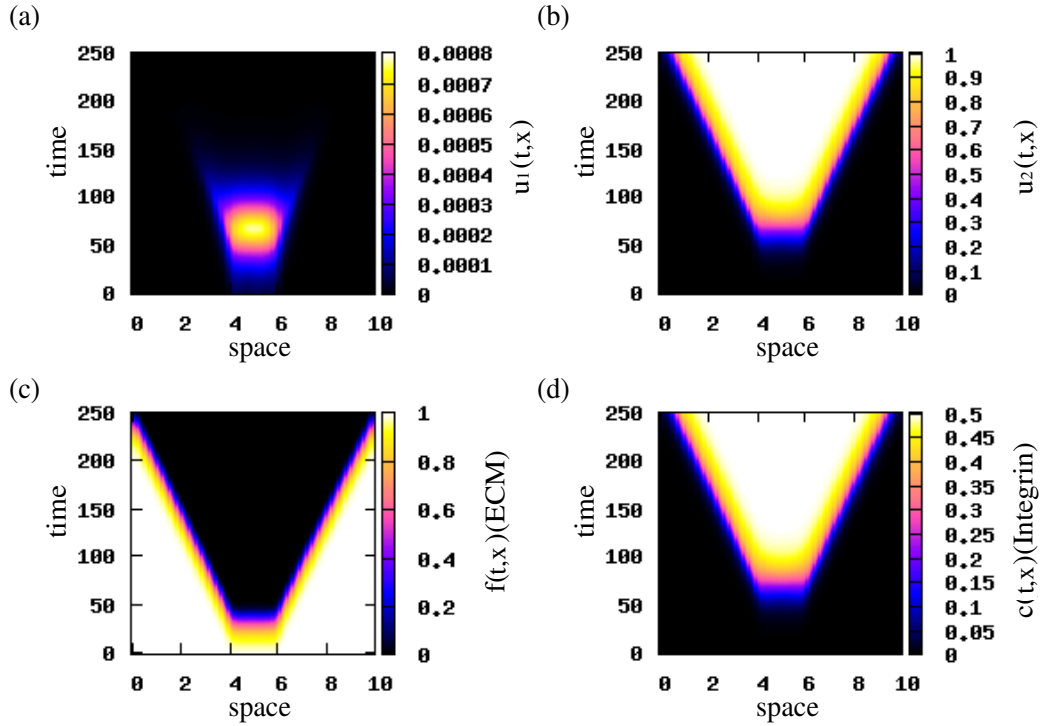
Figure 2.10: Patterns exhibited by model (2.21) for higher mutation rates ($M = 0.05$) and initial conditions for the two cancer cell populations consisting of a rectangular pulse with $u_2^c = 0.001$. Here, $q_r = 0.0005, q_a = 0.00025$, and the rest of the model parameters are given in Table 2.2. We use the interaction kernel given by (2.31). (a) Cell density for u_1 population; (b) Cell density for u_2 population; (c) ECM density f; (d) Integrin density c. Travelling waves are obtained for the translated Gaussian kernel given by relation (2.31)

Table 2.1: A list of model variables with their units. Since we are in 1D, length and volume coincide and we express the variables in terms of domain length.

Variable	Description	Dimensional Units
u_1	Early stage cancer cell density	$cell/length$
u_2	Late stage cancer cell density	$cell/length$
f	ECM density	$mg/length$
c	Integrin density	$integrins/cell$

- For the diffusion coefficient Chaplain and Lolas (2006) has shown a range between $\tilde{D} = 10^{-5}$ and $\tilde{D} = 10^{-3}$. In this chapter, we choose $\tilde{D} = 10^{-4}$.

- The sensing radius was based on the range of values given in (Armstrong et al., 2006; Gerisch and Chaplain, 2008). In this chapter, we choose $\tilde{R}_s = 0.99$.

- Attraction and repulsion ranges were chosen to be smaller or equal to sensing radius, with the repulsion range to be smaller than the attraction range (Green et al., 2010).

- Various experimental studies (Cunningham and You, 2015; Morani et al., 2014) have shown that doubling times for tumour cells range from $1 - 10$ days. This corresponds to growth rates between $\left(\ln\left(2\right)/10, \ln\left(2\right)/1\right) = (0.07, 0.7)$. In this chapter, we assume that $\tilde{r}_1 = \tilde{r}_2 = 0.1$.

- Experimental studies (Cillo et al., 1987; Hill et al., 1984; Mareel et al., 1991) have shown that the mutation rate ranges between $M = 10^{-3}/day$ and $M = 0.1/day$. Thus the non-dimensional value of the mutation rate is in the range between $\tilde{M} = 0.001$ and $\tilde{M} = 0.1$ (for highly aggressive tumours). In this chapter, we choose $\tilde{M} = 0.001$.

- The parameters $a_i, d, b_i, s_i^*, s^*, c_i^*, i = 1, 2$, were based on the range of the adhesion strength parameters used in Armstrong et al. (2006).

- Experimental studies (Kidera et al., 2010) have shown greater production of integrins for mutated cancer cells. Thus, we choose $\tilde{p}_1 < \tilde{p}_2$.

- Experimental studies (Delcommenne and Streuli, 1995; Davis et al., 2001; Liu et al., 2011; Lobert et al., 2010) have shown that the half-lifes of the integrins range from $0.04 - 4$ days. This corresponds to decay rate between $\left(\ln\left(2\right)/4, \ln\left(2\right)/0.04\right) = \left(0.17, 17.3\right)$. In this chapter, we assume that $\tilde{q} = 0.2$.

Table 2.2: A list of model parameters with their units and their non-dimensional values, obtained from (2.19) and (2.20), which we used during numerical simulations.

Param.	Description	Dimensional Units	Non-dim. value ($\tilde{p}$)	Reference
D	Diffusion coefficient	$length^2/time$	10^{-4}	Chaplain and Lolas (2006)
R_s	Sensing radius	$length$	0.99	Armstrong et al. (2006)
q_a	Magnitude of attraction	$length^2/cell$	0.09	Estimated
q_r	Magnitude of repulsion	$length^2/cell$	0.01	Estimated
s_a	Attraction range	$length$	0.99	Estimated
s_r	Repulsion range	$length$	0.25	Estimated
m_a	Width of attraction kernel	$length$	0.99/8	Estimated
m_r	Width of repulsion kernel	$length$	0.25/8	Estimated

Continued on next page

Table 2.2 – *Continued from previous page*

Param.	Description	Dimensional Units	Non-dim. value ($\tilde{p}$)	Reference
r_1	Growth rate of u_1	$1/time$	0.1	Cunningham and You (2015); Morani et al. (2014)
r_2	Growth rate of u_2	$1/time$	0.1	Cunningham and You (2015); Morani et al. (2014)
M	Mutation rate	$1/time$	0.001	Cillo et al. (1987); Hill et al. (1984); Mareel et al. (1991)
a_1	Coeff. related to the number of integrins necessary for max self-adhesion between u_1	$cell/integrins$	0.3	Estimated

Continued on next page

Table 2.2 – *Continued from previous page*

Param.	Description	Dimensional Units	Non-dim. value ($\tilde{p}$)	Reference
a_2	Coeff. related to the number of integrins necessary for max self-adhesion between u_2	$cell/integrins$	0.01	Estimated
d	Coeff. related to the number of integrins necessary for max cross-adhesion	$cell/integrins$	0.5	Estimated
b_1	Coeff. related to the number of integrins necessary for max cell-ECM adhesion for u_1	$cell/integrins$	1.8	Estimated
b_2	Coeff. related to the number of integrins necessary for max cell-ECM adhesion for u_2	$cell/integrins$	5	Estimated
s_1^*	Magnitude of self-adhesion forces of u_1	$length/(time \cdot cell)$	0.9	Estimated
s_2^*	Magnitude of self-adhesion forces of u_2	$length/(time \cdot cell)$	0.2	Estimated
s^*	Magnitude of cross-adhesion forces	$length/(time \cdot cell)$	1	Estimated
c_1^*	Magnitude of cell-ECM forces of u_1	$length/(time \cdot cell)$	1.5	Estimated
c_2^*	Magnitude of cell-ECM forces of u_2	$length/(time \cdot cell)$	5.5	Estimated

Table 2.2 – *Continued from previous page*

Param.	Description	Dimensional Units	Non-dim. value ($\tilde{p}$)	Reference
α	Rate of ECM degradation by u_1	$length/\left(time \cdot cell\right)$	1	Sherratt et al. (2009)
β	Rate of ECM degradation by u_2	$length/\left(time \cdot cell\right)$	2	Sherratt et al. (2009)
p_1	Production rate of c by u_1	$integrins/\left(time \cdot cell\right)$	0.05	Estimated
p_2	Production rate of c by u_2	$integrins/\left(time \cdot cell\right)$	0.1	Estimated
q	Decay rate of c	$1/time$	0.2	Liu et al. (2011)

2.5   Speed of travelling waves

The numerical simulations showed that the model exhibits travelling wave solutions (see Fig. 2.8 and 2.9). In this section we estimate the minimum speed at which these waves could propagate (assuming that the travelling waves do exist). We assume that close to the invading front, the nonlinear differential equations describing the spread of a population have similar speeds as their linear approximation (see the approaches in Medlock and Kot (2003); Mollison (1991)). Therefore, we first calculate the linearised system (2.26) at the steady state $\left(u_1^*, u_2^*, f^*, c^*\right) = \left(0, 1, 0, p_2/q\right)$. In travelling wave coordinates $z = x - wt$ (where $u_i\left(t, x\right) = U_i\left(z\right), i = 1, 2, \ f\left(t, x\right) = F\left(z\right), \ c\left(t, x\right) = C\left(z\right)$),

this system becomes:

$$-wU_1'(z) = DU_1''(z) - MU_1(z), \tag{2.55a}$$

$$-wU_2'(z) = -\frac{1}{R_s}\frac{\partial}{\partial z}\left\{\int_0^{R_s} K(r)\left[S_2(p_2/q)(U_2(z+r)-U_2(z-r))+\right.\right.$$

$$\left.\left.+S(p_2/q)(U_1(z+r)-U_1(z-r))+C_2(p_2/q)(F(z+r)-F(z-r))\right]dr\right\}$$

$$+MU_1(z)-r_2(U_1(z)+U_2(z)), \tag{2.55b}$$

$$-wF'(z) = -\beta F(z), \tag{2.55c}$$

$$-wC'(z) = p_1 U_1(z) + p_2 U_2(z) - qC(z). \tag{2.55d}$$

Let $s_1, s_2, s_3, s_4 > 0$ be the steepness (i.e., exponent of an exponential decay/increase profile) of u_1, u_2, f, c. The minimum of $w(s_j)$ for $s_j > 0$, $j = 1, \ldots, 4$, gives an upper bound on the rightward travelling wave speed of the nonlinear system. Thus, we make the general exponential ansatz

$$U_1(z) = A_1 e^{-s_1 z}, \ U_2(z) = A_2 e^{-s_2 z}, \ F(z) = A_3 e^{s_3 z} \text{ and } C(z) = A_4 e^{-s_4 z}, \tag{2.56}$$

where $A_j \in \mathbb{R}, j = 1, \ldots, 4$, such that asymptotically we have $U_i(z) \to 0, i = 1, 2, F(z) \to f^*, C(z) \to 0$ as $z \to +\infty$. First we investigate the s_j, $j = 1, \ldots, 4$, numerically. In Fig. 2.11 we fit these exponential ansatz profiles (given by (2.56)) to the numerical solutions $u_1(t, x), u_2(t, x), f(t, x)$ and $c(t, x)$ at time $t = 175$ (dotted curve). We obtain the

following ansatz profiles (continuous curve in Fig. 2.11):

$$E_1(x) = A_1 \cdot exp(-3.17x), \text{ with } A_1 = 0.063 \cdot \exp(24.5675), \qquad (2.57)$$

$$E_2(x) = A_2 \cdot exp(-3.17x), \text{ with } A_2 = 0.8 \cdot \exp(24.2505), \qquad (2.58)$$

$$E_3(x) = A_3 \cdot exp(6x), \text{ with } A_3 = 0.82 \cdot \exp(-52.5), \qquad (2.59)$$

$$E_4(x) = A_4 \cdot exp(-3.17x) \text{ with } A_4 = 0.4 \cdot \exp(24.092). \qquad (2.60)$$
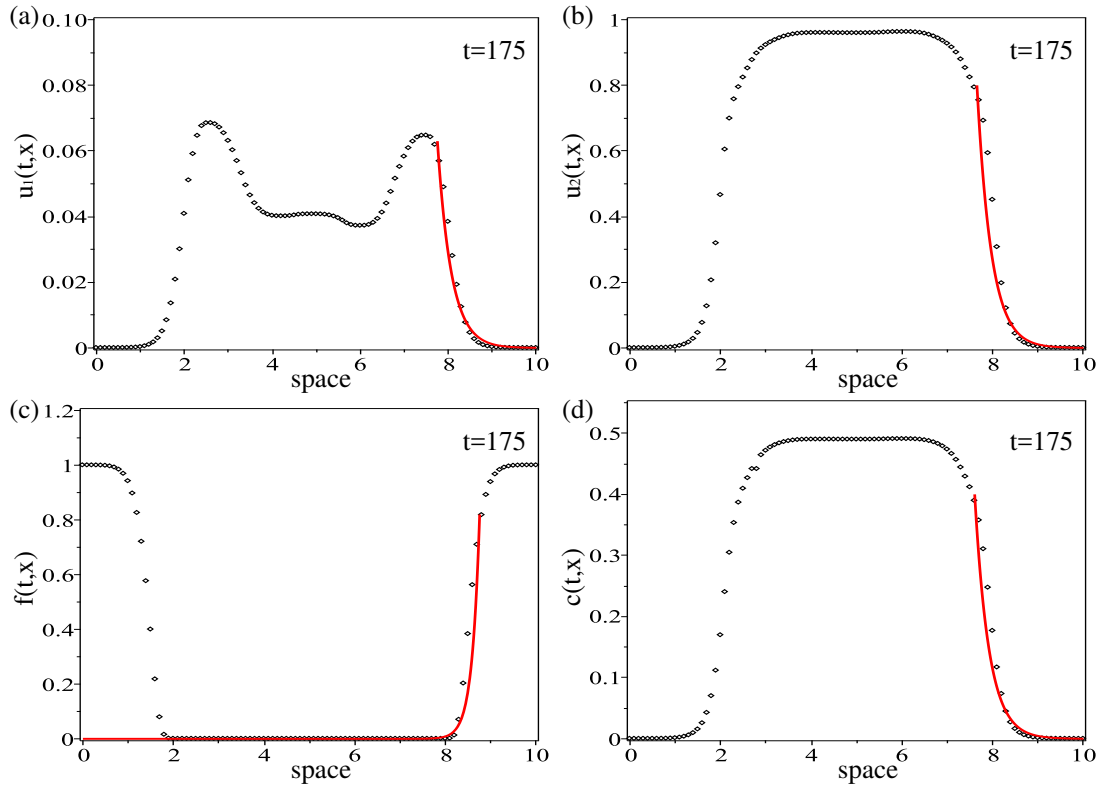
Figure 2.11: Plot of the numerical simulations of the travelling wave profile, shown in Figs. 2.8-2.9, for (a) population u_1 and the exponential ansatz function $E_1(x)$ given by relation (2.57) with $A_1 = 0.063 \cdot \exp(24.5675)$; (b) population u_2 and the exponential ansatz function $E_2(x)$ given by relation (2.58) with $A_2 = 0.8 \cdot \exp(24.2505)$; (c) ECM density, f, and the exponential ansatz function $E_3(x)$ given by relation (2.59) with $A_3 = 0.82 \cdot \exp(-52.5)$; (d) inttegrin density, c, and the exponential ansatz function $E_4(x)$ given by relation (2.60) with $A_4 = 0.4 \cdot \exp(24.092)$. Here, $q_r = 0.0005, q_a = 0.00025$, and the rest of the model parameters are given in Table 2.2.

Whence we deduce that the travelling wave profiles of $U_1(z), U_2(z)$ and $C(z)$ have

the same steepness $s := s_1 = s_2 = s_4 = 3.17$, while the profile of $F(z)$ has steepness $s_3 = 6$. Therefore, we replace the exponential ansatz given by (2.56) with $U_1(z) = A_1 e^{-sz}$, $U_2(z) = A_2 e^{-sz}$, $F(z) = A_3 e^{s_3 z}$ and $C(z) = A_4 e^{-sz}$. Let us assume that $K(r)$ has a moment generating function, $\tilde{M}(s)$, defined as $\tilde{M}(s) := \int_{-\infty}^{+\infty} K(r)\left(e^{-sr} - e^{sr}\right) dr$. Then we obtain from system (2.55):

$$A_1\left(sw - s^2 D + M\right) = 0, \tag{2.61a}$$

$$A_1\left(-S\left(p_2/q\right)\frac{s\tilde{M}(s)}{R_s} - M + r_2\right) + A_2\left(sw - S_2\left(p_2/q\right)\frac{s\tilde{M}(s)}{R_s} + r_2\right)$$

$$+ A_3 e^{(s+s_3)z}\left(-C_2\left(p_2/q\right)\frac{s_3\tilde{M}(s_3)}{R_s}\right) = 0,$$

$$\tag{2.61b}$$

$$A_3\left(s_3 w - \beta\right) = 0, \tag{2.61c}$$

$$-A_1 p_1 - A_2 p_2 + A_4\left(sw + q\right) = 0. \tag{2.61d}$$

Taking now the determinant of the system equal to zero we have the characteristic relation

$$\left(sw - s^2 D + M\right)\left(sw - S_2\left(p_2/q\right)\frac{s\tilde{M}(s)}{R_s} + r_2\right)\left(s_3 w - \beta\right)\left(sw + q\right) = 0. \tag{2.62}$$

Since we are looking for the minimum positive speed with respect to $s > 0$ and $s_3 > 0$, in Fig. 2.12(a) we plot implicitly equation (2.62) in the (s, s_3, w)-space. Note that the steepness coefficient s_3 (for the ECM degradation profile) does not have any significant effect on the minimum positive wave speed w (of the invading u_1 and u_2 populations). For this reason, in Fig. 2.12(b) we plot the relation (2.62) in the (s, w)-plane for fixed $s_3 > 0$. We see that indeed we cannot have a travelling wave with positive speed unless the wave has a steepness $s > 3.17$. Moreover, faster waves have higher steepness.
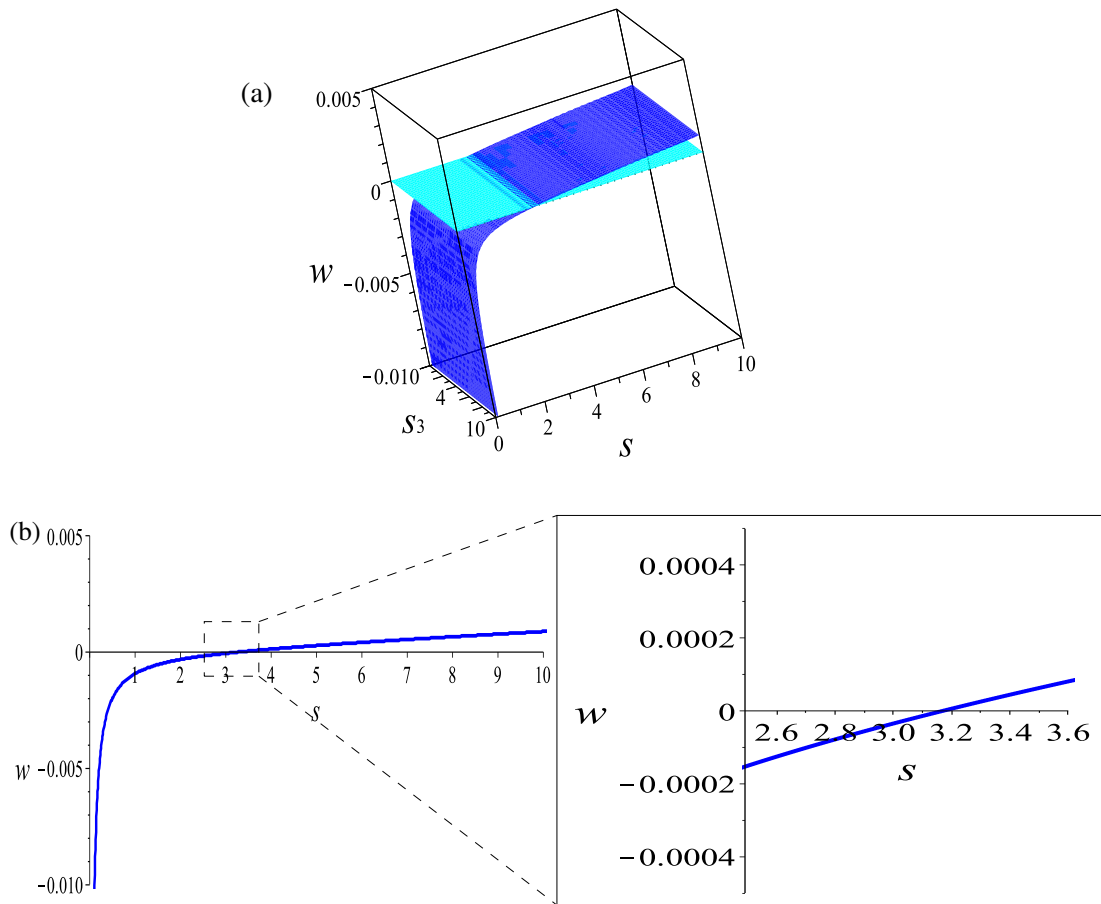
Figure 2.12: Plot of the relation (2.62) for $q_r = 0.0005, q_a = 0.00025$, and the rest of the model parameters as given in Table 2.2. The plot shows the relation between the speed and the steepness of the travelling waves in the (a) (s, s_3, w)-space; (b) (s, w)-plane.

Finally, we are interested in investigating how the speed of the invading waves correlates with their steepness, as we vary different model parameters. In Fig. 2.13(a) we see that a decrease in the diffusion coefficient D by one order of magnitude leads to a reduction in the velocity $w > 0$. In Fig. 2.13(b) we see that an increase in the mutation rate M (from 0.001 to 0.05) leads to a slightly lower velocity $w > 0$ and a higher steepness. (Note that for $s > 100$, the invading speed obtained for $M = 0.001$ and $M = 0.05$ is the same - not shown here.)
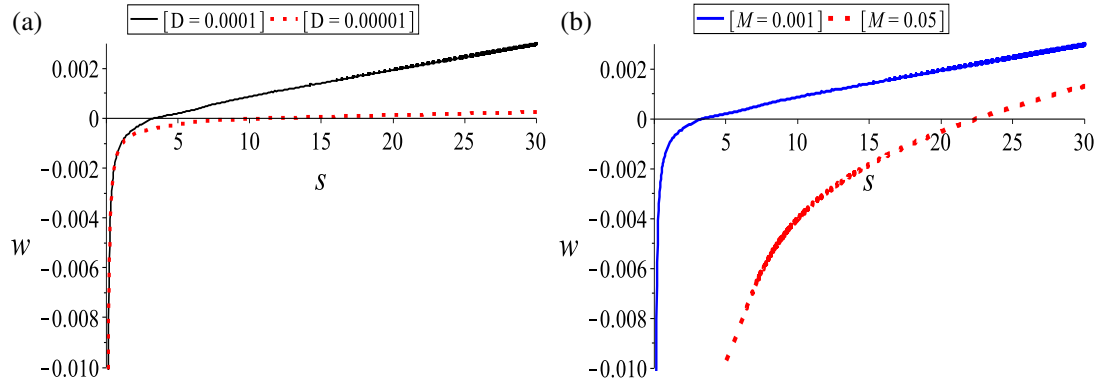
Figure 2.13: Plot of the relation (2.62) for $q_r = 0.0005, q_a = 0.00025$, and the rest of the model parameters given in Table 2.2, as we vary: (a) Diffusion coefficient D: $D = 10^{-4}$ (black solid line) and $D = 10^{-5}$ (red dashed line); (b) Mutation rate M: $M = 0.001$ (blue solid line) and $M = 0.05$ (red dashed line).

2.6 Conclusion and discussion

In this chapter we introduced a model of integro-differential equations describing the dynamics of two cancer cell populations: an early stage cell population that exhibits both random and directed movement, and a late stage cell population that exhibits only directed movement. The model incorporated both nonlocal cell-cell interactions and cell-matrix interactions. Moreover, unlike other models in the literature, in our model these interactions were not constant but depended on the cellular level of integrins.

Linear stability analysis of the non-dimensional model showed that aggregations could arise only via real bifurcations (the system could not exhibit Hopf bifurcations). We studied the effect of the interaction kernel on the formation of aggregations and we applied linear stability analysis for the 2D model to compare the results with the one dimensional case. Numerical results showed that these aggregations were described by a large number of stationary pulses (e.g., 13 pulses corresponding to the critical unstable wave number k_{13}). Moreover, numerics also showed the existence of travelling waves. We investigated the speed of these waves, which seemed to be affected by the

diffusion coefficient and the mutation rate of cells.

The rate at which cancer cells mutate seemed to play a critical role in our model. In Figs. 2.6 and 2.7 (as well as Figs. 2.8 and 2.10) we showed that depending on the magnitude of the mutation rate, either the u_1 or the u_2 cell populations can be eliminated (or, in some cases they can coexist - see Figs. 2.4 and 2.8). The existence of these dominant behaviours exhibited by the u_1 or u_2 populations are consistent with the principle of competitive exclusion of clonal sub-populations in heterogeneous tumours (Egan et al., 2012; Keats et al., 2012; Leith et al., 1989). In Fisher et al. (2013) the authors interpreted the experimental data, showing suppression and reappearance of cancer clones in myeloma patients (Keats et al., 2012) and chronic lymphocytic leukaemia patients (Schuh et al., 2012), by suggesting that two subclones can exist in a dynamic equilibrium. While all these experimental studies record the survival/suppression of tumour clones in various cancers, they do not offer a mechanistic explanation for the factors that could lead to these behaviours. In contrast, our numerical results (see Figs. 2.6 & 2.7, 2.8 & 2.10) offer such a mechanistic explanation by identifying the magnitude of the mutation rate as a factor that could explain the experimentally-observed suppression and reappearance of cancer clones.

This issue of cancer heterogeneity has significant implications of cancer drug therapies, since it can lead to drug resistance. For example, clinical studies have shown the emergence of imatinib-resistant mutations in patients with chronic myeloid leukaemia, which can co-exist with subclones that carry different imatinib-resistant mutations in treatment-naïve patients (Shah et al., 2002).

Overall, these clinical observations suggest that a single drug might not be successful in treating a genetically heterogeneous tumour, since sub-populations of cancer cells with drug-resistant mutations could become dominant, thus leading to therapeutic failure.

We note that the spatial distribution of the two cancer sub-populations – with the original u_1 population in the centre of the aggregation, surrounded by the mutated u_2 clones (see Fig. 2.5 for $t \in [0, 10]$ or Fig. 2.6 for $t \in [100, 300]$)– is consistent with experimental studies on the spatial relationship between clonal sub-populations of hepatocellular carcinoma (HCC) tumour (Ling et al., 2015). In this experimental study, the authors investigated the clonal diversity of a HCC-15 tumour (and the spatial distribution of these clones), and showed the ancestral clones being positioned in the middle of the tumour, with the descendant clones radiating outward.

In general, the numerical results of the model presented in this chapter, show that cell-cell/cell-matrix adhesion combined with cell proliferation (in the presence of cell competition) and cell mutation, can impact which tumour clones survive (see Figs. 2.4-2.8 and 2.10).

In this chapter we focused on a one-dimensional model. However, real life cell dynamics occurs in two or three dimensions. In Section 2.3.2 we extended model (2.21) to two spatial dimensions and applied linear stability analysis. We showed that for similar kernels, we obtained similar dispersion relations. Therefore, we expect that the 2D model (2.39) would exhibit stationary pulses similar to the ones exhibited by the 1D model (2.21). Future work will consider extending the numerical results in 2D. Moreover, an interesting future model derivation for integrin dynamics inside the cells would be an individual-based model.

Chapter 3

Modelling the multiple roles of TGF-β pathways on heterogeneous cancer cells proliferation and adhesion

3.1 Introduction

Cellular adhesion, i.e., cell-cell and cell-matrix adhesion, and cellular proliferation are fundamental features of multicellular organisms, linked to maintenance of order in the organisms, e.g., tissue formation, stability and breakdown (Armstrong et al., 2006). These interactions between cells and the extracellular matrix (ECM) are mediated though cell surface receptors, a major group of which is represented by the integrins (Weitzman et al., 1995), and various cytokines and chemokines. Another group of molecules involved in cell-cell adhesion is represented by the cadherin families (Hanahan and Weinberg, 2000). There are several signalling pathways that control normal cell processes like cell proliferation, division, cellular adhesion and apoptosis, with transforming growth factor β (TGF-β) pathway to be one of the most critical.

Belonging to a large family of multifunctional polypeptides, TGF-β regulates the proliferation, differentiation, adhesion, migration and apoptosis of many cell types, including endothelial cells, hematopoietic cells and lymphocytes (Miyazono, 2009), and extracellular matrix production (Kaminska et al., 2005).

Various signals, including integrin, Notch, Wnt, TNF-a, and EGF signals, have been reported to cooperate or synergize with TGF-β signalling and stimulate tumour invasion and metastasis (Miyazono, 2009). Experimental studies (Markowitz et al., 1995) showed that the loss of TGF-β responsiveness is one of the events that initiate fibrotic disease and malignant progression of cancer, as well as cancer metastasis (Venkatraman et al., 2012). TGF-β induces morphological, biochemical and transcriptional changes towards a mesenchymal phenotype, a process called epithelial to mesenchymal transition (EMT) (see Mamuya and Duncan (2012); Moustakas and Heldin (2007) and many references therein). EMT occurs when epithelial cells lose their epithelial cell characteristics and become mesenchymal. Mesenchymal cells can return to an epithelial phenotype, a process called mesenchymal-epithelial transition (MET). Through these processes, cancer cells become metastatic and form new colonies at distant sites.

Experimental studies (Khalique et al., 2007; Loeb and Loeb, 2000) have shown that tumours consist of heterogeneous populations of cells, which are the result of genetic instability. Intra-tumour heterogeneity appears in almost all phenotypic cell features: from cell morphology, to gene expression, motility, proliferation, immunogenicity and metastatic potential (Marusyk and Polyak, 2010). While both normal cells and cancer cells appear to be heterogeneous for various characteristics (e.g., surface antigens), cellular heterogeneity is shown (Nicholson, 1987) to be more pronounced in malignant neoplasms. As discussed in Chapter 2, experimental studies have shown complex interactions between clonal cancer cell sub-populations in heterogeneous tumours: from stable coexistence to competitive exclusion (Leith et al., 1989). The metastatic and invasive potential of heterogeneous tumours is influenced by the interactions among

the cells, and the interactions between cells and ECM components. To detach from the main aggregation/tissue, cells loose cell-cell adhesion and strengthen cell-matrix adhesion (these changes in cell-cell/cell-ECM adhesion can be influenced by TGF-β signalling), which leads to ECM remodelling and degradation (with the help of enzymes called matrix metalloproteinases; MMPs).

Over the last three decades there have been multiple mathematical models introduced to investigate the formation and movement of various cell aggregations (see, for example, Ambrosi and Preziosi (2002); Armstrong et al. (2006); Bellomo et al. (2016, 2008); Byrne and Preziosi (2003); Mogilner and Edelstein-Keshet (1995); Mogilner et al. (1996); Outada et al. (2016); Painter et al. (2010); Sherratt et al. (2009) and the many references therein). While there are mathematical models in the literature that investigate the roles of TGF-β on cancer dynamics, generally these models focus on particular aspects of cancer progression (e.g., growth (Michelson and Leith, 1991; Turner et al., 2004)). There are very few models that investigate, in an integrated manner, the multiple roles of TGF-β on cancer evolution (see, for example Ascolani and Liò (2014); Wang et al. (2009)), and in general these models focus on the motility and growth rate of early stage cancer cells.

In this chapter [1], we present a novel mathematical model which investigates in a integrated manner the various roles of TGF-β on tumour growth/decay, and on cell-cell and cell-matrix interactions, but paying particular attention to the opposite role of TGF-β on early stage versus late stage cancer cells. To this end, we generalise the mathematical model introduced in Chapter 2, described by a nonlocal hyperbolic-parabolic model for cell-cell and cell-matrix adhesion for two cancer cell populations: an early stage cancer population, moving both randomly and in a directed manner in

---

[1]A version of this chapter has been published.

response to cell-cell and cell-matrix adhesive forces, and a late stage cancer population (i.e., a mutated clone) moving only in a directed manner following self-adhesive and cross-adhesive cell-cell forces, as well as matrix interactions. Since TGF-β does not affect only tumour growth, but impacts also cell adhesion (Ascolani and Liò, 2014), we model the interactions between TGF-β and integrins that influence the cell-cell and cell-matrix adhesive forces. The computational results show a range of heterogeneous invasion patterns, as a result of the opposite role of TGF-β in early and late stages of cancer. Analytical results show the global existence of bounded solutions (hence existence of various types of invasion patterns). We note that existence results have been shown for local nonlinear parabolic PDEs for cell movement coupled with ODEs describing the ECM dynamics with tissue remodelling (Fan and Zhao, 2014; Kang and Lee, 2015; Tao, 2011; Tao and Winkler, 2014), as well as for nonlocal parabolic models describing cancer invasion when the ECM production is zero (Chaplain et al., 2011) and when it is nonzero (Szymańska et al., 2009). Existence results have been also shown for local hyperbolic models for chemo-sensitive movement (Hillen et al., 2001). However, in contrast to these previous results, here we show existence for a nonlocal parabolic-hyperbolic model for cancer cell movement.

The structure of this chapter is as follows. In Section 3.2 we present our mathematical model, which consists of partial integro-differential equations describing the dynamics of cell populations in early and late stages of cancer, coupled with ordinary differential equations describing ECM and integrins dynamics, and a parabolic partial differential equation describing TGF-β dynamics. In Section 3.3 we present a suitable notion of weak solution to the model and we prove the global-in-time existence of bounded solutions to our system as the vanishing viscosity limit of a classical solution to an associated parabolic problem. In Section 3.4 we undertake numerical simulations to investigate the effect of TGF-β on cancer cell movement, and observe a range of patterns obtained for different values of parameters of the model. Finally, in Section 3.5

we summarise our results and give some concluding remarks.

3.2 The mathematical model of TGF-β regulatory network in cancer

TGF-β plays a crucial role in embryonic development, wound healing and cancer. Moreover, TGF-β signalling stimulates EMT in certain epithelial cells (Moustakas and Heldin (2007) and many references therein) and consequently induces various diseases, including cancer. The way that TGF-β interacts with cancer cells varies between early and late stages of cancer (see Fig. 3.1), making its behaviour difficult to analyse. We consider a two-population model describing the behaviour of an early stage cancer population and a late stage cancer (descendant clone) population, which interact with each other, as well as with the ECM, via long-range integrin-controlled adhesive and repulsive forces (Deman et al., 1976; Geiger, 1991) on bounded spatial domain $\Omega \subset \mathbb{R}^n$ with smooth boundary $\partial \Omega$. The model presented in this chapter is similar to the one presented in the previous chapter. However, here we consider also the TGF-β consecration in the nonlinear differential equations.

For $T > 0$ let $\Omega_T = (0, T) \times \Omega$. As in Chapter 2 we denote by $u_1(t,x)$ and $u_2(t,x)$ the density of early and late stage cancer cells, respectively, at position x and time t, by $f(t,x)$ the ECM density, and by $c(t,x)$ the density of integrin receptors on the surface of cancer cells (receptors involved in cell-cell and cell-matrix interactions). Finally, we denote by $b(t,x)$ the TGF-β concentration. For compact notation, we define the vectors $\underline{u}(t,x) = \left(u_1(t,x), u_2(t,x)\right)^\top$ and $\underline{v}(t,x) = \left(\underline{u}(t,x), f(t,x)\right)^\top$.
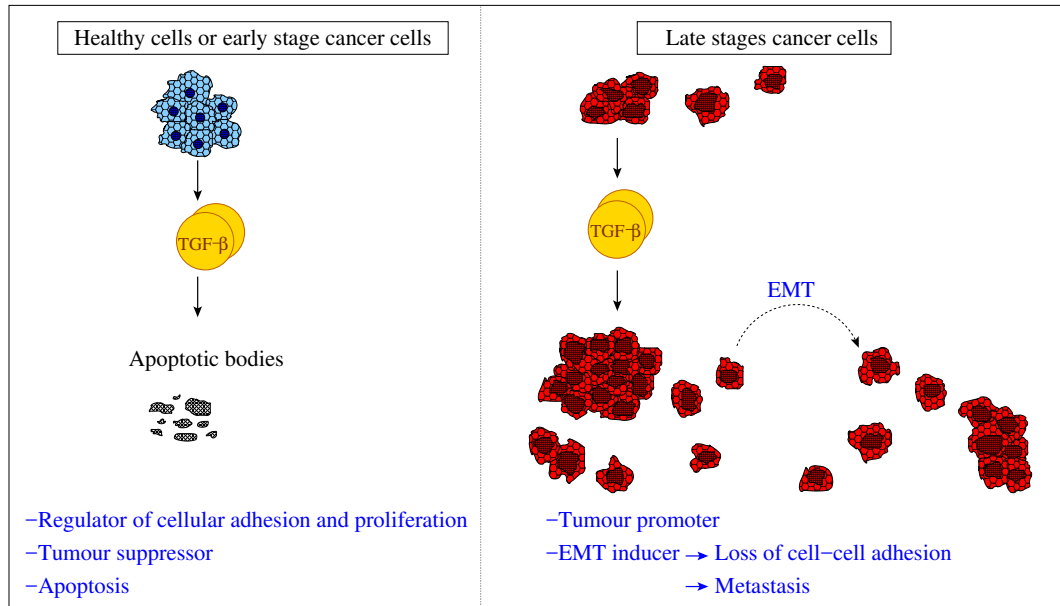
Figure 3.1: A caricature summarising the dual role of TGF-β in cancer progression.

Cancer cells dynamics. Cancer cells can switch from a homogeneous type of invasion to a heterogeneous type of invasion described by (directionally moving) invading chains (Chapman et al., 2014). Therefore, we assume that the movement of the early stage cancer cell population u_1 is governed by random motility (which underlines a homogeneous type of invasion), as well as directed motility in response to cell-cell and cell-matrix adhesive forces (which underlines the heterogeneous type of invasion) (Calvo and Sahai, 2011). Let D_u describe the random motility coefficient and $F_1^\beta[\underline{u}, f, c, b]$ describe the nonlocal directed motility. In contrast, the late stage cancer cell population, u_2, moves only in a directed manner (hence exhibiting a heterogeneous type of invasion) in response to cell-cell and cell-matrix adhesion forces (described by a nonlocal term $F_2^\beta[\underline{u}, f, c, b]$). Moreover, the u_1 cells can mutate into u_2 cells at a constant rate M. TGF-β has been found to have bidirectional functions in the progression of cancer. In early stages of cancer, TGF-β is an antiproliferative and proapoptotic signal, while in late stages of cancer it acts as a tumour promoter (Principe et al., 2014). Thus we have the following equations describing the dynamics of the two cancer cell

populations:

$$\frac{\partial u_1}{\partial t} = D_u \Delta u_1 - \nabla \cdot \left(u_1 F_1^\beta \left[\underline{u}, f, c, b \right] \right) - M u_1 + G_1 \left(\underline{u}, b \right), \tag{3.1a}$$

$$\frac{\partial u_2}{\partial t} = -\nabla \cdot \left(u_2 F_2^\beta \left[\underline{u}, f, c, b \right] \right) + M u_1 + G_2 \left(\underline{u}, b \right). \tag{3.1b}$$

Taking into account the effect of TGF-β on cancer cell proliferation and assuming that both u_1 and u_2 cells can proliferate in a logistic manner (to describe the observed slowdown in tumour growth following the loss of nutrients (Laird, 1964)), we choose the growth functions to be given by

$$G_i \left(\underline{u}, b \right) = r_i u_i \left(1 - \frac{u_1 + u_2}{k_u} \right) \left(1 + (-1)^i c_b \frac{b}{b_m} \right), \, i = 1, 2, \tag{3.2}$$

where r_1 and r_2 are the growth rates of the u_1 and u_2 populations, respectively, k_u is the carrying capacity, b_m is the maximum TGF-β concentration, and c_b is a coefficient related to the effect of TGF-β on cancer cell proliferation/decay. In particular, the term $(-1)^i$ models the anti-tumour effect of TGF-β on early tumours ($i = 1$), and the pro-tumour effect on late tumours ($i = 2$). Note that these growth functions incorporate also the principle of competition between clonal sub-populations in heterogeneous tumours (Leith et al., 1989).

The nonlocal cell-cell and cell-matrix adhesion and repulsion forces for cancer cell populations u_1 and u_2, are described by a function that depends on cell densities, ECM and integrin densities, and concentrations of TGF-β molecules

$$F_i^\beta : C \left(\bar{\Omega} : \mathbb{R} \right)^5 \mapsto C^{1,\zeta} \left(\bar{\Omega} : \mathbb{R}^n \right), \zeta \in (0,1], \, i = 1, 2, \tag{3.3}$$

given by the following relation

$$F_i^\beta [\underline{u}, f, c, b](x) := \int_\Omega K(|y - x|) g_i^\beta (\underline{u}(y), f(y), c(x), b(x)) \, dy, \ i = 1, 2, \qquad (3.4)$$

where $K \in L^\infty(\Omega)$, with $\partial_x K \in L^\infty(\Omega)$. The functions $g_i^\beta (\underline{u}, f, c, b), i = 1, 2$, describe the nature of the cell-cell and cell-matrix adhesive forces. These functions increase when the cell density and ECM density increase, and accordingly they decrease when the cell density and ECM density decrease. The functions $g_i^\beta, i = 1, 2$, are given by

$$g_i^\beta (\underline{u}, f, c, b) := S_i^\beta (c, b) u_i + S^\beta (c, b) u_j + C_i^\beta (c, b) f, \quad i, j = 1, 2, i \neq j, \qquad (3.5)$$

where $S_i^\beta (c, b)$ is the cell-cell self-adhesion strength function for populations u_i, $S^\beta (c, b)$ is the cell-cell cross-adhesion strength function between the two populations, and $C_i^\beta (c, b)$ is the adhesion strength function between population u_i and ECM.

Integrins are molecules known to have a regulative role in cell-cell and cell-matrix adhesion (Ascolani and Liò, 2014), while the role of TGF-β in cellular adhesion is dual: (i) Promotes cell-matrix adhesion by inducing the synthesis and the secretion of ECM-adhesion molecules laminin and fibronectin and the upregulation of integrin expression for these matrix-adhesion molecules (Huang and Chakrabarty, 1994; Wang et al., 2004); (ii) Decreases cell-cell adhesion (Nawshad et al., 2005; Wang et al., 2009). Thus, to define these adhesion strength functions we consider the integrin density, c, and TGF-β concentration, b. Since cell mutation could lead to more integrins (Kidera et al., 2010), we consider strength functions with different integrin levels for each of the two populations. The more integrins a cell has, the stronger its adhesion force (Gallant et al., 2005). Therefore, biologically realistic choices for these adhesion strength functions are the increasing, bounded and positive functions given by (see also Section

2.2) :

$$S_i^\beta (c,b) = s_i^* \left(1 + \tanh\left(a_i c - a_{b_i} b\right)\right), \; S^\beta (c,b) = s^* \left(1 + \tanh\left(dc - d_b b\right)\right),$$

$$C_i^\beta (c,b) = c_i^* \left(1 + \tanh\left(e_i c + e_{b_i} b\right)\right), \;\; i = 1,2, \tag{3.6}$$

where $a_i, a_{b_i}, d, d_b, e_i, e_{b_i}$ and $s_i^*, s^*, c_i^*, i = 1,2$, are positive real numbers.

ECM dynamics. The extracellular matrix is considered as non-motile matter, with changes to its density due to degradation by u_1 and u_2 cell populations upon contact at rates $\alpha > 0$ and $\beta > 0$, respectively, and ECM density remodelling back to normal levels, at a constant rate of δ. In contrast to equation (2.15) presented in Chapter 2, here we choose to consider the ECM remodelling term by choosing $\delta > 0$. Moreover, TGF-β induces the synthesis of extracellular matrix adhesion molecules (Wang et al., 2004, 2009), at a rate of $\theta_\beta > 0$. Thus the dynamics of ECM, $f(t,x)$, is described by:

$$\frac{\partial f}{\partial t} = -\alpha u_1 f - \beta u_2 f + \theta_\beta b f + \delta f \left(1 - \frac{f}{f_m}\right), \tag{3.7}$$

where f_m is the maximum ECM density at which the ECM fills up all available physical space.

Integrin dynamics. We assume that the level of integrins depends on cancer cell density, such that cell mutation changes the density of receptors (since in highly metastatic cancers, the expression of integrins is up-regulated (Kidera et al., 2010)). Moreover, TGF-β signalling up-regulates the integrin expression (Ascolani and Liò, 2014; Mamuya and Duncan, 2012), at a rate of p_3. Therefore, the dynamics of integrins, $c(t,x)$, can be described by:

$$\frac{\partial c}{\partial t} = p_1 u_1 + p_2 u_2 + p_3 b c - q c, \tag{3.8}$$

where q is the decay rate of c, and p_1 and p_2 are the production rates of integrins by u_1 and u_2 cancer cell populations, respectively. To model the increase in receptors on highly mutated cancer cells, we assume that $p_2 > p_1$ (see Table 3.2).

TGF-β dynamics. Finally, TGF-β is assumed to diffuse freely in the spatial domain, after being released by u_1 and u_2 cells, and decay at a rate of $q_b > 0$. Therefore, the dynamics of TGF-β, $b(t,x)$, is described by:

$$\frac{\partial b}{\partial t} = D_b \Delta b + \lambda\left(\underline{u}\right) - q_b b, \tag{3.9}$$

where D_b is the TGF-β diffusion coefficient and $\lambda\left(\underline{u}\right)$ is the TGF-β production term. Here, we choose $\lambda\left(\underline{u}\right) = \mu_1 u_1 + \mu_2 u_2$, with μ_1 and μ_2 to be the production rates of TGF-β by u_1 and u_2, respectively.

The relations (3.1)-(3.9) are summarised in the following system:

$$\frac{\partial u_1}{\partial t} = D_u \Delta u_1 - \nabla \cdot \left(u_1 F_1^\beta\left[\underline{u}, f, c, b\right]\right) - M u_1 + G_1\left(\underline{u}, b\right), \tag{3.10a}$$

$$\frac{\partial u_2}{\partial t} = -\nabla \cdot \left(u_2 F_2^\beta\left[\underline{u}, f, c, b\right]\right) + M u_1 + G_2\left(\underline{u}, b\right), \tag{3.10b}$$

$$\frac{\partial f}{\partial t} = -\alpha u_1 f - \beta u_2 f + \theta_\beta b f + \delta f\left(1 - \frac{f}{f_m}\right), \tag{3.10c}$$

$$\frac{\partial c}{\partial t} = p_1 u_1 + p_2 u_2 + p_3 b c - q c, \tag{3.10d}$$

$$\frac{\partial b}{\partial t} = D_b \Delta b + \mu_1 u_1 + \mu_2 u_2 - q_b b. \tag{3.10e}$$

We impose the following initial conditions

$$u_i(0,x) = u_{i_0}(x) \geq 0, \ i = 1, 2, \ f(0,x) = f_0(x) \geq 0, \ c(0,x) = c_0(x) \geq 0,$$

$$b(0,x) = b_0(x) \geq 0, \ \text{in} \ \Omega. \tag{3.11}$$

Finally, we assume that there is no-flux of both cancer cells and TGF-β proteins on the boundary of the domain,

$$\langle \nabla u_i, v \rangle = 0 = \langle \nabla b, v \rangle, \ i = 1, 2, \ \text{on} \ (0, \infty) \times \partial \Omega \tag{3.12}$$

and

$$\langle F_i^{\beta} [\underline{u}, f, c, b], v \rangle = 0, \ i = 1, 2, \ \text{on} \ (0, \infty) \times \partial \Omega, \tag{3.13}$$

where v is the outward unit normal vector to $\partial \Omega$.

3.3 Existence of solution

To prove the existence of solution for system (3.10) we use the theory of semigroups combined with the vanishing viscosity method (to transform equation (3.10b) into a parabolic equation). Then we show that in the vanishing viscosity limit, we obtain weak solutions for (3.10). We note that the steps in this proof of existence of approximate solution follow similar approaches taken in Chaplain et al. (2011), where a simpler parabolic-ODE model with no production term in the ODE (i.e., the ODE in Chaplain et al. (2011) contains only a decay term, which implies global boundedness of its solution) is considered, whereas in our model the production terms in (3.10c)-(3.10d) add an extra layer of complexity to the proof. Moreover, for the proof of vanishing viscosity limit we use techiques similar to those in Hillen et al. (2001) for a hyperbolic-elliptic model. The link between these two proofs is based on the extraction of the appropriate estimates for the vanishing viscosity limit, for our more complex system of nonlocal parabolic-hyperbolic equations coupled with ODEs.

3.3.1 Existence of approximate solution

We will approximate system (3.10) by the following system

$$
\frac{\partial u_1^\varepsilon}{\partial t} - D_u \Delta u_1^\varepsilon + M u_1^\varepsilon = - \nabla u_1^\varepsilon \cdot F_1^\beta \left[u_1^\varepsilon, u_2^\varepsilon, f^\varepsilon, c^\varepsilon, b^\varepsilon \right] - u_1^\varepsilon \left(\nabla \cdot F_1^\beta \left[u_1^\varepsilon, u_2^\varepsilon, f^\varepsilon, c^\varepsilon, b^\varepsilon \right] \right)
$$
$$
+ G_1 \left(u_1^\varepsilon, u_2^\varepsilon, b^\varepsilon \right), \tag{3.14a}
$$

$$
\frac{\partial u_2^\varepsilon}{\partial t} - \varepsilon \Delta u_2^\varepsilon + u_2^\varepsilon = - \nabla u_2^\varepsilon \cdot F_2^\beta \left[u_1^\varepsilon, u_2^\varepsilon, f^\varepsilon, c^\varepsilon, b^\varepsilon \right] - u_2^\varepsilon \left(\nabla \cdot F_2^\beta \left[u_1^\varepsilon, u_2^\varepsilon, f^\varepsilon, c^\varepsilon, b^\varepsilon \right] \right)
$$
$$
+ h_1 \left(u_1^\varepsilon, u_2^\varepsilon, b^\varepsilon \right), \tag{3.14b}
$$

$$
\frac{\partial f^\varepsilon}{\partial t} = h_2 \left(u_1^\varepsilon, u_2^\varepsilon, b^\varepsilon \right) f^\varepsilon - \frac{\delta}{f_m} f^{\varepsilon^2}, \tag{3.14c}
$$

$$
\frac{\partial c^\varepsilon}{\partial t} = h_3 \left(u_1^\varepsilon, u_2^\varepsilon \right) + c^\varepsilon h_4 \left(b^\varepsilon \right), \tag{3.14d}
$$

$$
\frac{\partial b^\varepsilon}{\partial t} - D_b \Delta b^\varepsilon + q_b b^\varepsilon = h_5 \left(u_1^\varepsilon, u_2^\varepsilon \right), \tag{3.14e}
$$

for $0 < \varepsilon \leq 1$, where

$$
h_1 \left(u_1^\varepsilon, u_2^\varepsilon, b^\varepsilon \right) = M u_1^\varepsilon + u_2^\varepsilon + G_2 \left(u_1^\varepsilon, u_2^\varepsilon, b^\varepsilon \right), \; h_2 \left(u_1^\varepsilon, u_2^\varepsilon, b^\varepsilon \right) = -\alpha u_1^\varepsilon - \beta u_2^\varepsilon + \theta_\beta b^\varepsilon + \delta,
$$

$$
h_3 \left(u_1^\varepsilon, u_2^\varepsilon \right) = p_1 u_1^\varepsilon + p_2 u_2^\varepsilon, \; h_4 \left(b^\varepsilon \right) = p_3 b^\varepsilon - q \;\; \text{and} \;\; h_5 \left(u_1^\varepsilon, u_2^\varepsilon \right) = \mu_1 u_1^\varepsilon + \mu_2 u_2^\varepsilon.
$$
$$
\tag{3.15}
$$

The ICs are given by

$$
u_i^\varepsilon (0,x) = u_{i_0} (x) \geq 0, \; i = 1,2, \; f^\varepsilon (0,x) = f_0 (x) \geq 0, \; c^\varepsilon (0,x) = c_0 (x) \geq 0,
$$

$$
b^\varepsilon (0,x) = b_0 (x) \geq 0, \; \text{in } \Omega. \tag{3.16}
$$

Finally, the BCs corresponding to (3.12)-(3.13) are given by the relations

$$
\langle \nabla u_i^\varepsilon, \nu \rangle = 0 = \langle \nabla b^\varepsilon, \nu \rangle, \; i = 1,2, \; \text{on } (0,\infty) \times \partial \Omega \tag{3.17}
$$

and

$$\langle F_i^\beta \left[u_1^\varepsilon, u_2^\varepsilon, f^\varepsilon, c^\varepsilon, b^\varepsilon \right], \nu \rangle = 0, \; i = 1, 2, \; \text{on} \; (0, \infty) \times \partial\Omega. \qquad (3.18)$$

For the full nonlocal interaction terms (3.3)-(3.4) we make the following assumptions:

$$F_i^\beta \left[u_1, u_2, f, c, b \right](x) = \int_\Omega N_i \left(x, y, u_1(y), u_2(y), f(y), c(x), b(x) \right) \mathrm{d}y, \qquad (3.19)$$

where $N_i : \Omega^2 \times \mathbb{R}^5 \mapsto \mathbb{R}^n$, $i = 1, 2$, is a continuous function, which satisfies

$$N_i(x, y, \underline{0}, c, b) = 0, \; i = 1, 2, \quad \text{for all} \quad (x, y) \in \Omega^2, c, b \in \mathbb{R}, \qquad (3.20)$$

and

$$N_i(\cdot, y, \phi, \chi, \psi, c, b) \in C^{1,\zeta} \left(\bar{\Omega} : \mathbb{R}^n \right), \; i = 1, 2, \; \text{for all } y \in \Omega, \; (\phi, \chi, \psi) \in \mathbb{R}^3. \quad (3.21)$$

Since functions $S_i^\beta(c, b), S^\beta(c, b), C_i^\beta(c, b), i = 1, 2$, (given by (3.6)) are bounded, we assume that there is a constant L_N, which depends on the bound for $S_i^\beta, S^\beta, C_i^\beta, i = 1, 2$, such that for any $\phi_1, \phi_2, \chi_1, \chi_2, \psi_1, \psi_2 \in \mathbb{R}$ we have

$$|N_i(x, y, \phi_1, \chi_1, \psi_1, c, b) - N_i(x, y, \phi_2, \chi_2, \psi_2, c, b)| + |\partial_x N_i(x, y, \phi_1, \chi_1, \psi_1, c, b)$$
$$- \partial_x N_i(x, y, \phi_2, \chi_2, \psi_2, c, b)| \leq L_N \left(|\phi_1 - \phi_2| + |\chi_1 - \chi_2| + |\psi_1 - \psi_2| \right), i = 1, 2,$$
$$(3.22)$$

uniformly with respect to $(x, y) \in \Omega^2$.

We assume that h_2', h_3' and h_4' exist, and that

$$h_2' : \mathbb{R} \times \mathbb{R} \times \mathbb{R} \mapsto \mathbb{R}, \;\; h_3' : \mathbb{R} \times \mathbb{R} \mapsto \mathbb{R} \;\; \text{and} \;\; h_4' : \mathbb{R} \mapsto \mathbb{R} \qquad (3.23)$$

are locally Lipschitz functions.

Based on relation (3.2) we can assume that there are constants $B_i, D_i > 0, i = 1, 2$, such that for $u_1^\varepsilon, u_2^\varepsilon, b^\varepsilon \geq 0, i = 1, 2$, we have

$$G_i\left(u_1^\varepsilon, u_2^\varepsilon, b^\varepsilon\right) \leq B_i - D_i u_i^\varepsilon, \ i = 1, 2. \tag{3.24}$$

Moreover, based on relation (3.15) we can assume that there are constants $\Lambda_j > 0, j = 1, \ldots, 4$, such that for $u_1^\varepsilon, u_2^\varepsilon, f^\varepsilon, c^\varepsilon, b^\varepsilon \geq 0$

$$f^\varepsilon h_2\left(u_1^\varepsilon, u_2^\varepsilon, b^\varepsilon\right) - \frac{\delta}{f_m} f^{\varepsilon^2} \leq \Lambda_1 b^\varepsilon - \Lambda_2 f^\varepsilon \tag{3.25}$$

and

$$c^\varepsilon h_4\left(b^\varepsilon\right) \leq \Lambda_3 b^\varepsilon - \Lambda_4 c^\varepsilon. \tag{3.26}$$

We now consider the sectorial operators

$$A_1 = -D_u \Delta + MI, \ A_2 = -\varepsilon \Delta + I \ \text{and} \ A_3 = -D_b \Delta + q_b I, \tag{3.27}$$

in the space $X = L^p(\Omega)$, with common domain of definition

$$D = D(A_1) = D(A_2) = D(A_3) = \left\{ w \in W^{2,p} : \frac{\partial w}{\partial v} = 0 \text{ on } \partial \Omega \right\}, \tag{3.28}$$

and $Re\left(\sigma\left(A_j\right)\right) > 0, \ j = 1, 2, 3$. Then the fractional powers are well defined

$$X^\gamma = D\left(A_1^\gamma\right) = D\left(A_2^\gamma\right) = D\left(A_3^\gamma\right), \ 0 < \gamma < 1, \tag{3.29}$$

with the graph norm

$$\|x\|_{X^\gamma} = \|A_j^\gamma x\|_X, \ \text{for} \ x \in X^\gamma, \ j = 1, 2, 3. \tag{3.30}$$

68

Then from Henry (1981) we have the following embeddings

$$X^\gamma \subset W^{1,p}(\Omega) \text{ for } \gamma > \frac{1}{2}, \tag{3.31}$$

$$X^\gamma \subset C^{0,r}(\bar{\Omega}) \text{ for } \frac{r}{2} + \frac{n}{2p} < \gamma < \frac{1}{2} + \frac{n}{2p}, \ 0 < r < 1, \tag{3.32}$$

where $C^{0,r}(\bar{\Omega})$ is the space of all Hölder continuous functions with exponent r in Ω. Notice that for

$$\gamma \in \left(\frac{1}{2}, \frac{1}{2} + \frac{1}{2p}\right) \text{ for } p > n, \tag{3.33}$$

(3.31) and (3.32) are satisfied.

Moreover, since A_1, A_2 and A_3 are sectorial operators, then each of $-A_1, -A_2$ and $-A_3$ is the infinitesimal generator of an analytic semigroup $\left\{e^{-tA_j}\right\}_{t \geq 0}$, $j = 1, 2, 3$. Therefore, there exists a positive constant C_γ such that the following inequality holds (Henry, 1981)

$$\|A_j^\gamma e^{-A_j t} w\|_X \leq C_\gamma t^{-\gamma} e^{-\xi_j t} \|w\|_X, \text{ for } w \in X, \tag{3.34}$$

where $0 < \xi_j < Re\left(\sigma(A_j)\right), j = 1, 2, 3$, and

$$\|A_j^\gamma e^{-A_j t} w\|_X \leq k_\gamma \|w\|_{X^\gamma}, \text{ for } w \in X^\gamma, \tag{3.35}$$

where k_γ positive constant.

Theorem 3.3.1. *Let $u_1^\varepsilon(0,x), u_2^\varepsilon(0,x), b^\varepsilon(0,x) \in X^\gamma$ and $f^\varepsilon(0,x), c^\varepsilon(0,x) \in W^{1,p}(\Omega)$. If assumptions (3.16)-(3.26) and (3.33) are satisfied, then for any $T > 0$ there exists a unique global in time solution $\left(u_1^\varepsilon, u_2^\varepsilon, f^\varepsilon, c^\varepsilon, b^\varepsilon\right) \in C\left([0,T); [X^\gamma]^2 \times \left[W^{1,p}(\Omega)\right]^2 \times X^\gamma\right)$ to (3.14)-(3.18), which remains bounded and the bounds are ε-independent. Moreover,*

the solution satisfies

$$\left(u_1^\varepsilon, u_2^\varepsilon, b^\varepsilon \right) \in C^1 \left((0,T); \left[X^\gamma \right]^3 \right) \cap C \left((0,T); \left[W^{2,p}(\Omega) \right]^3 \right), \qquad (3.36)$$

$$f^\varepsilon, c^\varepsilon \in C^1 \left((0,T); W^{1,p}(\Omega) \right). \qquad (3.37)$$

Proof. We will prove the existence of a local-in-time solution using the Banach contraction theorem. We first focus on the ODEs (3.14c) and (3.14d). We notice that relation (3.31) implies that $u_1^\varepsilon, u_2^\varepsilon, b^\varepsilon \in W^{1,p}(\Omega)$, and since the functions $h_2 : \mathbb{R} \times \mathbb{R} \times \mathbb{R} \mapsto \mathbb{R}, h_3 : \mathbb{R} \times \mathbb{R} \mapsto \mathbb{R}$ and $h_4 : \mathbb{R} \mapsto \mathbb{R}$ are locally Lipschitz, we have by the property of superposition operator that the value of the functions h_2, h_3 and h_4 is also in $W^{1,p}(\Omega)$ (Runst and Sickel, 1996). The space $W^{1,p}(\Omega)$ for $p > n$ is an algebra with pointwise multiplication, and thus it follows that the functions $\left(u_1^\varepsilon, u_2^\varepsilon, f^\varepsilon, b^\varepsilon \right) \mapsto P_1 = h_2 \left(u_1^\varepsilon, u_2^\varepsilon, b^\varepsilon \right) f^\varepsilon - \dfrac{\delta}{f_m} f^{\varepsilon^2}$ and $\left(u_1^\varepsilon, u_2^\varepsilon, c^\varepsilon, b^\varepsilon \right) \mapsto P_2 = h_3 \left(u_1^\varepsilon, u_2^\varepsilon \right) + c^\varepsilon h_4 \left(b^\varepsilon \right)$ are also $W^{1,p}$-valued. Since the right-hand-side functions of equations (3.14c) and (3.14d) are locally Lipschitz, it follows from assumption (3.23) and embeddings (3.31)-(3.32) that the mapping $P : \left(W^{1,p}(\Omega) \right)^5 \mapsto \left(W^{1,p}(\Omega) \right)^2, P = (P_1, P_2)$, is a locally Lipschitz function.

For a fixed $T > 0$ we note that functions

$$t \mapsto f_0 + \int_0^t P_1 \left(u_1^\varepsilon(s), u_2^\varepsilon(s), f^\varepsilon(s), b^\varepsilon(s) \right) \mathrm{d}s, \qquad (3.38)$$

$$t \mapsto c_0 + \int_0^t P_2 \left(u_1^\varepsilon(s), u_2^\varepsilon(s), c^\varepsilon(s), b^\varepsilon(s) \right) \mathrm{d}s, \qquad (3.39)$$

belong to the space $C \left([0,T]; W^{1,p}(\Omega) \right)$.

Then, the system of the PDEs (3.14a), (3.14b) and (3.14e) with (3.16) can be re-written

70

as:

$$z_t = Az + H(z) \qquad \text{in } \Omega_T$$

$$z(0,x) = z_0(x) \qquad \text{in } \Omega,$$

(3.40)

with

$$z = \begin{pmatrix} u_1^\varepsilon \\ u_2^\varepsilon \\ b^\varepsilon \end{pmatrix}, \quad A = \begin{pmatrix} A_1 & 0 & 0 \\ 0 & A_1 & 0 \\ 0 & 0 & A_3 \end{pmatrix},$$

and

$$H(z) = \begin{pmatrix} -\nabla u_1^\varepsilon \cdot F_1^\beta \left[u_1^\varepsilon, u_2^\varepsilon, f^\varepsilon, c^\varepsilon, b^\varepsilon\right] - u_1^\varepsilon \left(\nabla \cdot F_1^\beta \left[u_1^\varepsilon, u_2^\varepsilon, f^\varepsilon, c^\varepsilon, b^\varepsilon\right]\right) + G_1(z) \\ -\nabla u_2^\varepsilon \cdot F_2^\beta \left[u_1^\varepsilon, u_2^\varepsilon, f^\varepsilon, c^\varepsilon, b^\varepsilon\right] - u_2^\varepsilon \left(\nabla \cdot F_2^\beta \left[u_1^\varepsilon, u_2^\varepsilon, f^\varepsilon, c^\varepsilon, b^\varepsilon\right]\right) + h_1(z) \\ h_5\left(u_1^\varepsilon, u_2^\varepsilon\right) \end{pmatrix},$$

or, equivalently, we write that $A = A_1 \times A_2 \times A_3$ is sectorial in $X \times X \times X$, where $(A_1 \times A_2 \times A_3)\left(u_1^\varepsilon, u_2^\varepsilon, b^\varepsilon\right) = \left(A_1 u_1^\varepsilon, A_2 u_2^\varepsilon, A_3 b^\varepsilon\right)$ (Henry, 1981), and the mapping $H : (X^\gamma)^3 \mapsto (X)^3, H = (H_1, H_2, H_3)$ is defined as the mapping of the right-hand side of equations (3.14a), (3.14b) and (3.14e). Using similar arguments as before for P, and assumption (3.22) we deduce that $H : (X^\gamma)^3 \mapsto (X)^3$ is locally Lipschitz continuous.

Let us now denote $Y = X \times X \times W^{1,p}(\Omega) \times W^{1,p}(\Omega) \times X$. For a fixed $T > 0$ we define the space

$$Y_T^\gamma = C\left([0,T]; Y^\gamma\right),$$

(3.41)

where $Y^\gamma = X^\gamma \times X^\gamma \times W^{1,p}(\Omega) \times W^{1,p}(\Omega) \times X^\gamma$ equipped with the norm $\|y\|_{Y^\gamma} = \max\left\{\|y_1\|_{X^\gamma}, \|y_2\|_{X^\gamma}, \|y_3\|_{W^{1,p}(\Omega)}, \|y_4\|_{W^{1,p}(\Omega)}, \|y_5\|_{X^\gamma}\right\}$, for $y = (y_1, y_2, y_3, y_4, y_5) \in Y^\gamma$.

We define the mapping $J : Y_T^\gamma \mapsto Y_T^\gamma$ with $J = (J_1, J_2, J_3, J_4, J_5)$ given by the following

71

relation

$$
J =
\begin{cases}
J_1 = e^{-A_1 t} u_{1_0} + \int_0^t e^{-A_1(t-s)} H_1\left(u_1^\varepsilon(s), u_2^\varepsilon(s), f^\varepsilon(s), c^\varepsilon(s), b^\varepsilon(s)\right) ds \\[2mm]
J_2 = e^{-A_2 t} u_{2_0} + \int_0^t e^{-A_2(t-s)} H_2\left(u_1^\varepsilon(s), u_2^\varepsilon(s), f^\varepsilon(s), c^\varepsilon(s), b^\varepsilon(s)\right) ds \\[2mm]
J_3 = f_0 + \int_0^t P_1\left(u_1^\varepsilon(s), u_2^\varepsilon(s), f^\varepsilon(s), b^\varepsilon(s)\right) ds \\[2mm]
J_4 = c_0 + \int_0^t P_2\left(u_1^\varepsilon(s), u_2^\varepsilon(s), c^\varepsilon(s), b^\varepsilon(s)\right) ds \\[2mm]
J_5 = e^{-A_3 t} b_0 + \int_0^t e^{-A_3(t-s)} H_3\left(u_1^\varepsilon(s), u_2^\varepsilon(s)\right) ds.
\end{cases}
\tag{3.42}
$$

Let $R > 0$ be such that $\max\left\{\|u_{1_0}\|_{X^\gamma}, \|u_{2_0}\|_{X^\gamma}, \|b_0\|_{X^\gamma}\right\} < R/(2k_\gamma)$, where k_γ satisfies relation (3.35), and $\max\left\{\|f_0\|_{W^{1,p}(\Omega)}, \|c_0\|_{W^{1,p}(\Omega)}\right\} < R/2$ for $(u_{1_0}, u_{2_0}, f_0, c_0, b_0) \in Y^\gamma$. We define the ball

$$
B_R = \left\{ y \in Y_T^\gamma : \|y\|_{Y_T^\gamma} \le R \right\} \subset Y_T^\gamma.
\tag{3.43}
$$

Thus, there exists $M_R > 0$ such that $\sup_{y \in B_R} \|(H_1, H_2, P_1, P_2, H_3)(y)\|_Y < M_R$. We show that J maps B_R into itself and that J is a strict contraction. By using relations (3.34)-(3.35) and (3.42) we obtain, for T small enough,

$$
\|J_1\left[u_1^\varepsilon, u_2^\varepsilon, f^\varepsilon, c^\varepsilon, b^\varepsilon\right](t)\|_{X^\gamma} \le k_\gamma \|u_{1_0}\|_{X^\gamma} + M_R \int_0^T C_\gamma (t-s)^{-\gamma} e^{-\xi_1(t-s)} ds
$$
$$
\le \frac{R}{2} + M_R \frac{C_\gamma}{1-\gamma} T^{1-\gamma}.
\tag{3.44}
$$

Similarly we obtain

$$
\|J_2\left[u_1^\varepsilon, u_2^\varepsilon, f^\varepsilon, c^\varepsilon, b^\varepsilon\right](t)\|_{X^\gamma} \le \frac{R}{2} + M_R \frac{C_\gamma}{1-\gamma} T^{1-\gamma},
\tag{3.45}
$$

and

$$
\|J_5\left[u_1^\varepsilon, u_2^\varepsilon\right](t)\|_{X^\gamma} \le \frac{R}{2} + M_R \frac{C_\gamma}{1-\gamma} T^{1-\gamma}.
\tag{3.46}
$$

Moreover, for J_3 and J_4 we have

$$\left\| J_l \left[u_1^\varepsilon, u_2^\varepsilon, f^\varepsilon, c^\varepsilon, b^\varepsilon \right] (t) \right\|_{W^{1,p}(\Omega)} \leq \frac{R}{2} + M_R T, \quad l = 3,4. \tag{3.47}$$

Hence, we can choose T sufficiently small such that $\left\{ M_R \dfrac{C_\gamma}{1-\gamma} T^{1-\gamma}, M_R T \right\} < \dfrac{R}{2}$, to assert that $J(B_R) \subset B_R$. We note also that $J \left[u_1^\varepsilon, u_2^\varepsilon, f^\varepsilon, c^\varepsilon, b^\varepsilon \right]$ is continuous from $[0,T]$ to E^γ, as it can be easily proved using inequality (3.35). Thus J maps B_R into itself.

If $y^1, y^2 \in B_R$ then for $t \in [0,T]$ we have

$$\left\| J_1 \left[y^1 \right] (t) - J_1 \left[y^2 \right] (t) \right\|_{X^\gamma} \leq \int_0^t \| A_1^\gamma e^{-A_1(t-s)} \|_X \| H_1 \left(y^1 (s) \right) - H_1 \left(y^2 (s) \right) \|_X \mathrm{d}s$$

$$\leq C_\gamma L_R \int_0^T (t-s)^{-\gamma} e^{-\xi_1(t-s)} \| y^1 - y^2 \|_{Y_T^\gamma},$$

where L_R is the Lipschitz constant of H. Similar estimates can be obtained for the differences of the rest of the arguments. Therefore it follows that

$$\left\| J \left[y^1 \right] - J \left[y^2 \right] \right\|_{Y_T^\gamma} \leq \frac{1}{2} \| y^1 - y^2 \|_{Y_T^\gamma} \quad \text{for all} \quad y^1, y^2 \in B_R. \tag{3.48}$$

Hence for T small enough J is a contraction mapping. Therefore, by Banach fixed point theorem, J has a unique fixed point in B_R. Moreover, functions $f^\varepsilon, c^\varepsilon : [0,T] \mapsto C(\Omega)$ are locally Lipschitz, thus $f^\varepsilon, c^\varepsilon \in W^{1,\infty} \left([0,T]; W^{1,p}(\Omega) \right)$ (see Theorem 4, Sec. 5.8.2, in Evans (2010)). Therefore, it follows from Sec. 3.3 in Henry (1981) that there is a maximal time of existence T_{max} of regular solution $\left(u_1^\varepsilon, u_2^\varepsilon, b^\varepsilon \right) \in C \left([0, T_{max}); (X^\gamma)^3 \right)$ such that for $t \in (0, T_{max})$ we have $\left(u_1^\varepsilon, u_2^\varepsilon, b^\varepsilon \right) \in D(A)$. Then, from Henry (1981) (Sec. 3.3 and Theorem 3.5.2 in Sec. 3.5) we obtain that $\left(u_1^\varepsilon, u_2^\varepsilon, b^\varepsilon \right) \in C^\zeta \left((0, T_{max}); \left(X^\beta \right)^3 \right)$ for some $\zeta, \beta \in (0,1)$. Hence (3.14a), (3.14b) and (3.14e) are satisfied in a pointwise manner on $(0, T_{max}) \times \Omega$. It follows now from relations (3.21) and (3.32), and the regularity theory of parabolic systems, that $u_1^\varepsilon, u_2^\varepsilon$ and b^ε are classical solutions of (3.14a), (3.14b) and (3.14e), respectively.

Let us now prove the uniqueness of solution. Let $y^1 = \left(u_1^1, u_2^1, f^1, c^1, b^1\right)$ and $y^2 = \left(u_1^2, u_2^2, f^2, c^2, b^2\right)$ be two solutions of system (3.14), with the same initial conditions. By linearity $y = y^1 - y^2$ is a solution of (3.14) with zero initial conditions. Then, since all nonlinear terms are Lipschitz continuous and the components of the solution are L^∞-bounded functions on bounded time intervals, we have

$$\frac{\mathrm{d}}{\mathrm{d}t}\|y\|_{L^2(\Omega)}^2 \leq k_0\|y\|_{L^2(\Omega)}^2, \text{ for } t \in [0, T_{max}), y(0) = 0, \tag{3.49}$$

for a constant k_0, and since $\|y(0)\|_{L^2(\Omega)} = 0$, Gronwall's inequality implies that $\|y(t)\|_{L^2(\Omega)} = 0$ for all $t \geq 0$, so $y = 0$.

The equation for the ECM density given by (3.14c) does not involve any spatial derivatives and x behaves as a parameter. Thus, it is an ordinary differential equation in which the right-hand side is zero when $f^\varepsilon(t,x) = 0$ and for which local Lipschitz conditions hold. Therefore, from Picard-Lindelöf theorem we obtain a local unique solution for the initial value problem (3.14c), with $f^\varepsilon(0,x) = 0$. In the same way we obtain a local unique solution for the initial value problem (3.14c), with $f^\varepsilon(0,x) \geq 0$. Therefore, since $f^\varepsilon(0,x) \geq 0$, from uniqueness of solutions we have $f^\varepsilon(t,x) \geq 0$ for all $t > 0, x \in \Omega$. Then from maximum principle arguments it follows from system (3.40) that $u_1^\varepsilon, u_2^\varepsilon, b^\varepsilon \geq 0$ on $[0, T_{max}) \times \Omega$.

Finally, the equation for the integrin density given by (3.14d) can be treated in a similar manner as equation (3.14c) for the ECM density. Again we have an ordinary differential equation in which the right-hand side is greater than or equal to zero when $c^\varepsilon(t,x) = 0$, and for which local Lipschitz conditions hold. Therefore, $c^\varepsilon(t,x) \geq 0$ on $[0, T_{max}) \times \Omega$.

We proceed now with the proof of global in time solution. Let us first integrate equation (3.14a) on Ω. Then, from the boundary conditions (3.17)-(3.18) and relation (3.24) we

obtain

$$\frac{\mathrm{d}}{\mathrm{d}t} \int_{\Omega} u_1^{\varepsilon}(t,x)\,\mathrm{d}x \leq B_1|\Omega| - (M+D_1)\int_{\Omega} u_1^{\varepsilon}(t,x)\,\mathrm{d}x. \tag{3.50}$$

Thus Gronwall's inequality yields the estimate

$$\sup_{t\in[0,T_{max})} \|u_1^{\varepsilon}(t,\cdot)\|_{L^1(\Omega)} \leq \max\left\{\frac{B_1|\Omega|}{M+D_1}, \|u_{1_0}\|_{L^1(\Omega)}\right\} := M_{u_1}. \tag{3.51}$$

Similarly we have

$$\sup_{t\in[0,T_{max})} \|u_2^{\varepsilon}(t,\cdot)\|_{L^1(\Omega)} \leq \max\left\{\frac{MM_{u_1}+B_2|\Omega|}{D_2}, \|u_{2_0}\|_{L^1(\Omega)}\right\} := M_{u_2}, \tag{3.52}$$

and

$$\sup_{t\in[0,T_{max})} \|b^{\varepsilon}(t,\cdot)\|_{L^1(\Omega)} \leq \max\left\{\frac{\mu_1 M_{u_1}+\mu_2 M_{u_2}}{q_b}, \|b_0\|_{L^1(\Omega)}\right\} := M_b, \tag{3.53}$$

hence from relations (3.25)-(3.26) and Gronwall's inequality again we have

$$\sup_{t\in[0,T_{max})} \|f^{\varepsilon}(t,\cdot)\|_{L^1(\Omega)} \leq \max\left\{\frac{\Lambda_1 M_b}{\Lambda_2}, \|f_0\|_{L^1(\Omega)}\right\} := M_f, \tag{3.54}$$

and

$$\sup_{t\in[0,T_{max})} \|c^{\varepsilon}(t,\cdot)\|_{L^1(\Omega)} \leq \max\left\{\frac{p_1 M_{u_1}+p_2 M_{u_2}+\Lambda_3 M_b}{\Lambda_4}, \|c_0\|_{L^1(\Omega)}\right\} := M_c. \tag{3.55}$$

Thus, from relations (3.19)-(3.22) we have for all $t \in [0, T_{max})$

$$\left\| \left(\sum_{j=1}^{n} \partial_{x_j} F_i^{\beta} \left[u_1^{\varepsilon}, u_2^{\varepsilon}, f^{\varepsilon}, c^{\varepsilon}, b^{\varepsilon} \right] \right) + F_i^{\beta} \left[u_1^{\varepsilon}, u_2^{\varepsilon}, f^{\varepsilon}, c^{\varepsilon}, b^{\varepsilon} \right] \right\|_{L^{\infty}(\Omega)} \leq L_N \left(\left\| u_1^{\varepsilon}(t) \right\|_{L^1(\Omega)} \right.$$
$$\left. + \left\| u_2^{\varepsilon}(t) \right\|_{L^1(\Omega)} + \left\| f^{\varepsilon}(t) \right\|_{L^1(\Omega)} \right) \leq L_N \left(M_{u_1} + M_{u_2} + M_f \right), i = 1, 2.$$

$$(3.56)$$

From system (3.40), we rewrite the elliptic operators in the form:

$$- D_u \Delta u_1^{\varepsilon} + \sum_{j=1}^{n} b_1^j \partial_{x_j} u_1^{\varepsilon} + d_1 u_1^{\varepsilon},$$

$$- \varepsilon \Delta u_2^{\varepsilon} + \sum_{j=1}^{n} b_2^j \partial_{x_j} u_2^{\varepsilon} + d_2 u_2^{\varepsilon},$$

$$- D_b \Delta b^{\varepsilon} + q_b b^{\varepsilon},$$

where we denote by $b_i^j = F_{i_j} \left[u_1^{\varepsilon}, u_2^{\varepsilon}, f^{\varepsilon}, c^{\varepsilon}, b^{\varepsilon} \right]$ and by $d_i = \sum_{j=1}^{n} \partial_{x_j} F_i^{\beta} [u_1^{\varepsilon}, u_2^{\varepsilon}, f^{\varepsilon}, c^{\varepsilon}, b^{\varepsilon}]$, $i = 1, 2, j = 1, \ldots, n$. From relation (3.56) it follows that b_i^j and $d_i, i = 1, 2$, are bounded on $(0, \infty) \times \Omega$. Hence, from the fact that the reaction terms are dissipative (see Cholewa and Dlotko (2000)), it follows by Moser-Alikakos method (see Cholewa and Dlotko (2000), Section 9.3) that the uniform in time $L^1(\Omega)$ estimate implies the uniform in time $L^{\infty}(\Omega)$ estimate for the solution $\left(u_1^{\varepsilon}, u_2^{\varepsilon}, b^{\varepsilon} \right)$ of (3.40). Therefore, there is a constant M_{∞} independent of ε (see Remark 3.3.1), such that

$$\sup_{t \in [0, T_{max})} \left(\left\| u_1^{\varepsilon}(t) \right\|_{L^{\infty}(\Omega)} + \left\| u_2^{\varepsilon}(t) \right\|_{L^{\infty}(\Omega)} + \left\| b^{\varepsilon}(t) \right\|_{L^{\infty}(\Omega)} \right) < M_{\infty}. \qquad (3.57)$$

Moreover, from (3.25)-(3.26) and (3.57), and the comparison theorem it follows that

$$\sup_{t \in [0, T_{max})} \left\| f^{\varepsilon}(t) \right\|_{L^{\infty}(\Omega)} < \max \left\{ \left\| f_0 \right\|_{L^{\infty}(\Omega)}, \frac{\Lambda_1 M_{\infty}}{\Lambda_2} \right\}, \qquad (3.58)$$

and

$$\sup_{t\in[0,T_{max})} \|c^{\varepsilon}(t)\|_{L^{\infty}(\Omega)} < \max\left\{\|c_0\|_{L^{\infty}(\Omega)}, (p_1+p_2)M_{\infty}, \frac{\Lambda_3 M_{\infty}}{\Lambda_4}\right\}. \qquad (3.59)$$

Relations (3.57)-(3.59) can be used to show that

$$\|H_i\left(u_1^{\varepsilon}(s), u_2^{\varepsilon}(s), f^{\varepsilon}(s), c^{\varepsilon}(s), b^{\varepsilon}(s)\right)\|_X \le M_{\gamma_i}\left(1+\|u_i^{\varepsilon}(t)\|_{X^{\gamma}}\right) \text{ for } t\in[0,T_{max})$$

$$(3.60)$$

and

$$\|H_3\left(u_1^{\varepsilon}(s), u_2^{\varepsilon}(s)\right)\|_X \le M_{\gamma_3} \text{ for } t\in[0,T_{max}), \qquad (3.61)$$

where $M_{\gamma_i}, M_{\gamma_3}, i=1,2$, are constants depending on M_{∞}.

We show now the global existence of solution by contradiction. Let us suppose that for $T_{max} < \infty$ we have

$$\sup_{t\in[0,T_{max})} \left(\|u_1^{\varepsilon}(t)\|_{X^{\gamma}} + \|u_2^{\varepsilon}(t)\|_{X^{\gamma}} + \|f^{\varepsilon}(t)\|_{W^{1,p}(\Omega)} + \|c^{\varepsilon}(t)\|_{W^{1,p}(\Omega)} + \right.$$

$$\left. + \|b^{\varepsilon}(t)\|_{X^{\gamma}}\right) \to \infty \text{ as } t \to T_{max}. \qquad (3.62)$$

From relation (3.60) and Volterra type integral inequality (Cholewa and Dlotko, 2000) it follows, as in Corollary 3.3.5 in Henry (1981), that

$$\sup_{t\in[0,T_{max})} \|u_i^{\varepsilon}(t)\|_{X^{\gamma}} \le \left(k_{\gamma}\left\|u_{i_0}^{\varepsilon}\right\|_{X^{\gamma}} + C_{\gamma}M_{\gamma_i}\int_0^{T_{max}} \frac{e^{-\xi_i(t-s)}}{(t-s)^{\gamma}}\right) C_{T_{max}},$$

where $C_{T_{max}} := C_{C_{\gamma}M_{\gamma_i},\gamma,T_{max}}$, $i=1,2$, is a continuous function increasing with respect to T_{max}, while for the function b^{ε} we have from relation (3.61) that

$$\sup_{t\in[0,T_{max})} \|b^{\varepsilon}(t)\|_{X^{\gamma}} \le \left(k_{\gamma}\|b_0^{\varepsilon}\|_{X^{\gamma}} + C_{\gamma}M_{\gamma_3}\int_0^{T_{max}} \frac{e^{-\xi_3(t-s)}}{(t-s)^{\gamma}}\right).$$

Note that k_γ and C_γ are ε-independent constants since $0 < \varepsilon \le 1$ (see Theorem 1.3.4 in Henry (1981)). We conclude that

$$\sup_{t \in [0, T_{max})} \left(\|u_1^\varepsilon(t)\|_{X^\gamma} + \|u_2^\varepsilon(t)\|_{X^\gamma} + \|b^\varepsilon(t)\|_{X^\gamma} \right) < \infty. \tag{3.63}$$

Whence, by (3.31) it follows now that

$$\sup_{t \in [0, T_{max})} \left(\|u_1^\varepsilon(t)\|_{W^{1,p}(\Omega)} + \|u_2^\varepsilon(t)\|_{W^{1,p}(\Omega)} + \|b^\varepsilon(t)\|_{W^{1,p}(\Omega)} \right) < \infty. \tag{3.64}$$

By equation (3.14c) and direct calculations, we obtain

$$\nabla f_t^\varepsilon = \left(-\alpha \nabla u_1^\varepsilon - \beta \nabla u_2^\varepsilon + \theta_\beta \nabla b^\varepsilon \right) f^\varepsilon + h_6 \nabla f^\varepsilon, \tag{3.65}$$

where

$$h_6 := h_2 - \frac{2\delta}{f_m} f^\varepsilon = -\alpha u_1^\varepsilon - \beta u_2^\varepsilon + \theta_\beta b^\varepsilon + \delta - \frac{2\delta}{f_m} f^\varepsilon \le \theta_\beta b^\varepsilon + \delta. \tag{3.66}$$

For notational convenience, in what follows we denote various nonnegative constants, which are independent of T or t, by $c_j, j = 1, 2, \ldots, 8$.

Multiplying (3.65) by $p \nabla f^\varepsilon |\nabla f^\varepsilon|^{p-2}$, using (3.66), Young's inequality, and the estimates (3.57), (3.58) and (3.64), and integrating over Ω, we deduce that

$$\begin{aligned}
\frac{d}{dt} \|\nabla f^\varepsilon\|_{L^p(\Omega)}^p \le{}& p \int_\Omega \left(-\alpha \nabla u_1^\varepsilon - \beta \nabla u_2^\varepsilon + \theta_\beta \nabla b^\varepsilon \right) f^\varepsilon \nabla f^\varepsilon |\nabla f^\varepsilon|^{p-2} \mathrm{d}x \\
&+ p\theta_\beta \int_\Omega b^\varepsilon |\nabla f^\varepsilon|^p \mathrm{d}x + p\delta \|\nabla f^\varepsilon\|_{L^p(\Omega)}^p \\
\le{}& p \max\left\{ \alpha, \beta, \theta_\beta \right\} \|f^\varepsilon\|_{L^\infty(\Omega)} \left(\int_\Omega |\nabla u_1^\varepsilon| |\nabla f^\varepsilon|^{p-1} \mathrm{d}x \right. \\
&\left. + \int_\Omega |\nabla u_2^\varepsilon| |\nabla f^\varepsilon|^{p-1} \mathrm{d}x + \int_\Omega |\nabla b^\varepsilon| |\nabla f^\varepsilon|^{p-1} \mathrm{d}x \right)
\end{aligned}$$

$$+ p \left(\theta_\beta \|b^\varepsilon\|_{L^\infty(\Omega)} + \delta \right) \|\nabla f^\varepsilon\|_{L^p(\Omega)}^p$$

$$\leq c_1 \left(\|\nabla u_1^\varepsilon\|_{L^p(\Omega)}^p + \|\nabla u_2^\varepsilon\|_{L^p(\Omega)}^p + \|\nabla b^\varepsilon\|_{L^p(\Omega)}^p \right) + c_2 \|\nabla f^\varepsilon\|_{L^p(\Omega)}^p.$$

By Gronwall's inequality and previous estimates we have

$$\sup_{t \in [0, T_{max})} \|f^\varepsilon(t)\|_{W^{1,p}(\Omega)} \leq c_3 e^{c_4 t}, \ \text{ for } t \geq 0. \tag{3.67}$$

Similarly, by equation (3.14d) and direct calculations, we obtain

$$\nabla c_t^\varepsilon = p_1 \nabla u_1^\varepsilon + p_2 \nabla u_2^\varepsilon + p_3 \nabla b^\varepsilon c^\varepsilon + p_3 b^\varepsilon \nabla c^\varepsilon - q \nabla c^\varepsilon. \tag{3.68}$$

Multiplying now (3.68) by $p \nabla c^\varepsilon |\nabla c^\varepsilon|^{p-2}$, using the estimates (3.57), (3.59) and (3.64), as well as Young's inequality, and integrating over Ω, we obtain

$$\begin{aligned}
\frac{d}{dt} \|\nabla c^\varepsilon\|_{L^p(\Omega)}^p \leq{}& pp_1 \int_\Omega \nabla u_1^\varepsilon \nabla c^\varepsilon |\nabla c^\varepsilon|^{p-2} \mathrm{d}x + pp_2 \int_\Omega \nabla u_2^\varepsilon \nabla c^\varepsilon |\nabla c^\varepsilon|^{p-2} \mathrm{d}x \\
&+ pp_3 \int_\Omega \nabla b^\varepsilon c^\varepsilon \nabla c^\varepsilon |\nabla c^\varepsilon|^{p-2} \mathrm{d}x + pp_3 \int_\Omega b^\varepsilon |\nabla c^\varepsilon|^p \mathrm{d}x - pq \int_\Omega |\nabla c^\varepsilon|^p \mathrm{d}x \\
\leq{}& p \max \left\{ p_1, p_2, p_3 \|c^\varepsilon\|_{L^\infty(\Omega)} \right\} \left(\int_\Omega |\nabla u_1^\varepsilon| |\nabla c^\varepsilon|^{p-1} \mathrm{d}x \right. \\
&+ \left. \int_\Omega |\nabla u_2^\varepsilon| |\nabla c^\varepsilon|^{p-1} \mathrm{d}x + \int_\Omega |\nabla b^\varepsilon| |\nabla c^\varepsilon|^{p-1} \mathrm{d}x \right) \\
&+ p \left(p_3 \|b^\varepsilon\|_{L^\infty(\Omega)} - q \right) \|\nabla c^\varepsilon\|_{L^p(\Omega)}^p \\
\leq{}& c_5 \left(\|\nabla u_1^\varepsilon\|_{L^p(\Omega)}^p + \|\nabla u_2^\varepsilon\|_{L^p(\Omega)}^p + \|\nabla b^\varepsilon\|_{L^p(\Omega)}^p \right) + c_6 \|\nabla c^\varepsilon\|_{L^p(\Omega)}^p.
\end{aligned}$$

This, together with Gronwall's inequality and previous estimates, yields

$$\sup_{t \in [0, T_{max})} \|c^\varepsilon(t)\|_{W^{1,p}(\Omega)} \leq c_7 e^{c_8 t}, \ \text{ for } t \geq 0. \tag{3.69}$$

Bounds (3.63), (3.67) and (3.69) contradict (3.62), therefore the solution exists glob-

ally. □

Remark 3.3.1. *It is easy to see how the proof of Moser-Alikakos method in Cholewa*

and Dlotko (2000) can be used in our case to show the ε-independent L^∞-estimates

given in relation (3.57). Following along the same lines with the proof of Lemma

9.3.1 in Cholewa and Dlotko (2000), we obtain a constant c' (as described in relation

(9.3.11) of the proof in Cholewa and Dlotko (2000)) such that

$$c' := max\left\{ const.a_0, 1, D|\Omega|, K^2 \right\}, \tag{3.70}$$

where a_0 will be each of the diffusion coefficients D_u, ε and D_b. Using the fact that

$0 < D_u, \varepsilon, D_b \leq 1$ it follows that c' is ε-independent.

By this result, it follows that the rest of the estimates given by relations (3.58)-(3.61),

(3.63)-(3.64), (3.67) and (3.69) are ε-independent.

3.3.2 Vanishing viscosity limit

Now we are ready to take the vanishing viscosity limit $\varepsilon \to 0$ and prove the existence of

solution for system (3.10). First we introduce the notion of a weak solution to problem

(3.10)-(3.11) with (3.12)-(3.13).

Definition 3.3.1. *A function $(u_1, u_2, f, c, b) \in L^\infty\left(\bar{\Omega}_T\right) \cap L^\infty\left(0, T; \left[L^1\left(\Omega\right)\right]^5\right)$ is called*

a weak solution of the problem (3.10)-(3.11) with (3.12)-(3.13) if

80

(i) For all $\phi \in C_0^\infty (\Omega_T)$ we have

$$- \int_{\bar{\Omega}_T} u_1 \phi_t - D_u \nabla u_1 \cdot \nabla \phi + u_1 F_1^\beta [\underline{u}, f, c, b] \cdot \nabla \phi$$
$$= \int_{\bar{\Omega}_T} \left[-Mu_1 + G_1 (\underline{u}, b) \right] \phi, \qquad (3.71)$$

$$- \int_{\bar{\Omega}_T} u_2 \phi_t + u_2 F_2^\beta [\underline{u}, f, c, b] \cdot \nabla \phi = \int_{\bar{\Omega}_T} \left[Mu_1 + G_2 (\underline{u}, b) \right] \phi, \qquad (3.72)$$

$$- \int_{\bar{\Omega}_T} f \phi_t = \int_{\bar{\Omega}_T} \left[-\alpha u_1 f - \beta u_2 f + \theta_\beta b f + \delta f \left(1 - \frac{f}{f_m} \right) \right] \phi, \qquad (3.73)$$

$$- \int_{\bar{\Omega}_T} c \phi_t = \int_{\bar{\Omega}_T} \left[p_1 u_1 + p_2 u_2 + p_3 b c - q c \right] \phi, \qquad (3.74)$$

$$- \int_{\bar{\Omega}_T} b \phi_t - D_b \nabla b \cdot \nabla \phi = \int_{\bar{\Omega}_T} \left[\mu_1 u_1 + \mu_2 u_2 - q_b b \right] \phi. \qquad (3.75)$$

(ii) The functions u_1, u_2, f, c and b satisfy the initial conditions $u_{1_0}(x)$, $u_{2_0}(x)$, $f_0(x)$, $c_0(x)$ and $b_0(x)$, respectively, given by (3.11), in the weak sense, i.e., there exists a set $E \subset [0, T]$ of Lebesgue measure zero such that $u_1(t_0, \cdot), u_2(t_0, \cdot), f(t_0, \cdot)$, $c(t_0, \cdot)$ and $b(t_0, \cdot)$ are defined almost everywhere in Ω for $t_0 \in [0, T] \setminus E$ and satisfy

$$\lim_{t_0 \to 0, t_0 \in [0, T] \setminus E} \int_\Omega |u_i(t_0, x) - u_{i_0}(x)| \mathrm{d}x = 0, \; i = 1, 2, \qquad (3.76)$$

$$\lim_{t_0 \to 0, t_0 \in [0, T] \setminus E} \int_\Omega |f(t_0, x) - f_0(x)| \mathrm{d}x = 0, \qquad (3.77)$$

$$\lim_{t_0 \to 0, t_0 \in [0, T] \setminus E} \int_\Omega |c(t_0, x) - c_0(x)| \mathrm{d}x = 0, \qquad (3.78)$$

$$\lim_{t_0 \to 0, t_0 \in [0, T] \setminus E} \int_\Omega |b(t_0, x) - b_0(x)| \mathrm{d}x = 0. \qquad (3.79)$$

We show now the L^1-estimates with respect to time, which will be used in the proof of existence of solution to model (3.10).

Theorem 3.3.2. *Let the assumptions of Theorem 3.3.1 hold. Then for each $\rho > 0$ there exist nondecreasing functions $\omega_\rho^{u_i}, \omega_\rho^f, \omega_\rho^c, \omega_\rho^b \in C([0, \infty))$ with $\omega_\rho^{u_i}(0) = \omega_\rho^f(0) =$*

$\omega_\rho^c(0) = \omega_\rho^b(0) = 0, i = 1, 2$, *such that for any* $\varepsilon \in (0,1]$ *and for any* $t, t + \Delta t \in$ $[0,T], \Delta t \geq 0$ *we have for a ball* $B_\rho = \{|x| \leq \rho\}$ *that*

$$\int_{B_\rho} |u_i^\varepsilon(t + \Delta t, x) - u_i^\varepsilon(t, x)| dx \leq \omega_\rho^{u_i}(\Delta t), \ i = 1, 2, \tag{3.80}$$

$$\int_{B_\rho} |f^\varepsilon(t + \Delta t, x) - f^\varepsilon(t, x)| dx \leq \omega_\rho^f(\Delta t), \tag{3.81}$$

$$\int_{B_\rho} |c^\varepsilon(t + \Delta t, x) - c^\varepsilon(t, x)| dx \leq \omega_\rho^c(\Delta t), \tag{3.82}$$

$$\int_{B_\rho} |b^\varepsilon(t + \Delta t, x) - b^\varepsilon(t, x)| dx \leq \omega_\rho^b(\Delta t). \tag{3.83}$$

Proof. Let us consider a function $g \in C_0^2(\Omega)$ with $\text{supp}(g) \subset B_\rho$. Then from the estimates obtained by Theorem 3.3.1 we have

$$\left| \int_\Omega \left(u_2^\varepsilon(t + \Delta t, x) - u_2^\varepsilon(t, x) \right) g(x) dx \right| = \left| \int_\Omega g(x) \int_t^{t + \Delta t} u_{2_t}^\varepsilon(s, x) ds dx \right|$$

$$\leq \left| \int_t^{t + \Delta t} \int_\Omega \varepsilon u_2^\varepsilon(s, x) \Delta g(x) dx ds \right|$$

$$+ \left| \int_t^{t + \Delta t} \int_\Omega u_2^\varepsilon(s, x) F_2^\beta \left[u_1^\varepsilon, u_2^\varepsilon, f^\varepsilon, c^\varepsilon, b^\varepsilon \right] \nabla g(x) dx ds \right|$$

$$+ \left| \int_t^{t + \Delta t} \int_\Omega \left[M u_1^\varepsilon(s, x) + G_2 \left(u_1^\varepsilon, u_2^\varepsilon, b^\varepsilon \right) \right] g(x) dx ds \right|$$

$$\leq C(\rho, M_\infty) \Delta t \|g\|_{C^2(\Omega)}.$$

Similarly we can obtain estimates for u_1, f, c and b. Then, as in Hillen et al. (2001), the L^1-estimates of $u_1^\varepsilon, u_2^\varepsilon, f^\varepsilon, c^\varepsilon$ and b^ε with respect to time t follow. $\square$

Theorem 3.3.3. *Let* $u_i(0, x), b(0, x) \in X^\gamma, i = 1, 2$, *and* $f(0, x), c(0, x) \in W^{1,p}(\Omega)$. *If assumptions of Theorem 3.3.1 are satisfied, then there exists a weak solution* (u_1, u_2, f, c, b) *of model (3.10) with (3.11)-(3.13), such that for all* $T > 0$ *the weak solution satisfies*

for almost all $(t, x) \in \bar{\Omega}_T$

$$0 \leq u_1(t, x), u_2(t, x), f(t, x), c(t, x), b(t, x) \leq C(M_\infty). \tag{3.84}$$

Proof. By Theorem 3.3.1, we have that for all $0 < \varepsilon \leq 1$ and $T > 0$ there exists a classical solution $\left(u_1^\varepsilon, u_2^\varepsilon, f^\varepsilon, c^\varepsilon, b^\varepsilon\right)$ of problem (3.14)-(3.16), which is uniformly bounded in $L^\infty\left(\bar{\Omega}_T\right)$. From estimates (3.64), (3.67) and (3.69) it follows that

$$\sup_{t \in [0,T)} \left(\|u_1^\varepsilon(t)\|_{W^{1,1}(\Omega)} + \|u_2^\varepsilon(t)\|_{W^{1,1}(\Omega)} + \|f^\varepsilon(t)\|_{W^{1,1}(\Omega)} + \|c^\varepsilon(t)\|_{W^{1,1}(\Omega)} \right.$$
$$\left. + \|b^\varepsilon(t)\|_{W^{1,1}(\Omega)} \right) < C. \tag{3.85}$$

We consider for $m \in \mathbb{N}$ a sequence ε_m with $\varepsilon_m \to 0$ for $m \to \infty$. Then by estimate (3.85) and L^1-estimates with respect to time, obtained from Theorem 3.3.2, it follows by Fréchet-Kolmogorov theorem that the sequences $\left\{u_1^{\varepsilon_m}, u_2^{\varepsilon_m}, f^{\varepsilon_m}, c^{\varepsilon_m}, b^{\varepsilon_m}\right\}$ are precompact in $L^1_{loc}\left(\bar{\Omega}_T\right)$. Using a standard diagonal extraction argument we obtain subsequences, denoted also as $\left\{u_1^{\varepsilon_m}, u_2^{\varepsilon_m}, f^{\varepsilon_m}, c^{\varepsilon_m}, b^{\varepsilon_m}\right\}$, and functions u_1, u_2, f, c, $b \in L^1_{loc}\left(\bar{\Omega}_T\right)$ with $u_i^{\varepsilon_m} \to u_i, i = 1, 2$, $f^{\varepsilon_m} \to f$, $c^{\varepsilon_m} \to c$ and $b^{\varepsilon_m} \to b$ in $L^1_{loc}\left(\bar{\Omega}_T\right)$. This implies that the convergence is even pointwise a.e. for a suitable subsequence. From uniform L^1-bounds of $\left\{u_1^{\varepsilon_m}(t, \cdot), u_2^{\varepsilon_m}(t, \cdot), f^{\varepsilon_m}(t, \cdot), c^{\varepsilon_m}(t, \cdot), b^{\varepsilon_m}(t, \cdot)\right\}$ we have that $u_1(t, \cdot), u_2(t, \cdot), f(t, \cdot), c(t, \cdot), b(t, \cdot) \in L^1(\Omega)$. Multiplying now equations (3.10a)-(3.10e) with a test function $\phi \in C_0^\infty(\Omega_T)$, taking the integral and integrating by parts

over $\bar{\Omega}_T$ yields

$$- \int_{\bar{\Omega}_T} u_1^{\varepsilon_m} \phi_t + D_u u_1^{\varepsilon_m} \cdot \Delta \phi + u_1^{\varepsilon_m} F_1^{\beta} \left[\underline{u}^{\varepsilon_m}, f^{\varepsilon_m}, c^{\varepsilon_m}, b^{\varepsilon_m} \right] \cdot \nabla \phi$$

$$= \int_{\bar{\Omega}_T} \left[-M u_1^{\varepsilon_m} + G_1 \left(\underline{u}^{\varepsilon_m}, b^{\varepsilon_m} \right) \right] \phi, \qquad (3.86)$$

$$- \int_{\bar{\Omega}_T} u_2^{\varepsilon_m} \phi_t + u_2^{\varepsilon_m} F_2^{\beta} \left[\underline{u}^{\varepsilon_m}, f^{\varepsilon_m}, c^{\varepsilon_m}, b^{\varepsilon_m} \right] \cdot \nabla \phi = \int_{\bar{\Omega}_T} \left[M u_1^{\varepsilon_m} + G_2 \left(\underline{u}^{\varepsilon_m}, b^{\varepsilon_m} \right) \right] \phi$$

$$+ \varepsilon \int_{\bar{\Omega}_T} u_2^{\varepsilon_m} \Delta \phi, \qquad (3.87)$$

$$- \int_{\bar{\Omega}_T} f^{\varepsilon_m} \phi_t = \int_{\bar{\Omega}_T} \left[-\alpha u_1^{\varepsilon_m} f^{\varepsilon_m} - \beta u_2^{\varepsilon_m} f^{\varepsilon_m} + \theta_{\beta} b^{\varepsilon_m} f^{\varepsilon_m} + \delta f^{\varepsilon_m} \left(1 - f^{\varepsilon_m} / f_m \right) \right] \phi,$$

$$\qquad (3.88)$$

$$- \int_{\bar{\Omega}_T} c^{\varepsilon_m} \phi_t = \int_{\bar{\Omega}_T} \left[p_1 u_1^{\varepsilon_m} + p_2 u_2^{\varepsilon_m} + p_3 b^{\varepsilon_m} c^{\varepsilon_m} - q c^{\varepsilon_m} \right] \phi, \qquad (3.89)$$

$$- \int_{\bar{\Omega}_T} b^{\varepsilon_m} \phi_t + D_b b^{\varepsilon_m} \cdot \Delta \phi = \int_{\bar{\Omega}_T} \left[\mu_1 u_1^{\varepsilon_m} + \mu_2 u_2^{\varepsilon_m} - q_b b^{\varepsilon_m} \right] \phi. \qquad (3.90)$$

The last term in (3.87) vanishes in the limit due to the uniform L^{∞}-bound on $\left\{ u_2^{\varepsilon_m} \right\}$ and from the pointwise convergence the Lebesgue's dominated convergence theorem ensures that the limit (u_1, u_2, f, c, b) satisfies (3.71)-(3.75). Moreover, $(u_1, u_2, f, c, b) \in L^{\infty} \left(\bar{\Omega}_T \right)$, and by relations (3.57)-(3.59) and Remark 3.3.1 we obtain the bounds (3.84).

It remains to show the initial conditions (3.76)-(3.79). Let us first define the set $E \subset [0, T]$ such that for all $t_0 \in [0, T] \setminus E$ we have for almost all $x \in \Omega$ that (t_0, x) is Lebesgue point of u_1, u_2, f, c and b. The set E has Lebesgue measure zero. For any fixed $t_0 \in [0, T] \setminus E$ and $\rho > 0$ it follows from Theorem 3.3.2 that

$$\int_{B_{\rho}} |u_i(t_0, x) - u_{i_0}(x)| \mathrm{d}x \leq \int_{B_{\rho}} |u_i(t_0, x) - u_i^{\varepsilon_m}(t_0, x)| \mathrm{d}x + \omega_{\rho}^{u_i}(t_0), \quad i = 1, 2.$$

The pointwise convergence of $\left\{ u_i^{\varepsilon_m} \right\}, i = 1, 2,$ yields

$$\int_{B_{\rho}} |u_i(t_0, x) - u_{i_0}(x)| \mathrm{d}x \leq \omega_{\rho}^{u_i}(t_0), \quad i = 1, 2.$$

The properties of $\omega_\rho^{u_i}(t_0), i = 1, 2$, give (3.76) since u_i has compact support. Similarly we obtain relations (3.77)-(3.79). $\qquad\qquad\square$

Remark 3.3.2. *Note that a similar approach can be applied also for the proof of existence of solutions to the model presented in Chapter 2 in $\Omega \subset \mathbb{R}^n$. A detailed proof will be the subject of future work.*

3.4   Numerical results

3.4.1   Non-dimensionalisation of the model

In this Section we investigate numerically the type of patterns exhibited by model (3.10) in the one dimensional case. Let $R_s > 0$ be the cells sensing radius (i.e., the maximum range over which cells can detect other surrounding cells). We consider a bounded domain $\Omega = [0, R_s]$, and following the approach in Gerisch and Chaplain (2008) we choose the nonlocal terms $F_i^\beta [\underline{u}, f, c, b], i = 1, 2$, to be given by

$$
F_i^\beta [\underline{u}, f, c, b](t, x) := \frac{1}{R_s} \int_0^{R_s} \sum_{k=0}^1 \eta(k) K(r) g_i \left(\underline{v}(t, x + r\eta(k)), c(t, x), b(t, x) \right) dr,
$$

(3.91)

where $\eta(k) = (-1)^k, k = 0, 1$ and $g_i^\beta, i = 1, 2$, as described in Section 3.2 (see relation (3.5)).

As in Chapter 2, let us define the kernel K, assuming that it is attractive at medium/long ranges (i.e., at the edges of the cell) and repulsive at very short ranges (i.e., over cell surface), and thus can be defined as

$$
K(x) := q_a K_a(x) - q_r K_r(x),
$$

(3.92)

with q_a and q_r describing the magnitudes of attractive and repulsive interactions, respectively, and $K_a(x)$ and $K_r(x)$ describe the spatial ranges over which these interactions take place. Similar to Chapter 2 (equations (2.31)), we consider translated Gaussian attraction and repulsion kernels (as in Eftimie et al. (2007)):

$$K(x) = \frac{q_a}{\sqrt{2\pi m_a^2}} e^{-\frac{(x-s_a)^2}{2m_a^2}} - \frac{q_r}{\sqrt{2\pi m_r^2}} e^{-\frac{(x-s_r)^2}{2m_r^2}}, \qquad (3.93)$$

where s_a and s_r represent half of the length of attraction and repulsion ranges, respectively, with $s_r < s_a$. Also, $m_j = s_j/8, j = a, r$, represent the width of the attractive and the repulsive interaction ranges.

To perform numerical simulations we first non-dimensionalise system (3.10) by using the following quantities:

$$\tilde{t} = \frac{t}{\tau}, \ \ \tilde{x} = \frac{x}{L_0}, \ \ \tilde{u}_i = \frac{u_i}{k_u}, \ \ \tilde{f} = \frac{f}{f_m}, \ \ \tilde{c} = \frac{c}{c_m}, \ \ \tilde{b} = \frac{b}{b_m}, \ \ \tilde{R}_s = \frac{R_s}{L_0}, \ \ \tilde{r} = \frac{r}{L_0},$$

$$\tilde{S}\left(\tilde{c},\tilde{b}\right) = \frac{\tau k_u}{L_0^2} S^\beta \left(c_m \tilde{c} + b_m \tilde{b}\right), \ \ \tilde{S}_i\left(\tilde{c},\tilde{b}\right) = \frac{\tau k_u}{L_0^2} S_i^\beta \left(c_m \tilde{c} + b_m \tilde{b}\right),$$

$$\tilde{C}_i\left(\tilde{c},\tilde{b}\right) = \frac{\tau f_m}{L_0^2} C_i^\beta \left(c_m \tilde{c} + b_m \tilde{b}\right), \ \ i = 1, 2. \qquad (3.94)$$

The length scale, L_0, is in the range of 0.1-1cm, and is defined as the maximum invasion distance of the cancer cells at the early stage of invasion (Anderson et al., 2000). The time scale is defined as $\tau := L_0^2/D_\tau$, where D_τ is the characteristic diffusion coefficient ($\sim 10^{-6} \mathrm{cm}^2\mathrm{s}^{-1}$). Furthermore, we rescale the cancer cells, the ECM, the integrins and the TGF-β with k_u, f_m, c_m and b_m, respectively. Here k_u is the carrying capacity of the cancer cell populations and it is taken to be $\sim 6.7 \cdot 10^7$cell/volume, and f_m is the maximum ECM density at which the ECM fills up all available physical space and it is taken to be equal to $4 \, mg/$volume, as in Domschke et al. (2014). Finally, c_m is the maximum integrin density and it is taken to be $5 \cdot 10^4$ integrins per cell (as in Benedetto et al. (2006)), while b_m is the maximum TGF-β concentration taken to be

equal to 141.59 ng/volume (as in Khan et al. (2012)).

We choose the dimensionless functions $\tilde{K}(\tilde{r}) := L_0 K(L_0 \tilde{r}) = L_0 K(r)$ and $\tilde{g}_i^\beta\left(\tilde{\underline{u}}, \tilde{f}, \tilde{c}, \tilde{b}\right) := \left(\tau / L_0^2\right) g_i^\beta\left(\underline{u}, f, c, b\right), i = 1, 2$. Therefore, the nonlocal terms are given by $\tilde{F}_i^\beta\left[\tilde{\underline{u}}, \tilde{f}, \tilde{c}, \tilde{b}\right] := \left(\tau / L_0\right) F_i^\beta\left[\underline{u}, f, c, b\right], i = 1, 2$.

Finally, we obtain the dimensionless parameters:

$$
\tilde{D}_u = \frac{D_u}{D_\tau}, \ \tilde{D}_b = \frac{D_b}{D_\tau}, \ \tilde{M} = \tau M, \ \tilde{\alpha} = \tau \alpha k_u, \ \tilde{\beta} = \tau \beta k_u, \ \tilde{\theta}_\beta = \tau \theta_\beta b_m, \ \tilde{\delta} = \tau \delta,
$$

$$
\tilde{p}_3 = \tau p_3 b_m, \ \tilde{q} = \tau q, \ \tilde{q}_b = \tau q_b, \ \tilde{r}_i = \tau r_i, \ \tilde{p}_i = \frac{\tau p_i k_u}{c_m} \text{ and } \tilde{\mu}_i = \frac{\tau \mu_i k_u}{b_m}, \ i = 1, 2.
$$

$$
(3.95)
$$

After dropping the tildes for notational convenience, we obtain the following non-dimensionalised system:

$$
\frac{\partial u_1}{\partial t} = D_u \frac{\partial^2 u_1}{\partial x^2} - \frac{\partial}{\partial x}\left(u_1 F_1^\beta\left[\underline{u}, f, c, b\right]\right) - M u_1 + r_1 u_1 \left(1 - u_1 - u_2\right)\left(1 - c_b b\right),
$$

$$
(3.96a)
$$

$$
\frac{\partial u_2}{\partial t} = -\frac{\partial}{\partial x}\left(u_2 F_2^\beta\left[\underline{u}, f, c, b\right]\right) + M u_1 + r_2 u_2 \left(1 - u_1 - u_2\right)\left(1 + c_b b\right), \quad (3.96b)
$$

$$
\frac{\partial f}{\partial t} = -\alpha u_1 f - \beta u_2 f + \theta_\beta b f + \delta f \left(1 - f\right), \quad (3.96c)
$$

$$
\frac{\partial c}{\partial t} = p_1 u_1 + p_2 u_2 + p_3 b c - q c, \quad (3.96d)
$$

$$
\frac{\partial b}{\partial t} = D_b \frac{\partial^2 b}{\partial x^2} + \mu_1 u_1 + \mu_2 u_2 - q_b b. \quad (3.96e)
$$

3.4.2 Pattern formation

As in Chapter 2, we discretise our model by using a time-splitting approach. We use a Crank-Nicolson scheme to propagate the solution of the diffusion term. Then, we use the Nessyahu-Tadmor scheme (Nessyahu and Tadmor, 1990) for the time-propagation of the advection terms. Finally, for the time-propagation of the reaction terms we use a fourth order Runge-Kutta algorithm, where the integrals are further discretized using the Simpson's rule. All simulations are performed on a domain of length $L = 10$ with periodic boundary conditions (introduced to approximate the dynamics on an infinite domain). For this reason, the integrals are wrapped-up at the boundaries. The simulations are ran for times up to $t = 1000$, but for clarity in Figures 3.2-3.5 we show mainly the dynamics for $t \leq 400$. If the patterns do not reach a steady state before $t = 400$, we add inset figures showing the dynamics for $t \leq 1000$.

The initial conditions for the cancer cell populations are small random perturbations of rectangular-shaped aggregations located in the middle of the domain

$$u_i(0,x) = \begin{cases} u_i^c + rand(0, 10^{-4}), & x \in (L/2 - 1, L/2 + 1) \\ 0, & \text{everywhere else} \end{cases} \tag{3.97}$$

with $u_1^c = 0$ and $u_2^c = 0.1$. As in Chapter 2, for the ECM density, f, we assume that the tumour has already degraded some of its surrounding tissues:

$$f(0,x) = 1 - 0.5u_1(0,x) - 0.5u_2(0,x). \tag{3.98}$$

Finally, the integrin density and TGF-β concentration, c and b, respectively, are proportional to the initial tumour cell density

$$c(0,x) = 0.5u_1(0,x) + 0.5u_2(0,x), \tag{3.99}$$

and

$$b(0,x) = 0.05u_1(0,x) + 0.05u_2(0,x). \qquad (3.100)$$

To investigate the effect of TGF-β signalling on cell proliferation, movement and aggregation (the last two aspects being controlled by cell adhesion), we focus on three possible cases for the magnitudes of cell-cell and cell-matrix adhesion. For each of these three cases, we investigate the dynamics of u_1 and u_2 populations when TGF-β is absent and does not influence cell proliferation or cell adhesion (i.e., for $c_b = a_{b_i} = d_b = e_{b_i} = \theta_\beta = p_3 = \mu_1 = \mu_2 = 0, i = 1, 2$), and when TGF-$\beta$ is present and influences both cell proliferation and cell adhesion (i.e., for $c_b = 20$ and $a_{b_i}, d_b, e_{b_i}, \theta_\beta, p_3, \mu_1, \mu_2, \neq 0, i = 1, 2$).
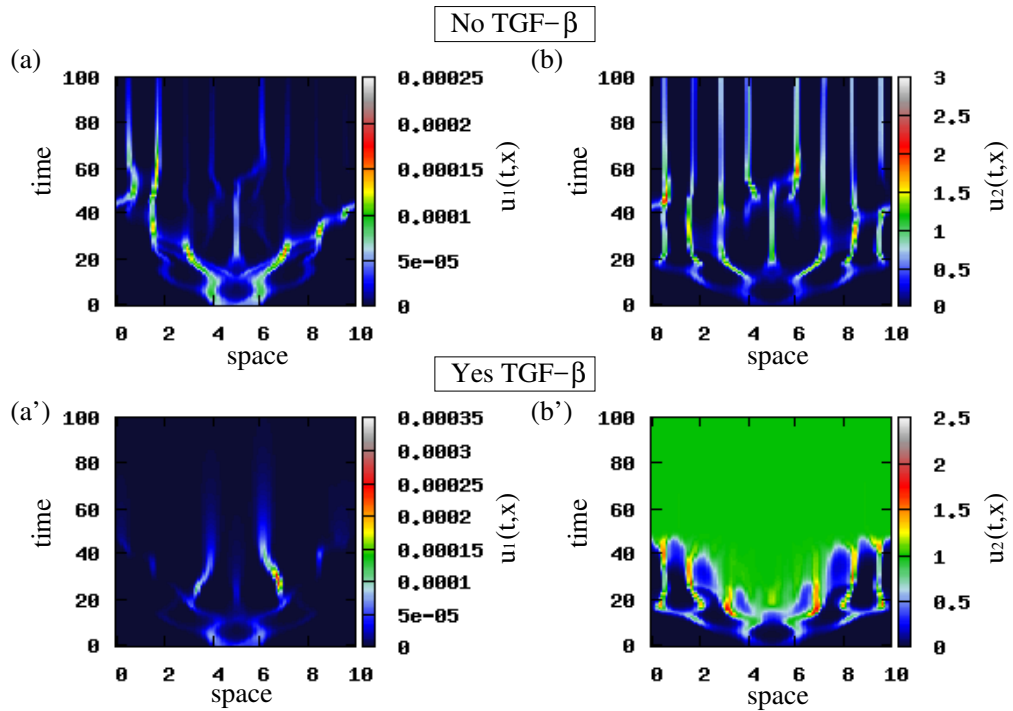
Figure 3.2: Patterns exhibited by model (3.96) showing the effect of TGF-β on cancer cell density, for cell-matrix adhesion greater than cell-cell adhesion, i.e., $s_1^* = 1.8, s_2^* = 0.6, s^* = 1, c_1^* = 1.9$ and $c_2^* = 2.5$. The rest of model parameters are given in Table 3.2. (a), (b) Density of u_1 and u_2 populations in the absence of TGF-β; (a'), (b') Density of u_1 and u_2 populations in the presence of TGF-β.

Figure 3.3: Patterns exhibited by model (3.96) showing the effect of TGF-β on cancer cell density, for cell-cell adhesion greater than cell-matrix adhesion, i.e., $s_1^* = 2.4, s^* = 2.1, s_2^* = 2, c_1^* = 1.1$ and $c_2^* = 0.9$. The rest of model parameters are given in Table 3.2. (a), (b) Density of u_1 and u_2 populations in the absence of TGF-β. The inset in panel (b) shows the long-term dynamics of $u_2(t,x)$ (for $t \leq 1000$); (a'), (b') Density of u_1 and u_2 populations in the presence of TGF-β.

(i) *Cell-cell adhesion < cell-matrix adhesion.* To investigate the effect of greater cell-matrix adhesion, we choose $s_1^* = 1.8, s_2^* = 0.6, s^* = 1, c_1^* = 1.9$ and $c_2^* = 2.5$ and the rest of model parameters as given in Table 3.2. We see in Figs. 3.2(a)-(b) that in the absence of TGF-β, the population of early-stage cancer cells (u_1) decreases, while the population of late-stage cancer cells (u_2) increases and dominates the long-term dynamics. This behaviour is expected due to the mutation term "$-Mu_1$", and due to large cell-matrix adhesion, which impedes cells to move and thus leads to the formation of stationary pulses for $t > 50$. Considering now the effect of TGF-β, we see in Figs. 3.2(a')-(b') that population u_1 vanishes faster, due to the presence of antiproliferative and proapoptotic signals

90

from TGF-β (described by $c_b > 0$ in equation (3.96a)). Population u_2 persists and increases significantly, due to the promoting effects of TGF-β on the late stages of cancer, which also induces the movement of the cancer cells (via EMT) thus leading to their spread over the domain until they reach the boundaries.
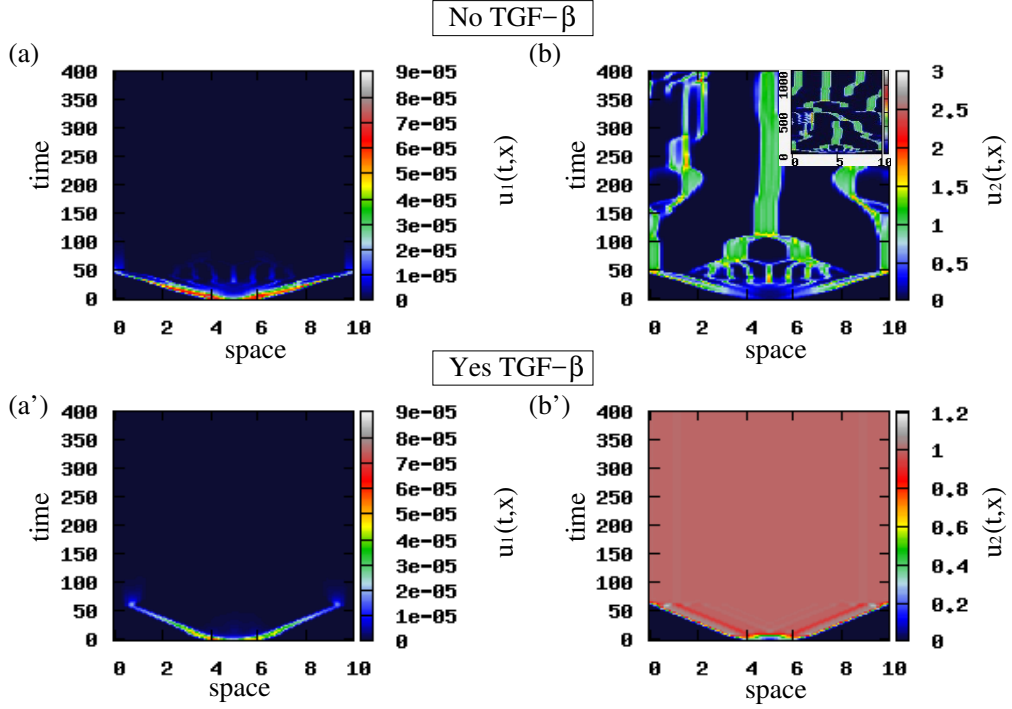
Figure 3.4: Patterns exhibited by model (3.96) showing the effect of the TGF-β on the cancer cell density for the same cell-cell and cell-matrix adhesion, i.e., $s_i^* = s^* = c_i^* = 0.8$ and $a_i = d = e_i = 0.5, i = 1, 2$. The rest of model parameters are given in Table 3.2. (a), (b) Density of u_1 and u_2 populations in the absence of TGF-β. The inset in panel (b) shows the long-term dynamics of $u_2(t,x)$ (for $t \leq 1000$); (a'), (b') Density of u_1 and u_2 populations in the presence of TGF-β.

(ii) *Cell-cell adhesion > cell-matrix adhesion.* To investigate the effect of greater cell-cell adhesion, we choose $s_1^* = 2.4, s^* = 2.1, s_2^* = 2, c_1^* = 1.1$ and $c_2^* = 0.9$, and the rest of model parameters as given in Table 3.2. We see in Fig. 3.3(a)-(b) that due to the weak cell-matrix adhesive forces, u_1 and u_2 cells start to move through the domain in a collective manner. Figs. 3.3(a)-(a') show that u_1 population

vanishes in the absence and in the presence of TGF-β (due to the mutation term). We also note that the spread of u_1 cells is reduced in the presence of TGF-β, likely due to the positive effect of TGF-β on cell-matrix adhesion (see the term "$+e_{b_i}b$" in equations (3.6)). In Figs. 3.3(b)-(b') we see that the u_2 population changes its movement from a chaotic-like dynamics (in the absence of TGF-β; panel (b)) to a spread over the whole domain (in the presence of TGF-β; panel (b')), as a result of a decrease in the cell-cell adhesion induced by the tumour growth factor.
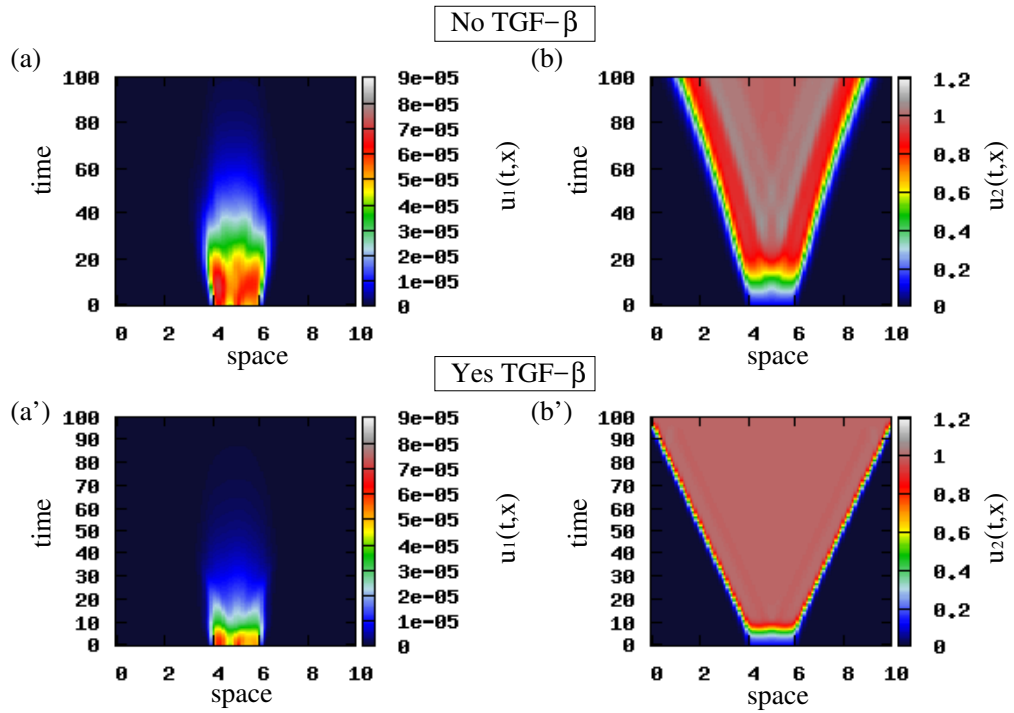
Figure 3.5: Patterns exhibited by model (3.96) showing the effect of the TGF-β on the cancer cell density for the same cell-cell and cell-matrix adhesion, i.e., $s_i^* = s^* = c_i^* = 0.1$ and $a_i = d = e_i = 0.5, i = 1, 2$. The rest of model parameters are given in Table 3.2. (a), (b) Density of u_1 and u_2 populations in the absence of TGF-β; (a'), (b') Density of u_1 and u_2 populations in the presence of TGF-β.
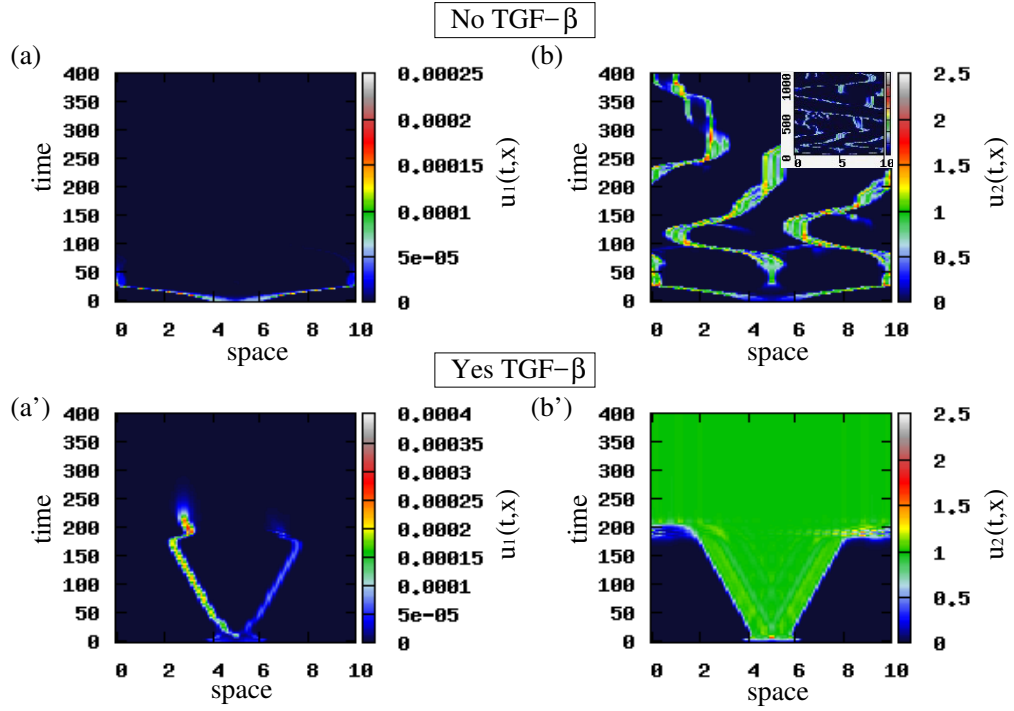
(iii) *Cell-cell adhesion = cell-matrix adhesion.* To ensure the same values for the adhesive strength functions (3.6) when there is no TGF-β in the system, we choose

$s_i^* = s^* = c_i^* = 0.8$ and $a_i = d = e_i = 0.5, i = 1, 2$. In Figs. 3.4(a)-(b) we see that some cells in the two cancer sub-populations move quickly to the left and the right, reaching the boundaries, while other cells (both u_1 and u_2) stay in the middle of the domain and create a chaotic-like pattern (even if u_1 is slowly eliminated for $t > 50$). If we now add TGF-β to the system, we see in Figs. 3.4(a')-(b') that both u_1 and u_2 populations move slower towards the edges of the domain. In contrast to the u_2 population in the absence of TGF-β, which exhibits a chaotic clumping and splitting behaviour (panel (b)), the u_2 population in the presence of TGF-β exhibits travelling-wave dynamics (panel (b')). This is different from the dynamics observed in Fig.3.3(b') where the u_2 cells move in a travelling-wave manner up to $t = 200$, after which they quickly move towards the boundaries.

Reducing now the magnitudes of cellular adhesion forces to $s_i^* = s^* = c_i^* = 0.1, i = 1, 2$, we see in Fig. 3.5 that irrespective of the absence/presence of TGF-β, population u_1 forms a stationary aggregation that eventually vanishes for large times, while population u_2 exhibits a travelling wave. This behaviour might be explained by the combined effect of high mutation rate and clonal competition (see the logistic growth terms in (3.2)), since adhesive forces are very small and lead to the spread of population u_2. In contrast to the dynamics in Figs. 3.3(b),(b') and 3.4(b),(b') where the u_2 cells seem to travel slower towards the boundaries in the presence of TGF-β (compared to the absence of TGF-β), in Fig. 3.5 the u_2 cells travel faster to the boundaries in the presence of TGF-β. We deduce from here that the spread of tumour cells depends both on the magnitude of adhesive forces as well as on the presence of TGF-β molecules.

We note here that we also investigated numerically the case when TGF-β is present, but does not influence cell proliferation or cell adhesion (i.e., for $\theta_\beta, p_3, \mu_1, \mu_2, \neq 0$, and $c_b = a_{b_i} = d_b = e_{b_i} = 0, i = 1, 2$). The patterns (not shown here) that we obtained were similar to those presented in Figs. 3.2(a)-(b), 3.3(a)-(b), 3.4(a)-(b) and 3.5(a)-(b).

This suggests that the effect of TGF-β on the cancer cell density is greater than the effect on the ECM and on the integrins density.

3.4.3 Summary of model variables and parameters

Here we present two tables with the model variables and parameters. In Table 3.1 we list the model variables with their units. In Table 3.2 we list the parameters of our model and their corresponding units and non-dimensional values used in the simulations.

Table 3.1: A list of model variables with their units. Since we are in 1D, length and volume coincide and we express the variables in terms of domain length.

Variable	Description	Dimensional Units
u_1	Early stage cancer cell density	$cell/length$
u_2	Late stage cancer cell density	$cell/length$
f	ECM density	$mg/length$
c	Integrin density	$integrins/cell$
b	TGF-β concentration	$mg/length$

Parameter estimation. Here we refer only to the parameter estimation related to TGF-β. For a detailed discussion on the estimation of the rest parameters see Section 2.4.1.

- The parameters $a_i, d, e_i, s_i^*, s^*, c_i^*, i = 1, 2$, were based on the range of the adhesion strength parameters used in Armstrong et al. (2006).

- The remodelling rate was chosen to be greater than cell proliferation rate, as considered also in Chaplain and Lolas (2006).

Table 3.2: A list of model parameters with their units and their non-dimensional values, obtained from (3.94) and (3.95), which we used during numerical simulations.

Param.	Description	Dimensional Units	Non-dim. value ($\tilde{p}$)	Reference
D_u	Diffusion coefficient of u_1	$length^2/time$	0.0001	Chaplain and Lolas (2006)
R_s	Sensing radius	$length$	0.99	Armstrong et al. (2006); Gerisch and Chaplain (2008)
q_a	Magnitude of attraction	$length^2/cell$	0.09	Estimated
q_r	Magnitude of repulsion	$length^2/cell$	0.01	Estimated
s_a	Attraction range	$length$	0.99	Estimated
s_r	Repulsion range	$length$	0.25	Estimated
m_a	Width of attraction kernel	$length$	0.99/8	Estimated
m_r	Width of repulsion kernel	$length$	0.25/8	Estimated

Continued on next page

Table 3.2 – *Continued from previous page*

Param.	Description	Dimensional Units	Non-dim. value ($\tilde{p}$)	Reference
r_1	Growth rate of u_1	$1/time$	0.1	Cunningham and You (2015); Morani et al. (2014)
r_2	Growth rate of u_2	$1/time$	0.2	Cunningham and You (2015); Morani et al. (2014)
M	Mutation rate	$1/time$	0.05	Cillo et al. (1987); Hill et al. (1984); Mareel et al. (1991)
c_b	Coeff. related to the effect of TGF-β on cancer cell proliferation	Non-dim.	20	Estimated

Continued on next page

Table 3.2 – *Continued from previous page*

Param.	Description	Dimensional Units	Non-dim. value ($\tilde{p}$)	Reference
a_1	Coeff. related to the number of integrins necessary for max self-adhesion between u_1	*cell/integrins*	0.7	Estimated
a_2	Coeff. related to the number of integrins necessary for max self-adhesion between u_2	*cell/integrins*	0.3	Estimated
d	Coeff. related to the number of integrins necessary for max cell-cell cross-adhesion	*cell/integrins*	0.5	Estimated
e_1	Coeff. related to the number of integrins necessary for max cell-ECM adhesion for u_1	*cell/integrins*	1.8	Estimated
e_2	Coeff. related to the number of integrins necessary for max cell-ECM adhesion for u_2	*cell/integrins*	2.5	Estimated
a_{b_1}	Coeff. related to the effect of TGF-β on self-adhesion between u_1 cells	*length/mg*	0.5	Estimated

Continued on next page

Table 3.2 – *Continued from previous page*

Param.	Description	Dimensional Units	Non-dim. value ($\tilde{p}$)	Reference
a_{b_2}	Coeff. related to the effect of TGF-β on self-adhesion between u_2 cells	$length/mg$	0.3	Estimated
d_b	Coeff. related to the effect of TGF-β on cell-cell cross-adhesion	$length/mg$	0.4	Estimated
e_{b_1}	Coeff. related to the effect of TGF-β on cell-ECM adhesion for u_1 cells	$length/mg$	0.8	Estimated
e_{b_2}	Coeff. related to the effect of TGF-β on cell-ECM adhesion for u_2 cells	$length/mg$	0.9	Estimated
s_1^*	Magnitude of self-adhesion forces of u_1	$length/(time \cdot cell)$	$0.1 - 2.4$	Estimated
s_2^*	Magnitude of self-adhesion forces of u_2	$length/(time \cdot cell)$	$0.1 - 2$	Estimated
s^*	Magnitude of cross-adhesion forces	$length/(time \cdot cell)$	$0.1 - 2.1$	Estimated
c_1^*	Magnitude of cell-ECM forces of u_1	$length/(time \cdot cell)$	$0.1 - 1.9$	Estimated
c_2^*	Magnitude of cell-ECM forces of u_2	$length/(time \cdot cell)$	$0.1 - 2.5$	Estimated

Table 3.2 – *Continued from previous page*

Param.	Description	Dimensional Units	Non-dim. value ($\tilde{p}$)	Reference
α	Rate of ECM degradation by u_1	$length/(time \cdot cell)$	1	Sherratt et al. (2009)
β	Rate of ECM degradation by u_2	$length/(time \cdot cell)$	2	Sherratt et al. (2009)
θ_β	Binding rate of TGF-β to ECM components	$length/(time \cdot mg)$	0.77	Estimated
δ	ECM remodelling rate	$1/time$	0.25	Chaplain and Lolas (2006)
p_1	Production rate of c by u_1	$integrins/(time \cdot cell)$	0.05	Estimated
p_2	Production rate of c by u_2	$integrins/(time \cdot cell)$	0.1	Estimated
p_3	Up-regulation rate of c by b	$length/(time \cdot mg)$	0.2	Estimated
q	Decay rate of c	$1/time$	0.3	Liu et al. (2011)
D_b	Diffusion coefficient of TGF-β	$length^2/time$	0.007	Van Schepdael et al. (2016)

Continued on next page

Table 3.2 – *Continued from previous page*

Param.	Description	Dimensional Units	Non-dim. value ($\tilde{p}$)	Reference
μ_1	Production rate of b by u_1	$mg/(time \cdot cell)$	0.05	Kim and Othmer (2013); Wu et al. (2007)
μ_2	Production rate of b by u_2	$mg/(time \cdot cell)$	0.05	Kim and Othmer (2013); Wu et al. (2007)
q_b	Decay rate of b	$1/time$	0.05	Liu et al. (2011)

3.5 Conclusion and discussion

In this chapter we introduced a model of integro-differential equations describing the dynamics of early stage and late stage cancer cell populations, under the effect of TGF-β signalling. The model was then used to investigate the role of TGF-β on cellular adhesion and proliferation.

We first proved the global existence of bounded solutions to our nonlocal model by taking a vanishing viscosity approach and approximating our model with a nonlocal parabolic PDE. The proof used the Banach contraction mapping theorem, the Moser-Alikakos method and the vanishing viscosity method.

We then investigated numerically the solution of this nonlocal model, paying particular attention to the effect of TGF-β on cell-cell and cell-matrix interactions. We showed that: (i) In the absence of TGF-β, the magnitudes of cell-cell and cell-matrix interactions influenced the formation of cancer cell aggregation at specific position in space (see Figs. 3.2(b), 3.3(b), 3.4(b)); (ii) The consideration of TGF-β leads to the spread of mutated (i.e., u_2) cancer cells over the whole domain mainly in a travelling-wave manner (with no cell aggregations; see Figs. 3.3(b'), 3.4(b'), 3.5(b')). We also emphasise that the speed at which cells spread depended on the presence/absence of TGF-β and on the magnitudes of cell adhesion forces (see Figs. 3.4(b),(b') vs. Figs. 3.5(b),(b')).

While the numerical investigation of cancer spread uncovered an interesting combined effect of cell adhesion and presence/absence of TGF-β, in the future we plan to investigate analytically the travelling waves and study the effect of parameters related to TGF-β and cell adhesion on the speed of these waves.

Chapter 4

An alternative model incorporating alignment

4.1 Introduction

Collective cell movement (Friedl and Wolf, 2003; Rørth, 2009) can be observed in many types of cells and plays an important role in many physiological processes, including wound healing, embryonic development and metastasis of cancer cells. The cancer cells' movement and aggregations are influenced by external factors, e.g., concentration of food, as well as internal factors, which are social forces among cells, i.e., attraction, repulsion and polarisation. These internal factors lead to self-organised cell aggregation and the formation of a wide variety of patterns. Apart from the attraction-repulsion forces, that has been extensively studied in the previous chapters, alignment seems to play a crucial role in cell movement. Experimental studies (Omelchenko et al., 2003; Rørth, 2012) have shown that alignment (polarisation) has been reported as the initial cellular response in wound healing and cancer invasion. By alignment we mean the process where cells turn to adapt their orientation to that of their neighbours,

which leads to a polarised group of cells having the same orientation in space and travelling large distances together. In contrast, there are non-polarised groups in which all cells move individually, while the group as a whole can remain stationary or drift only slowly (Lutscher, 2002). Cells interact with their neighbours and change their shape and direction of movement as a result of this collective movement and a process known as contact inhibition of locomotion (CIL) (Vicente-Manzanares and Sánchez-Madrid, 2000), which plays a crucial role in cancer invasion and metastasis. During this process cells alter their direction of movement when contact other cells in order to avoid collision.

Although, the exact mechanism that makes the cells cooperate with each other and migrate collectively in one direction is not fully clear, it has been observed that "leader" cells at the tops of outgrowths (e.g., an epithelial cell at the edge of an epithelial sheet that adopts a fibroblast-like morphology extending a wide lamellipodium) are accompanied by many "follower" cells along the sides, both migrating to distant sites (Haga et al., 2005; Omelchenko et al., 2003). As cells move in a collective manner, only the cells in the free edge will produce lamellipodia, while cells inside the group will form smaller protrusions or no protrusion. Although, CIL process will lead to a change in the direction of movement of the cells in the edges, the whole group of cells will follow this movement as a result of cell-cell interactions, ending up in the re-alignment of the cell populations (Mayor and Carmona-Fontaine, 2010). What also seems to play an important role in the direction of cell migration is the front-back orientation of cells (Reffay et al., 2011), thus it is very important to consider all the cells detected around it that interact with each other.

In the mathematical literature there are various models that consider the effect of nonlocal social interactions on the collective movement of cells and animals. A large number of models for the collective movement of animals consider the interplay between all

three social interactions: repulsion, attraction and alignment (Canizo et al., 2010; Cavagna et al., 2010; Gautrais et al., 2012; Huth and Wissel, 1992; Kunz and Hemelrijk, 2003; Lukeman et al., 2010). Some of these models consider nonlocal turning rates and constant speeds (see, for example Buono and Eftimie (2015); Fetecau (2011)). Other models investigate the effect of social interactions also on animals speed (Fetecau and Eftimie, 2010; Topaz et al., 2006). In regard to the models for the collective movement of cells, the majority of these models focus on attractive-repulsive interactions (Armstrong et al., 2006; Domschke et al., 2014; Painter et al., 2015; Sherratt et al., 2009). Very few nonlocal models incorporate cell alignment (see for instance Mogilner and Edelstein-Keshet (1995)). Therefore, it is very important to develop nonlocal models that consider cell polarization and describe the way that all three social forces affect the velocity and the turning behaviour of cells.

In this chapter [1], we introduce a new model describing better the interplay between cell polarisation and cell repulsive-attractive interactions. In contrast to the models mentioned in the previous paragraphs, here we consider both nonlocal speed and turning rates. To this end we derive a model of nonlinear nonlocal first order hyperbolic equations describing the dynamics of polarised early and late stage cancer cell populations. In addition to cell movement and cell turning behaviours (which depend on repulsive, attractive and polarising forces), we also consider mutation and proliferation. We investigate numerically the patterns generated by this hyperbolic model - by focusing on the effect of the following parameters: (i) Social interactions (and mainly alignment); (ii) Turning rates and (iii) Base-line speed. Since the majority of papers describing collective movement of cells are of parabolic type, in this chapter we also take a parabolic limit to investigate the preservation of patterns in this limit.

---

[1]A version of this chapter has been submitted for publication.

Bitsouni and Eftimie (2017), A nonlocal model for cell polarisation in heterogeneous cancer cell populations

We should emphasize here that we focus on the interactions between the cells and the effect of the social forces (paying mainly attention to the alignment forces) on the behaviour of the heterogeneous populations. For this reason we choose to ignore the ECM and integrin density in this model.

This chapter is organized as follows. In Section 4.2 we present a model of nonlocal nonlinear hyperbolic equations describing the dynamics of two sub-populations of polarised cancer cells, with different levels of mutation. In Section 4.3 we derive the parabolic limit of this hyperbolic model. In Section 4.4 we perform linear stability analysis of both hyperbolic and limiting parabolic model to investigate the ability of these models to form cell aggregation. In Section 4.5 we investigate numerically the spatiotemporal patterns obtained by the hyperbolic model and compare the results with the patterns obtained by the limiting parabolic model. We conclude in Section 4.6 with a discussion of the results.

4.2 A nonlocal hyperbolic model for cancer cell polarisation

In this section, we introduce a new nonlocal model that incorporates the tendency of cancer cells to align with other cells that are within a range (alignment range). The model describes the movement of two cancer cell populations, an early and a late stage population. Here, we assume that the movement of cancer cells is governed by directed motility in response explicitly to cell- cell adhesive forces, choosing to ignore the cell-ECM interactions. For this situation speed depends on attractive and repulsive interactions only between cancer cells.

Let $\Omega \subset \mathbb{R}$ be a bounded spatial domain with smooth boundary $\partial\Omega$. Let $I_T = [0, \infty)$

be the time interval. We denote by $u_1^+(t,x)$ ($u_1^-(t,x)$) the density of early stage cancer cells at (t,x) that move to the right (left), and respectively by $u_2^+(t,x)$ ($u_2^-(t,x)$) the density of late stage cancer cells at (t,x) that move to the right (left). The total cancer cell population density is given by the relation $u_1 = u_1^+ + u_1^-$ for the early stage cancer cell population, and respectively by $u_2 = u_2^+ + u_2^-$ for the late stage cancer cell population. For compact notation, we define the vector $\underline{u}(t,x) = \big(u_1(t,x), u_2(t,x)\big)^T$. We also define the cell population flows by $v_i = u_i^+ - u_i^-$, $i = 1, 2$, for early ($i = 1$) and late ($i = 2$) stage cancer cells. Thus, we derive the following hyperbolic system of conservation laws that describe the evolution of densities of left-moving and right-moving early and late stage cancer cells:

$$\frac{\partial u_1^+}{\partial t} + \frac{\partial}{\partial x}\left(u_1^+\Gamma^+[u_1,u_2]\right) = -\lambda_{u_1}^+\left[u_1^+,u_1^-,u_2^+,u_2^-\right]u_1^+ + \lambda_{u_1}^-\left[u_1^+,u_1^-,u_2^+,u_2^-\right]u_1^-$$
$$-Mu_1^+ + r_1\frac{u_1}{2}(1 - u_1 - u_2), \qquad (4.1a)$$

$$\frac{\partial u_1^-}{\partial t} - \frac{\partial}{\partial x}\left(u_1^-\Gamma^-[u_1,u_2]\right) = \lambda_{u_1}^+\left[u_1^+,u_1^-,u_2^+,u_2^-\right]u_1^+ - \lambda_{u_1}^-\left[u_1^+,u_1^-,u_2^+,u_2^-\right]u_1^-$$
$$-Mu_1^- + r_1\frac{u_1}{2}(1 - u_1 - u_2), \qquad (4.1b)$$

$$\frac{\partial u_2^+}{\partial t} + \frac{\partial}{\partial x}\left(u_2^+\Gamma^+[u_1,u_2]\right) = -\lambda_{u_2}^+\left[u_1^+,u_1^-,u_2^+,u_2^-\right]u_2^+ + \lambda_{u_2}^-\left[u_1^+,u_1^-,u_2^+,u_2^-\right]u_2^-$$
$$+M\frac{u_1}{2} + r_2\frac{u_2}{2}(1 - u_1 - u_2), \qquad (4.1c)$$

$$\frac{\partial u_2^-}{\partial t} - \frac{\partial}{\partial x}\left(u_2^-\Gamma^-[u_1,u_2]\right) = \lambda_{u_2}^+\left[u_1^+,u_1^-,u_2^+,u_2^-\right]u_2^+ - \lambda_{u_2}^-\left[u_1^+,u_1^-,u_2^+,u_2^-\right]u_2^-$$
$$+M\frac{u_1}{2} + r_2\frac{u_2}{2}(1 - u_1 - u_2), \qquad (4.1d)$$

$$u_i^\pm(0,x) = u_{i_0}^\pm(x) \geq 0, \quad i = 1, 2, \text{ in } \Omega, \qquad (4.1e)$$

where $\Gamma^\pm[u_1,u_2]$ are the density-dependent speeds, and $\lambda_{u_i}^+$ ($\lambda_{u_i}^-$) are the density dependent turning rates for the cancer cells initially moving to the right (left) and then turn to the left (right). As in the previous two chapters we denote by M the mutation

rate of cancer cells and by r_i, $i = 1, 2$, the proliferation rate of population u_i. Note that we consider a non-dimensionalised model, where the cancer cell densities $u_i, i = 1, 2$, are non-dimensionalised by the carrying capacity for the cells, k_u (see Chapters 2 and 3), leading to logistic growth functions with unit-valued carrying capacity for the cells.

The turning rates are functions of the cell-cell interactions, $y^\pm \left[u_1^+, u_1^-, u_2^+, u_2^- \right]$, described as in Eftimie et al. (2007):

$$
\begin{aligned}
\lambda_{u_i}^\pm \left[u_1^+, u_1^-, u_2^+, u_2^- \right] &:= \lambda_i^r + \lambda_i^b p \left(y^\pm \left[u_1^+, u_1^-, u_2^+, u_2^- \right] \right) \\
&= \lambda_i^r + \lambda_i^b \left(0.5 + 0.5 \tanh \left(y^\pm \left[u_1^+, u_1^-, u_2^+, u_2^- \right] - 2 \right) \right), \quad (4.2)
\end{aligned}
$$

where the constants λ_i^r and $\lambda_i^b, i = 1, 2$, represent a base-line random turning rate and a biased turning rate, respectively. The dimensionless functionals $y^\pm \left[u_1^+, u_1^-, u_2^+, u_2^- \right]$ of the densities of right moving, u_i^+, and left moving, u_i^-, cancer cells, incorporate nonlocal interactions between the two sub-populations of polarised cancer cells, and can be described by the following relation

$$
y^\pm \left[u_1^+, u_1^-, u_2^+, u_2^- \right] = y_a^\pm \left[u_1^+, u_1^-, u_2^+, u_2^- \right] - y_r^\pm \left[u_1^+, u_1^-, u_2^+, u_2^- \right] + y_{al}^\pm \left[u_1^+, u_1^-, u_2^+, u_2^- \right],
$$

$$(4.3)$$

where $y_j^\pm \left[u_1^+, u_1^-, u_2^+, u_2^- \right], j = a, r, al$, denote the attraction, repulsion and alignment functional, respectively, which influence the likelihood of a cancer cell to turn to the left (+) or to the right (-). We note here that stronger interaction forces lead to higher turning rates. The attraction and repulsion interactions are described by the following nonlocal terms (Buono and Eftimie, 2015):

$$
y_{a,r}^\pm [u_1, u_2] = \frac{q_{a,r}}{R_s} \int_0^{R_s} K_{a,r}(s) \left(u_1(t, x \pm s) + u_2(t, x \pm s) - u_1(t, x \mp s) - u_2(t, x \mp s) \right) ds,
$$

$$(4.4)$$

with q_a and q_r describing the magnitudes of attractive and repulsive interactions, respectively, and $K_a(x)$ and $K_r(x)$ describe the spatial ranges over which these interactions take place. As in the previous two chapters, we denote by $K(x) := q_a K_a(x) - q_r K(x)$ the attraction-repulsion kernel, assuming that it is attractive at medium/long ranges (i.e., at the edges of the cell) and repulsive at very short ranges (i.e., over the cell surface).

The nonlocal alignment term is given by the relation (Buono and Eftimie, 2015):

$$
\begin{aligned}
y_{al}^{\pm}\left[u_1^+, u_1^-, u_2^+, u_2^-\right] = \frac{q_{al}}{R_s} \int_0^{R_s} K_{al}(s) \Bigg(& u_1^{\mp}(t, x \mp s) + u_1^{\mp}(t, x \pm s) + u_2^{\mp}(t, x \mp s) \\
& + u_2^{\mp}(t, x \pm s) - u_1^{\pm}(t, x \mp s) - u_1^{\pm}(t, x \pm s) - u_2^{\pm}(t, x \mp s) \\
& - u_2^{\pm}(t, x \pm s) \Bigg) \mathrm{d}s,
\end{aligned} \tag{4.5}
$$

with q_{al} describing the magnitude of alignment and $K_{al}(x)$ describing the spatial range over which alignment takes place.

Let us now focus on the density dependent speeds $\Gamma^{\pm}[u_1, u_2]$. Here, we choose the nonlocal speeds of the two-population cancer cells to be described by non-negative, bounded and increasing functionals of cell-cell interactions, thus $\Gamma^{\pm}[u_1, u_2]$ are given by the following relations

$$
\Gamma^{\pm}[u_1, u_2] = \gamma\left(1 + \tanh\left(y_a^{\pm}[u_1, u_2] - y_r^{\pm}[u_1, u_2]\right)\right), \tag{4.6}
$$

where γ is a constant base-line speed describing the behaviour of the cancer cell populations in the absence of cell-cell interactions (see Fetecau and Eftimie (2010)).

For the nonlocal terms, we choose as in the previous chapters, translated Gaussian

kernels

$$K_j(x) = \frac{1}{\sqrt{2\pi m_j^2}} e^{-\frac{\left(x-s_j\right)^2}{2m_j^2}}, j = a, r, al, \tag{4.7}$$

with s_j representing half the length of the interaction ranges and $m_j = s_j/8$ representing the widths of the interaction kernels. (The constants $m_j, j = a, r, al$, are chosen such that the support of more than 98% of the mass of the kernels is inside the interval $[0, \infty)$ (Eftimie et al., 2007).)

We study the hyperbolic model (4.1) on a finite domain of length L, that is $x \in [0, L]$. To complete the model, we have to impose boundary conditions. Note that since the system (4.1) is hyperbolic, we have to follow the characteristics of the system when imposing these boundary conditions. For this reason, u_i^+, $i = 1, 2$, are prescribed only at $x = 0$, while u_i^-, $i = 1, 2$ are prescribed only at $x = L$. For this model we choose periodic boundary conditions, where the cancer cells move on a circular domain, leaving the domain at one end and entering it again at the other end. The boundary conditions are described by:

$$u_i^+(t, 0) = u_i^+(t, L) \text{ and } u_i^-(t, L) = u_i^-(t, 0), \, i = 1, 2. \tag{4.8}$$

4.3   Parabolic limit for nonlocal interactions

In this section, we take a formal parabolic limit to investigate the connection between the hyperbolic model (4.1) and other nonlocal parabolic models with density-dependent speed for collective cell dynamics in the literature (see for example Domschke et al. (2014); Painter et al. (2015) and many references therein). To study the parabolic limit of our hyperbolic model we assume that there is no alignment, i.e., $q_{al} = 0$. The main reason for choosing to ignore alignment is that we aim to obtain

parabolic equations for the total densities of the cancer cells, thus terms that incorporate left and right moving cancer cells (which would appear when $q_{al} \neq 0$) are currently being ignored. Note that the speed and the turning rates depend on attraction and repulsion, which are defined in terms of the total densities $u_i = u_i^+ + u_i^-$, $i = 1, 2$.

We denote by $g[\underline{u}] := \tanh\left(y^+[\underline{u}]\right)$. Since the function $\tanh(\cdot)$ is an odd function, we have from relation (4.6) (and the fact that $q_{al} = 0$):

$$\Gamma^{\pm}[\underline{u}] = \gamma\left(1 \pm g[\underline{u}]\right). \tag{4.9}$$

Adding and subtracting equations (4.1a)-(4.1b) for population u_1 and similarly equations (4.1c)-(4.1d) for population u_2, yields the following system:

$$\frac{\partial u_1}{\partial t} + \gamma \frac{\partial v_1}{\partial x} + \gamma \frac{\partial}{\partial x}\left(u_1 g[\underline{u}]\right) = -M u_1 + R_1(\underline{u}), \tag{4.10}$$

$$\frac{\partial v_1}{\partial t} + \gamma \frac{\partial u_1}{\partial x} + \gamma \frac{\partial}{\partial x}\left(v_1 g[\underline{u}]\right) = f_1[\underline{u}] u_1 - h_1[\underline{u}] v_1 - M v_1, \tag{4.11}$$

$$\frac{\partial u_2}{\partial t} + \gamma \frac{\partial v_2}{\partial x} + \gamma \frac{\partial}{\partial x}\left(u_2 g[\underline{u}]\right) = M u_1 + R_2(\underline{u}), \tag{4.12}$$

$$\frac{\partial v_2}{\partial t} + \gamma \frac{\partial u_2}{\partial x} + \gamma \frac{\partial}{\partial x}\left(v_2 g[\underline{u}]\right) = f_2[\underline{u}] u_2 - h_2[\underline{u}] v_2, \tag{4.13}$$

where

$$R_i(\underline{u}) = r_i u_i (1 - u_1 - u_2), \quad f_i[\underline{u}] = \lambda_{u_i}^-\left[u_1^+, u_1^-, u_2^+, u_2^-\right] - \lambda_{u_i}^+\left[u_1^+, u_1^-, u_2^+, u_2^-\right],$$

$$h_i[\underline{u}] = \lambda_{u_i}^-\left[u_1^+, u_1^-, u_2^+, u_2^-\right] + \lambda_{u_i}^+\left[u_1^+, u_1^-, u_2^+, u_2^-\right], i = 1, 2. \tag{4.14}$$

Next we differentiate equations (4.10) and (4.12) with respect to t, and equations (4.11)

and (4.13) with respect to x, to obtain

$$\frac{\partial^2 u_1}{\partial t^2} + \gamma \frac{\partial^2 v_1}{\partial x \partial t} + \gamma \frac{\partial^2}{\partial x \partial t} \left(u_1 g\left[\underline{u}\right] \right) = -M \frac{\partial u_1}{\partial t} + \frac{\partial}{\partial t} R_1\left(\underline{u}\right), \tag{4.15}$$

$$\frac{\partial^2 v_1}{\partial t \partial x} + \gamma \frac{\partial^2 u_1}{\partial x^2} + \gamma \frac{\partial^2}{\partial x^2} \left(v_1 g\left[\underline{u}\right] \right) = \frac{\partial}{\partial x} \left(u_1 f_1\left[\underline{u}\right] \right) - v_1 \frac{\partial}{\partial x} h_1\left[\underline{u}\right] - \left(h_1\left[\underline{u}\right] + M \right) \frac{\partial v_1}{\partial x}, \tag{4.16}$$

$$\frac{\partial^2 u_2}{\partial t^2} + \gamma \frac{\partial^2 v_2}{\partial x \partial t} + \gamma \frac{\partial^2}{\partial x \partial t} \left(u_2 g\left[\underline{u}\right] \right) = M \frac{\partial u_1}{\partial t} + \frac{\partial}{\partial t} R_2\left(\underline{u}\right), \tag{4.17}$$

$$\frac{\partial^2 v_2}{\partial t \partial x} + \gamma \frac{\partial^2 u_2}{\partial x^2} + \gamma \frac{\partial^2}{\partial x^2} \left(v_2 g\left[\underline{u}\right] \right) = \frac{\partial}{\partial x} \left(u_2 f_2\left[\underline{u}\right] \right) - v_2 \frac{\partial}{\partial x} h_2\left[\underline{u}\right] - h_2\left[\underline{u}\right] \frac{\partial v_2}{\partial x}. \tag{4.18}$$

We eliminate the terms $\frac{\partial^2 v_1}{\partial t \partial x}$ and $\frac{\partial^2 v_2}{\partial t \partial x}$ from equations (4.15)-(4.16) and (4.17)-(4.18), respectively. We assume that the flows $v_i, i = 1, 2$, are zero at the boundaries. Using equations (4.10) and (4.12) we replace $v_i, i = 1, 2$, with

$$v_i = \int^x \left(-\frac{1}{\gamma} \frac{\partial u_i}{\partial t} - \frac{\partial}{\partial x} \left(u_i g\left[\underline{u}\right] \right) + (-1)^i \frac{M}{\gamma} u_1 + \frac{1}{\gamma} R_i\left(\underline{u}\right) \right) ds, \tag{4.19}$$

and $\dfrac{\partial v_i}{\partial x}, i = 1, 2$, with

$$\frac{\partial v_i}{\partial x} = -\frac{1}{\gamma} \frac{\partial u_i}{\partial t} - \frac{\partial}{\partial x} \left(u_i g\left[\underline{u}\right] \right) + (-1)^i \frac{M}{\gamma} u_1 + \frac{1}{\gamma} R_i\left(\underline{u}\right). \tag{4.20}$$

Therefore, we obtain the following second-order equations

$$\frac{\partial^2 u_1}{\partial t^2} - \gamma^2 \frac{\partial^2 u_1}{\partial x^2} + \gamma \frac{\partial}{\partial x} \left(u_1 f_1\left[\underline{u}\right] \right) + \gamma \frac{\partial^2}{\partial x \partial t} \left(u_1 g\left[\underline{u}\right] \right) + M \frac{\partial u_1}{\partial t} - \frac{\partial}{\partial t} \left(R_1\left(\underline{u}\right) \right)$$

$$+ \left(-\gamma \frac{\partial^2}{\partial x^2} g\left[\underline{u}\right] - \frac{\partial}{\partial x} h_1\left[\underline{u}\right] \right) \left(\int^x \left(-\frac{\partial u_1}{\partial t} - \gamma \frac{\partial}{\partial x} \left(u_1 g\left[\underline{u}\right] \right) - M u_1 + R_1\left(\underline{u}\right) \right) ds \right)$$

$$+ \left(-2\gamma \frac{\partial}{\partial x} g\left[\underline{u}\right] - h_1\left[\underline{u}\right] - M \right) \left(-\frac{\partial u_1}{\partial t} - \gamma \frac{\partial}{\partial x} \left(u_1 g\left[\underline{u}\right] \right) - M u_1 + R_1\left(\underline{u}\right) \right)$$

$$- \gamma g\left[\underline{u}\right] \frac{\partial}{\partial x} \left(-\frac{\partial u_1}{\partial t} - \gamma \frac{\partial}{\partial x} \left(u_1 g\left[\underline{u}\right] \right) - M u_1 + R_1\left(\underline{u}\right) \right) = 0, \tag{4.21}$$

$$\frac{\partial^2 u_2}{\partial t^2} - \gamma^2 \frac{\partial^2 u_2}{\partial x^2} + \gamma \frac{\partial}{\partial x}\left(u_2 f_2\left[\underline{u}\right]\right) + \gamma \frac{\partial^2}{\partial x \partial t}\left(u_2 g\left[\underline{u}\right]\right) - M \frac{\partial u_1}{\partial t} - \frac{\partial}{\partial t}\left(R_2\left(\underline{u}\right)\right)$$

$$+ \left(-\gamma \frac{\partial^2}{\partial x^2} g\left[\underline{u}\right] - \frac{\partial}{\partial x} h_2\left[\underline{u}\right]\right)\left(\int^x \left(-\frac{\partial u_2}{\partial t} - \gamma \frac{\partial}{\partial x}\left(u_2 g\left[\underline{u}\right]\right) + M u_1 + R_2\left(\underline{u}\right)\right) ds\right)$$

$$+ \left(-2\gamma \frac{\partial}{\partial x} g\left[\underline{u}\right] - h_2\left[\underline{u}\right]\right)\left(-\frac{\partial u_2}{\partial t} - \gamma \frac{\partial}{\partial x}\left(u_2 g\left[\underline{u}\right]\right) + M u_1 + R_2\left(\underline{u}\right)\right)$$

$$- \gamma g\left[\underline{u}\right] \frac{\partial}{\partial x}\left(-\frac{\partial u_2}{\partial t} - \gamma \frac{\partial}{\partial x}\left(u_2 g\left[\underline{u}\right]\right) + M u_1 + R_2\left(\underline{u}\right)\right) = 0. \tag{4.22}$$

To transform these equations into parabolic equations, we assume that cancer cells move very fast and change direction even faster. This behaviour leads to a reduced sensitivity to the environment. With these assumptions, we introduce a small parameter $\varepsilon > 0$ and we make the following rescaling

(i) $\lambda_i^r = \dfrac{\tilde{\lambda}_i^r}{\varepsilon^2}, \quad \lambda_i^b = \dfrac{\tilde{\lambda}_i^b}{\varepsilon^2}, \; i = 1, 2,$

(ii) $\gamma = \dfrac{\tilde{\gamma}}{\varepsilon},$

(iii) $g\left[\underline{u}\right] = \varepsilon \tilde{g}\left[\underline{u}\right],$

(iv) $p\left(y^{\pm}\left[\underline{u}\right]\right) = \varepsilon \tilde{p}\left(y^{\pm}\left[\underline{u}\right]\right).$

This reduction of the sensitivity in the environment leads to the following rescaling

$\bullet \; f_i\left[\underline{u}\right] = \dfrac{\tilde{\lambda}_i^b \tilde{f}\left[\underline{u}\right]}{\varepsilon}, \;$ with $\tilde{f}\left[\underline{u}\right] = \tilde{p}\left(y^-\left[\underline{u}\right]\right) - \tilde{p}\left(y^+\left[\underline{u}\right]\right), \; i = 1, 2,$ (4.23)

$\bullet \; h_i\left[\underline{u}\right] = \dfrac{2\tilde{\lambda}_i^r + 2\tilde{\lambda}_i^b \varepsilon \tilde{h}\left[\underline{u}\right]}{\varepsilon^2}, \;$ with $\tilde{h}\left[\underline{u}\right] = \tilde{p}\left(y^-\left[\underline{u}\right]\right) + \tilde{p}\left(y^+\left[\underline{u}\right]\right), \; i = 1, 2.$ (4.24)

Substituting these terms into system (4.21)-(4.22) and multiplying with ε^2, taking the limit as $\varepsilon \to 0$ and dropping the tildes (for simplicity), leads to the following parabolic

112

equations

$$\frac{\partial u_1}{\partial t} = D_{u_1} \frac{\partial^2 u_1}{\partial x^2} - \frac{\gamma \lambda_1^b}{2\lambda_1^r} \frac{\partial}{\partial x} \left(u_1 f[\underline{u}] \right) - \gamma \frac{\partial}{\partial x} \left(u_1 g[\underline{u}] \right) - Mu_1 + R_1(\underline{u}), \qquad \text{(4.25a)}$$

$$\frac{\partial u_2}{\partial t} = D_{u_2} \frac{\partial^2 u_2}{\partial x^2} - \frac{\gamma \lambda_2^b}{2\lambda_2^r} \frac{\partial}{\partial x} \left(u_2 f[\underline{u}] \right) - \gamma \frac{\partial}{\partial x} \left(u_2 g[\underline{u}] \right) + Mu_1 + R_2(\underline{u}), \qquad \text{(4.25b)}$$

where $D_{u_i} = \frac{(\gamma)^2}{2\lambda_i^r}$, $i = 1, 2$, is the diffusion coefficients. Here the initial conditions are given by the functions $u_i(0, x) = u_{i_0}(x) \geq 0$, $i = 1, 2$.

To fully define the parabolic model (4.25), we need to impose boundary conditions. To be consistent with the hyperbolic model (4.1), we impose again periodic boundary conditions on a finite domain of length L:

$$u_1(t, 0) = u_1(t, L) \text{ and } u_2(t, 0) = u_2(t, L). \qquad \text{(4.26)}$$

We note here that the nonlocal terms $f[\underline{u}]$ and $g[\underline{u}]$ now depend only on the repulsive and attractive interactions. The reason for this is that the alignment interactions are defined in terms of $u_i^{\pm}$, $i = 1, 2$.

4.4 Linear stability analysis

In this section, we investigate the possibility of pattern formation for models (4.1) and (4.25) via linear stability analysis. As it was shown also in Chapter 2, what seems to play an important role in the pattern formation is the social interactions (i.e., attraction, repulsion, alignment) between cancer cells (Mogilner and Edelstein-Keshet, 1996; Topaz et al., 2006).

4.4.1 Linear stability analysis of the hyperbolic model

We start with the linear stability analysis of the hyperbolic model (4.1). First, we look for the spatially homogeneous steady states $u_i^{\pm,*}, i = 1, 2$, assuming that cancer cells are spread evenly over the domain. We denote the constant total density of the populations by $u_i^*, i = 1, 2$. From the right-hand-side of equations (4.1a)-(4.1d) we have the following system:

$$-Mu_1^* + r_1 u_1^* \left(1 - u_1^* - u_2^*\right) = 0, \qquad (4.27a)$$

$$Mu_1^* + r_2 u_2^* \left(1 - u_1^* - u_2^*\right) = 0, \qquad (4.27b)$$

which has the solutions $\left(u_1^*, u_2^*\right) = (0,0)$ and $\left(u_1^*, u_2^*\right) = (0,1)$. Note that we consider only non-negative solutions for biological realism. If we consider the states where both cell populations are evenly spread in both directions over the domain, then these states $\left(u_1^{+,*}, u_1^{-,*}, u_2^{+,*}, u_2^{-,*}\right)$ are given by

$$(0,0,0,0) \quad \text{and} \quad (0,0,0.5,0.5). \qquad (4.28)$$

If we consider populations that are evenly spread over the domain and also have a preference in directionality, then the steady states are the following

$$(0,0,0,0) \quad \text{and} \quad \left(0,0,u_2^{+,*}, 1 - u_2^{+,*}\right), \qquad (4.29)$$

for $0 \le u_2^{+,*} \le 1$.

Now that we know the steady states, we proceed with the study of the local stability of these solutions under small perturbations caused by spatially non-homogeneous terms. We let $u_1^{\pm} = u_1^{\pm,*} + A_{u_1}^{\pm} e^{ikx+\lambda t}$ and $u_2^{\pm} = u_2^{\pm,*} + A_{u_2}^{\pm} e^{ikx+\lambda t}$ with $|A_{u_1}^{\pm}|, |A_{u_2}^{\pm}| \ll 1$, where k and λ are the wave number and frequency, respectively. Let $\hat{K}_j^{\pm}, j = a, r, al$, be the

Fourier transform of the interaction kernel K_j, given by the following relation

$$\hat{K}_j^{\pm}(k) = \int_{-\infty}^{\infty} K_j(s)\, e^{\pm iks_j} ds, \quad j = a, r, al. \tag{4.30}$$

We denote by $\hat{K}^s(k) = \hat{K}^+(k) - \hat{K}^-(k) = q_a \hat{K}^s{}_a(k) - q_r \hat{K}^s{}_r(k)$ the Fourier sine transform of kernel K, and respectively by $\hat{K}^c{}_{al}(k) = \hat{K}^+_{al}(k) + \hat{K}^-_{al}(k)$ the Fourier cosine transform of kernel K_{al}. Throughout this chapter we will consider translated Gaussian kernels given by relation (4.7). Then the Fourier transform of these kernels is given by

$$\hat{K}_j^{\pm}(k) = \exp\left(\pm iks_j - k^2 m_j^2/2\right), \quad j = a, r, al, \tag{4.31}$$

and the Fourier sine and cosine transforms are given by

$$\hat{K}_j^s(k) = \exp\left(-k^2 m_j^2/2\right)\sin(ks_j), \quad \text{and} \quad \hat{K}_j^c(k) = \exp\left(-k^2 m_j^2/2\right)\cos(ks_j). \tag{4.32}$$

To simplify the results of this section, we set the following parameter values:

$$
\begin{aligned}
L_i^{\pm} &= \lambda_i^r + 0.5\lambda_i^b + 0.5\lambda_i^b \tanh\left(\pm Q^* - 2\right), \ i = 1, 2, \\
Q^* &= \frac{2q_{al}}{R_s}\left(u_1^{-,*} + u_2^{-,*} - u_1^{+,*} - u_2^{+,*}\right), \\
f(u) &= 0.5\tanh(u), \\
f'(u) &= 0.5 - 2f^2(u), \\
B_i &= u_i^{+,*} f'\left(Q^* - 2\right) + u_i^{-,*} f'\left(-Q^* - 2\right), \\
Y(k) &= -\frac{2k\gamma}{R_s}\hat{K}^s(k), \\
W_i^{\pm}(k) &= \frac{B_i \lambda_i^b}{R_s}\left[i\hat{K}^s(k) \mp q_{al}\hat{K}^c{}_{al}(k)\right], \ i = 1, 2.
\end{aligned}
\tag{4.33}
$$

Substituting now the expressions $u_j^{\pm} = u_j^{\pm,*} + A_{u_j}^{\pm} e^{ikx + \lambda t}$, $j = 1, 2$, into the system (4.1), we obtain the following dispersion relations:
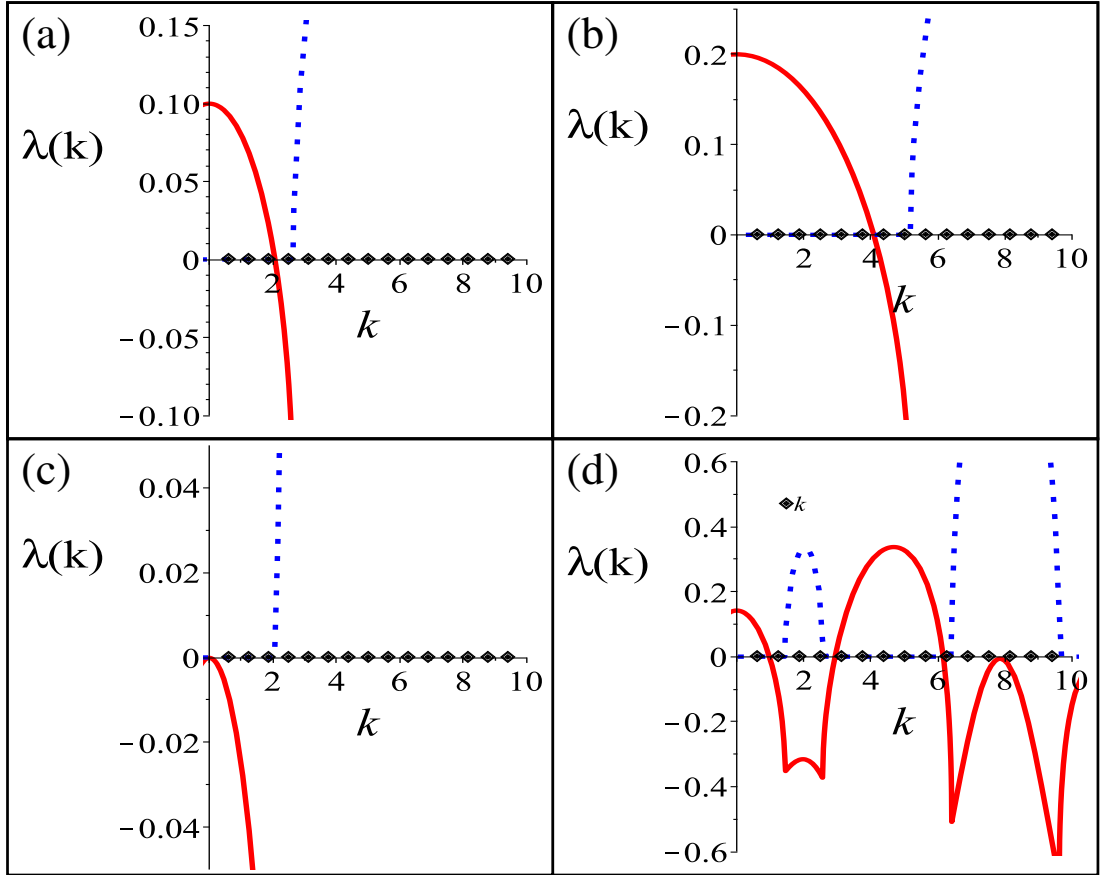
Figure 4.1: Plot of the larger eigenvalues $\lambda_l = -D_l + \sqrt{D_l^2 - 4E_l}$, $l = 1,\ldots 4$, obtained by dispersion relations (4.34) and (4.39) for (a) D_1, E_1, for the steady state $(0,0,0,0)$; (b) D_2, E_2, for the steady state $(0,0,0,0)$; (c) D_3, E_3, for the steady state $(0,0,0.5,0.5)$; (d) D_4, E_4, for the steady state $(0,0,0.5,0.5)$. The continuous curves represent the $Re(\lambda(k))$, while the dashed curves represent the $Im(\lambda(k))$. The model parameters are given in Table 4.2. The diamonds on the x-axis represent the discrete wave numbers $k_j = 2\pi j/L, j = 1,2,\ldots$.

- For the steady state $(0,0,0,0)$ we have:

$$\left(\lambda^2 + \lambda D_1(k) + E_1(k)\right) \cdot \left(\lambda^2 + \lambda D_2(k) + E_2(k)\right) = 0 \qquad (4.34)$$

116

with

$$D_1(k) = L_1^+ + L_1^- + 2M - r_1, \tag{4.35}$$

$$E_1(k) = k^2\gamma^2 - \left(L_1^+ - L_1^-\right)ik\gamma + \left(L_1^+ + L_1^- + M - r_1\right)M - \left(L_1^+ + L_1^-\right)r_1, \tag{4.36}$$

and

$$D_2(k) = L_2^+ + L_2^- - r_2, \tag{4.37}$$

$$E_2(k) = k^2\gamma^2 - \left(L_2^+ - L_2^-\right)ik\gamma - \left(L_2^+ + L_2^-\right)r_2. \tag{4.38}$$

- For the steady state $\left(0, 0, u_2^{+,*}, 1 - u_2^{+,*}\right)$ we have:

$$\left(\lambda^2 + \lambda D_3(k) + E_3(k)\right) \cdot \left(\lambda^2 + \lambda D_4(k) + E_4(k)\right) = 0 \tag{4.39}$$

with

$$D_3(k) = L_1^+ + L_1^- + 2M, \tag{4.40}$$

$$E_3(k) = k^2\gamma^2 - \left(L_1^+ - L_1^-\right)ik\gamma + \left(L_1^+ + L_1^- + M\right)M, \tag{4.41}$$

and

$$D_4(k) = L_2^+ + L_2^- + r_2 + W_2^+(k) - W_2^-(k) + Y(k), \tag{4.42}$$

$$E_4(k) = k^2\gamma^2 - \left(L_2^+ - L_2^- + W_2^+(k) + W_2^-(k) + \left(2u_2^{+,*} - 1\right)Y(k)\right)ik\gamma$$

$$+ \left(L_2^+ + L_2^- + W_2^+(k) - W_2^-(k)\right)\left(Y(k) + r_2\right). \tag{4.43}$$

Equations (4.34) and (4.39) show that the steady states are unstable, i.e., $Re\left(\lambda(k)\right) > 0$, when $D_l(k) < 0$ or $E_l(k) < 0$, $l = 1, \ldots, 4$. Examples of such dispersion relations are shown in Fig. 4.1. There is a range of k-values for which $Re\left(\lambda(k)\right)$ is positive, and thus aggregation can arise from spatial perturbations of the steady states $(0, 0, 0, 0)$ (see

117

Fig. 4.1(a), (b)) and $(0,0,0.5,0.5)$ (see Fig. 4.1(c), (d)). Note that similar results (not shown here) are obtained for any steady state $\left(0,0,u_2^{+,*},1-u_2^{+,*}\right)$, with $0 \leq u_2^{+,*} \leq 1$.

4.4.2 Linear stability analysis of the parabolic model

Next, we investigate the conditions under which aggregations can arise for the limiting parabolic model (4.25). We first calculate the spatially homogeneous steady states of the parabolic model. We see from equations (4.25a)-(4.25b) that the ODE model associated to system (4.25) is described by system (4.27), which has the solutions $\left(u_1^*, u_2^*\right) = (0,0)$ and $(0,1)$ (considering again only non-negative solutions).

Proceeding with the linear stability analysis of the spatial system (4.25), we apply small spatial perturbations to the homogeneous steady states: $u_1 = u_1^* + A_{u_1} e^{ikx+\lambda t}$ and $u_2 = u_2^* + A_{u_2} e^{ikx+\lambda t}$ with $|A_{u_1}|, |A_{u_2}| \ll 1$. Substituting these terms into system (4.25), using the parameter values (4.33) and replacing $u_1^* = 0$, yields the following dispersion relation:

$$\left[-k^2 D_{u_1} - M + r_1\left(1-u_2^*\right) - \lambda\right] \cdot \left[-k^2 D_{u_2} + Y(k)\left(\frac{\lambda_2^b f'(-2)}{2\lambda_2^r} - 1\right) u_2^*\right.$$
$$\left. + r_2\left(1-2u_2^*\right) - \lambda\right] = 0. \quad (4.44)$$

Therefore, for the steady state $(0,0)$ we have the solutions:

$$\lambda_1 = -k^2 D_{u_1} - M + r_1 \text{ and } \lambda_2 = -k^2 D_{u_2} + r_2, \quad (4.45)$$

and for the steady state $(0,1)$ the solutions:

$$\lambda_1 = -k^2 D_{u_1} - M < 0 \text{ and } \lambda_2 = -k^2 D_{u_2} + Y(k)\left(\frac{\lambda_2^b f'(-2)}{2\lambda_2^r} - 1\right) - r_2. \quad (4.46)$$
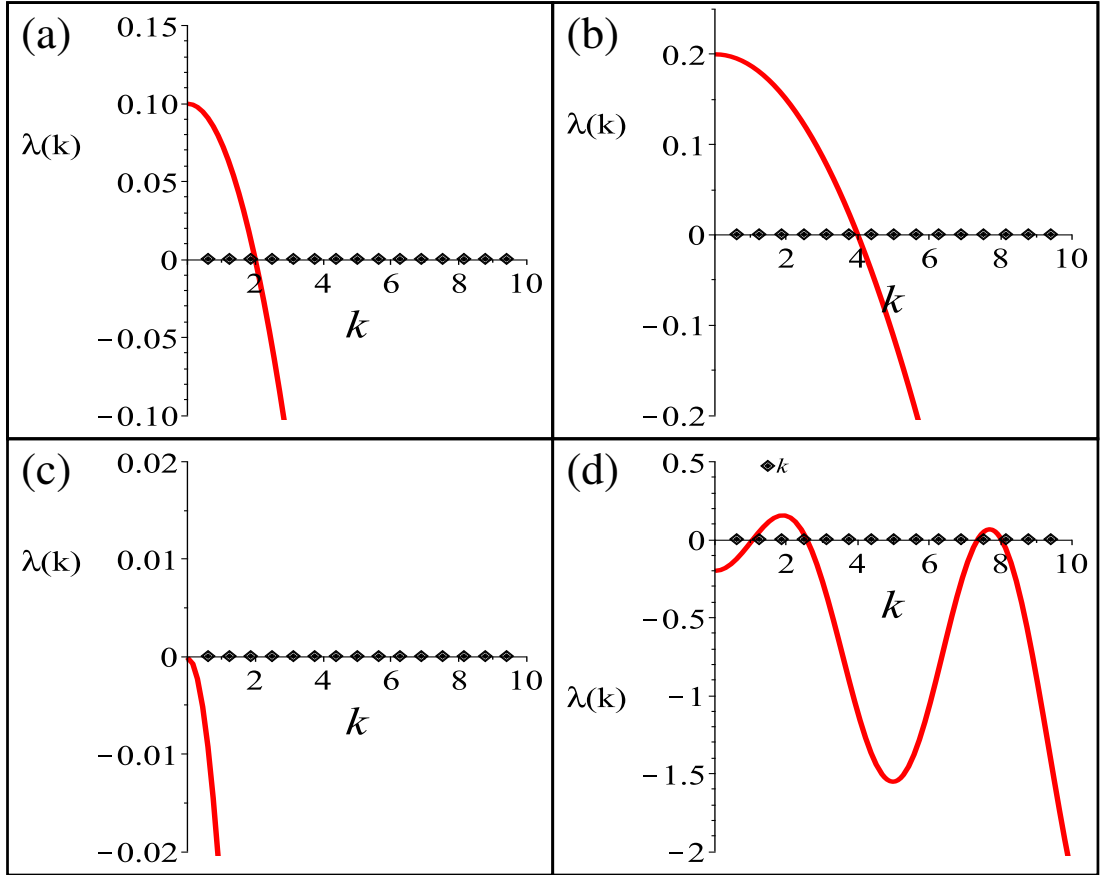
Figure 4.2: Plot of the eigenvalues obtained by dispersion relation (4.44). (a) $\lambda = -k^2 D_{u_1} - M + r_1$, for the steady state $(0,0)$; (b) $\lambda = -k^2 D_{u_2} + r_2$, for the steady state $(0,0)$; (c) $\lambda = -k^2 D_{u_1} - M$, for the steady state $(0,1)$; (d) $\lambda = -k^2 D_{u_2} + Y(k)\left(\lambda_2^b f'(-2)/(2\lambda_2^r) - 1\right) - r_2$, for the steady state $(0,1)$. The model parameters are given in Table 4.2. The continuous curves represent the $Re\left(\lambda(k)\right)$, as the imaginary part of the eigenvalues is zero in the case of the parabolic model (see relations (4.44)-(4.46)). The diamonds on the x-axis represent the discrete wave numbers $k_j = 2\pi j/L, j = 1, 2, \ldots$.

As in the case of the hyperbolic model, we see in Fig. 4.2 that there is a range of k-values for which $Re\left(\lambda(k)\right) > 0$, and thus aggregation can arise from spatial perturbations of the steady states $(0,0)$ and $(0,1)$ of the parabolic model.

4.5 Numerical results

To understand the behaviour of systems (4.1) and (4.25), we investigate them numerically. The aim of this section is to study the effect of the cell-cell interactions, base-line speed and turning rates on the pattern formation for both models.

As in the previous two chapters, we use a time-splitting approach to discretise our model. We use a Crank-Nicolson scheme to propagate the solution of the diffusion term for the parabolic equations (4.25), obtained with the formal parabolic limit of equations (4.1). For the time-propagation of the advection terms in both models (4.1) and (4.25) we use the Nessyahu-Tadmor scheme (Nessyahu and Tadmor, 1990). Finally, for the time-propagation of the reaction terms in (4.1) and (4.25) we use a fourth order Runge-Kutta algorithm, where the integrals are further discretised using the Simpson's rule. All simulations are performed on a domain of length $L = 10$ with periodic boundary conditions (introduced to approximate the dynamics on an infinite domain).

4.5.1 Pattern formation for the nonlocal hyperbolic model

Let us focus first on the numerical simulations for the nonlocal hyperbolic model (4.1). The initial conditions for the cancer cell populations are either small random perturbations of spatially homogeneous steady states

$$u_i^{\pm}(0,x) \quad = \quad u_i^{\pm,*} + rand(0, 10^{-4}), \ i = 1, 2, \tag{4.47}$$
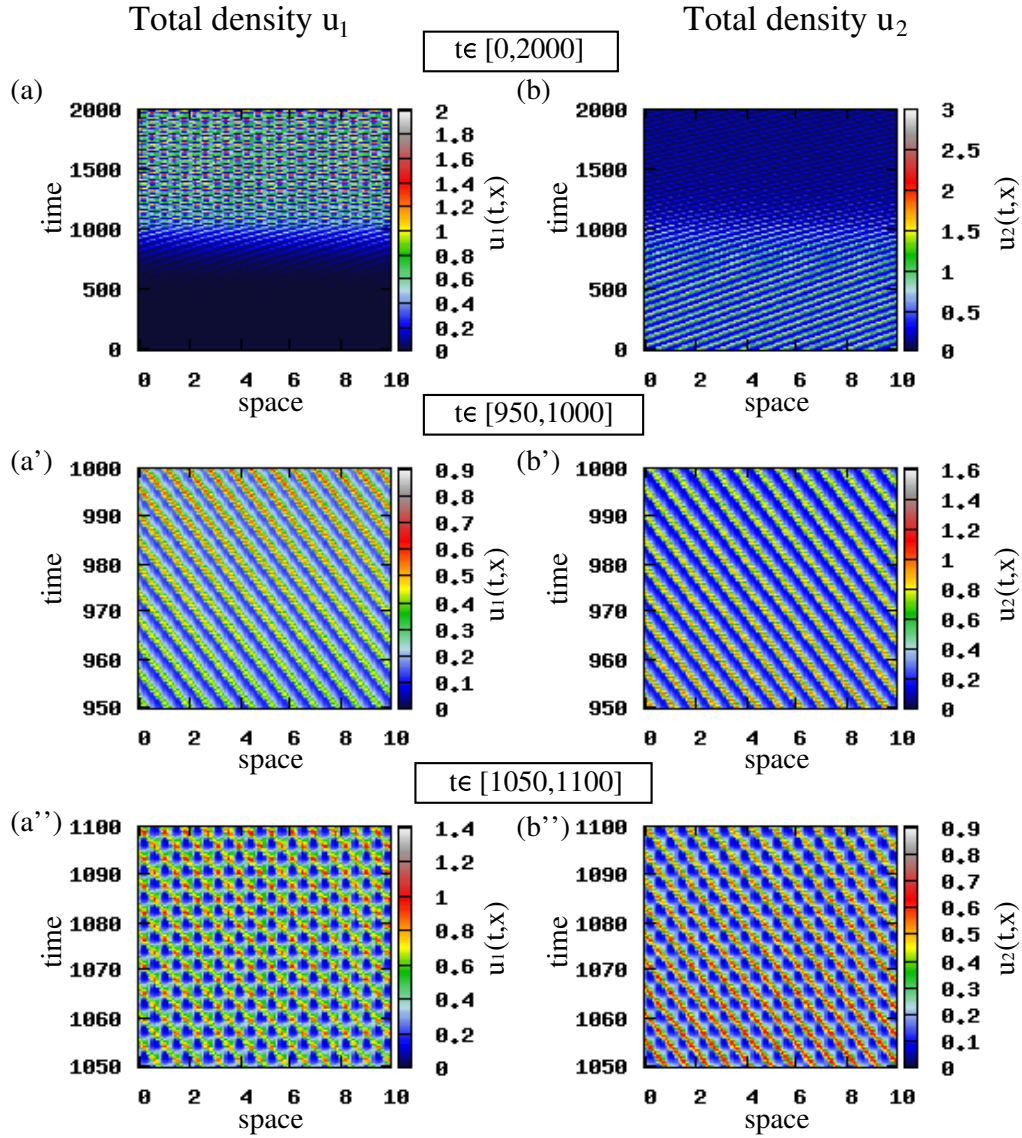
Figure 4.3: Short-term and long-term patterns exhibited by hyperbolic model (4.1). The initial conditions for the two cancer cell populations are described by small random perturbations of the steady state $(0, 0, 0.5, 0.5)$ (see (4.47)). (a)-(a") Total density of $u_1 = u_1^+ + u_1^-$; (b)-(b") Total density of $u_2 = u_2^+ + u_2^-$, for $q_a = 1.2, q_r = 0.1$ and $q_{al} = 0.5$. The rest of model parameters are given in Table 4.2.

or small random perturbations of rectangular-shaped aggregations located in the middle of the domain

$$u_i^{\pm}(0, x) = \begin{cases} 0.1 + rand(0, 10^{-4}), & x \in (L/2 - 1, L/2 + 1) \\ 0, & \text{everywhere else} \end{cases} \qquad (4.48)$$
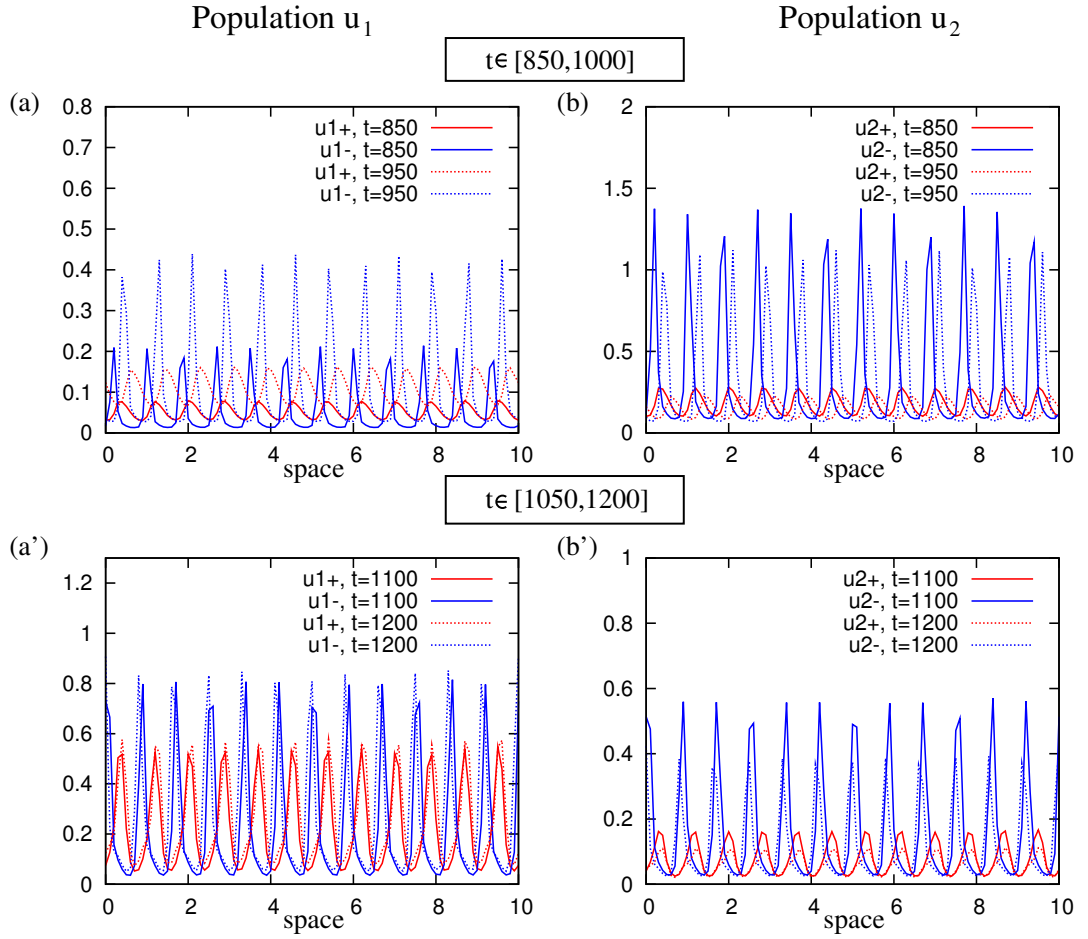
Figure 4.4: Spatial distribution of left and right moving cancer cells satisfying system (4.1), for $q_a = 1.2, q_r = 0.1$ and $q_{al} = 0.5$. The rest of model parameters are given in Table 4.2. The initial conditions for the two cancer cell populations are described by small random perturbations of the steady state $(0, 0, 0.5, 0.5)$ (see (4.47)). (a) , (b) Spatial distribution of cancer cells $u_1^\pm$ and $u_2^\pm$ for $t \in [850, 1000]$; (a'), (b') Spatial distribution of cancer cells $u_1^\pm$ and $u_2^\pm$ for $t \in [1050, 1200]$.

To begin we first run numerical simulations for small random perturbations of the steady states $(0, 0, 0.5, 0.5)$ and $(0, 0, 0, 0)$. Fig. 4.3 shows the patterns displayed by system (4.1) for the initial conditions given by (4.47) for $\left(u_1^{+,*}, u_1^{-,*}, u_2^{+,*}, u_2^{-,*}\right) = (0, 0, 0.5, 0.5)$, and for $q_a = 1.2, q_r = 0.1$ and $q_{al} = 0.5$. We see that for $t < 1050$ we obtain rotating waves, while for $t \geq 1050$ cancer cell populations change their movement to standing waves. This behaviour can be explained by the instability of the rotating waves, which undergo a bifurcation to standing waves.

122

In Fig. 4.4 we graph the spatial distribution of populations $u_i^\pm, i = 1, 2$, for $t \in [850, 1000]$ and for $t \in [1050, 1200]$. We notice that for $t \in [850, 1000]$, where cancer cell populations u_1 and u_2 exhibit rotating waves, both u_i^+ and u_i^- move in the same direction. For $t \in [1050, 1200]$, u_i^+ and u_i^- move in opposite directions thus describing standing waves.

Attraction-repulsion interactions Let us now choose the initial conditions to be given by relation (4.47) for $(u_1^{+,*}, u_1^{-,*}, u_2^{+,*}, u_2^{-,*}) = (0, 0, 0, 0)$. To see the effect of attraction and repulsion on the pattern formation, we focus on two different cases: (i) $q_a > q_r$ and (ii) $q_a < q_r$, while $q_{al} = 0$ in both cases. We see in Fig. 4.5 that when $q_a > q_r$ (Fig. 4.5(a)-(b)) then cancer cell populations move in rotating wave manner, while for $q_a < q_r$ (Fig. 4.5(a')-(b')) they exhibit standing waves. Note that similar patterns (not shown here) are obtained if we choose the initial conditions for the two cancer cell populations consisting of a rectangular pulse (see relation (4.48)).

Clonal competition We have seen in Chapters 2 and 3, that for parabolic-hyperbolic coupled systems it is usual to have persistence of u_2 population, but not of u_1. Here, we investigate again this phenomenon of clonal competition for the case of a hyperbolic system.

In Figs. 4.3 and 4.5 we notice that early stage cancer cells, u_1, dominate the dynamics, while late stage cancer cells, u_2, start to reduce for $t \geq 1000$. We should mention here that this behaviour has been displayed also for the case that $q_{al} > 0$ (patterns not shown here). If we choose now smaller base-line random turning rate $\lambda_i^r = 0.1, i = 1, 2$, then we see in Fig. 4.6 the inverse behaviour. The cancer cell populations exhibit semi-zigzag pattern, with u_1 population being reduced to low cell density for $t > 600$, while u_2 population persists. This can be possibly explained by the effect that the reduction of turning frequency has on the sensitivity of cancer cells and eventually
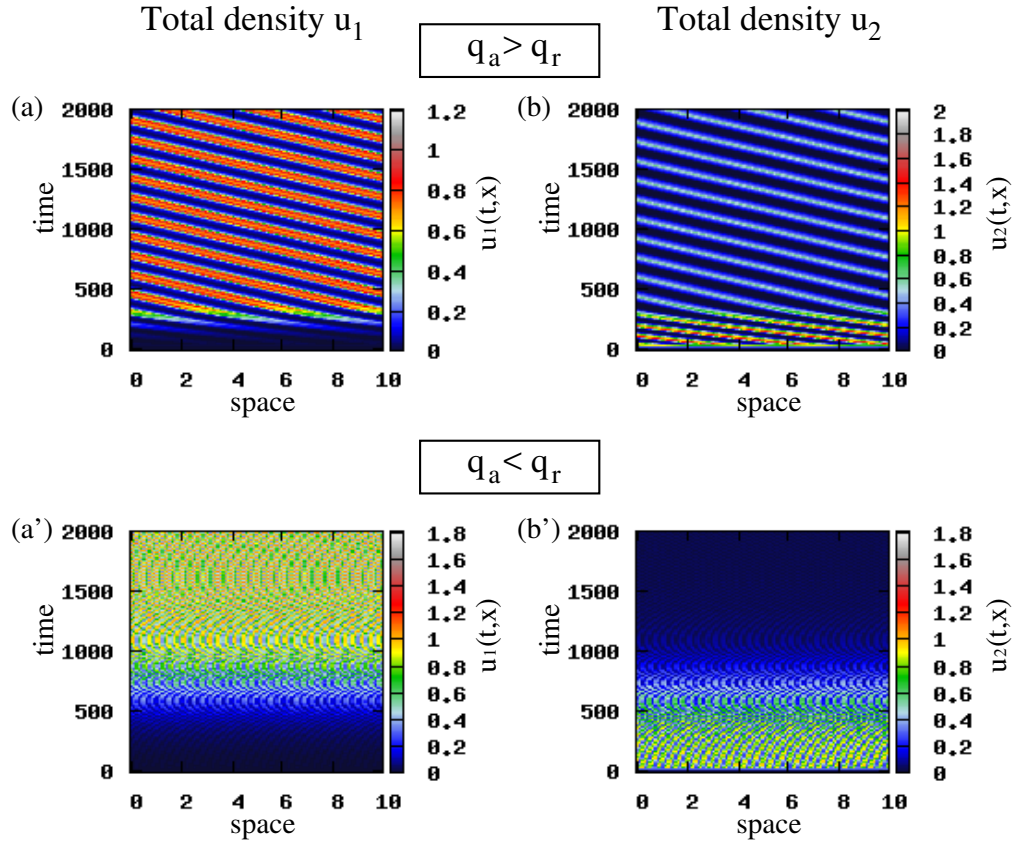
Figure 4.5: Patterns exhibited by the hyperbolic model (4.1). The initial conditions for the two cancer cell populations are described by small random perturbations of the steady state $(0,0,0,0)$ (see (4.47)) . (a), (b) Total density of $u_1 = u_1^+ + u_1^-$ and $u_2 = u_2^+ + u_2^-$ for $q_a = 1.2, q_r = 0.1$ and $q_{al} = 0$; (a'), (b') Total density of $u_1 = u_1^+ + u_1^-$ and $u_2 = u_2^+ + u_2^-$ for $q_a = 1.2, q_r = 2.5$ and $q_{al} = 0$. The rest of model parameters are given in Table 4.2.

on their migration, and therefore in the dynamics of late stage cancer cells that are considered as more metastatic cancer cells.

We see in Fig. 4.6 that for $\left(u_i^+, u_i^-\right)$ there is a periodic transition between two different types of patterns: a stationary aggregation and a travelling aggregation, which seems to be similar to a heteroclinic connection. Note that the standing waves (see Fig. 4.3(a'')-(b'') and 4.5(a')-(b')) are generated by mode interactions that become unstable at the same time. Due to the complexity of the theory behind these heteroclinic connections
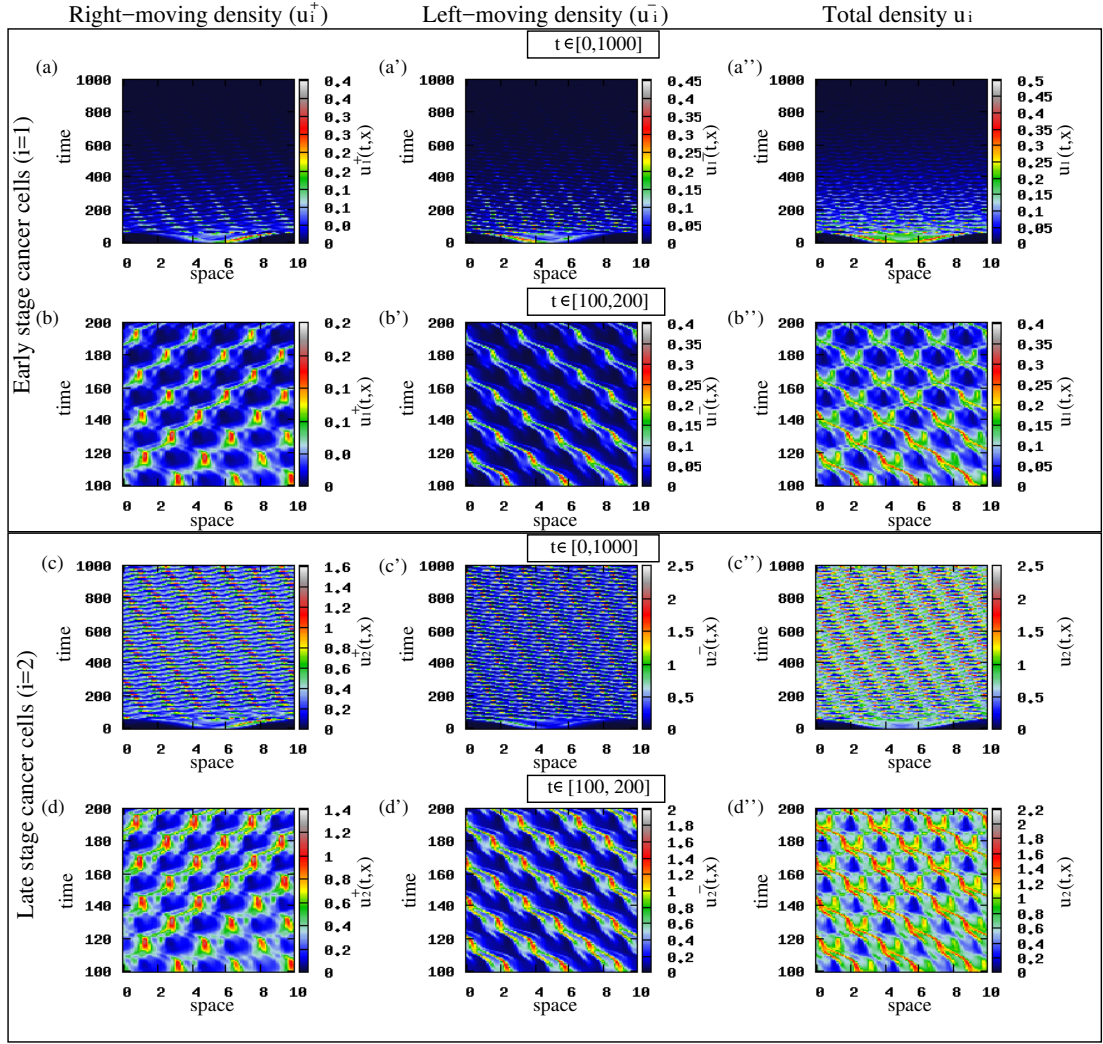
Figure 4.6: Patterns exhibited by the hyperbolic model (4.1) for $q_a = 1.2, q_r = 0.1, q_{al} = 0.5$ and $\lambda_i^r = 0.1, i = 1, 2$. The rest of model parameters are given in Table 4.2. The initial conditions for the two cancer cell populations consist of a rectangular pulse (see (4.48)). Panels (a)-(d) show the density of right-moving cancer cells u_1^+ (panels (a)-(b)) and u_2^+ (panels (c)-(d)). Panels (a')-(d') show the density of left-moving cancer cells u_1^- (panels (a')-(b')) and u_2^- (panels (c')-(d')). Panels (a'')-(d'') show the total density of cancer cells u_1 (panels (a'')-(b'')) and u_2 (panels (c'')-(d'')).

in infinite dimensional dynamical systems, it is beyond the purpose of this study to investigate them further. This will be the subject of future research.

Similar competitive excluding behaviour is exhibited when we consider very small speed, i.e., $\gamma = 0.01$, as it can be seen in Fig. 4.7. This behaviour is expected due to

125

the mutation rate and the small speed, which leads to the formation of stationary aggregations with highly mutated population u_2 spreading throughout the whole domain.

The effect of alignment on cancer cell movement and aggregation An interesting fact that we discuss in this paragraph is the effect of alignment on the cell movement and aggregation. We see in Figs. 4.7(a),(b) and 4.7(c),(d) that when alignment is absent ($q_{al} = 0$) cells form stationary aggregations, while when it is present ($q_{al} > 0$) we see in Figs. 4.7(a'),(b') and 4.7(c'),(d') that some groups of cells have a directed movement forming rotating waves. We notice that for $q_{al} > 0$, the rotating waves for the case $q_a > q_r$ (see Figs. 4.7(a'),(b')) are larger that those displayed for $q_a < q_r$ (see Figs. 4.7(c'),(d')), due to the strong attractive forces making the cells stay aggregated.

To see more clearly that the patterns in Fig. 4.7(c)-(d') show spatial oscillations, we show in Fig. 4.8 a time snapshot of the spatial distribution of the densities of u_1 and u_2 cancer cells, for $t = 300$.

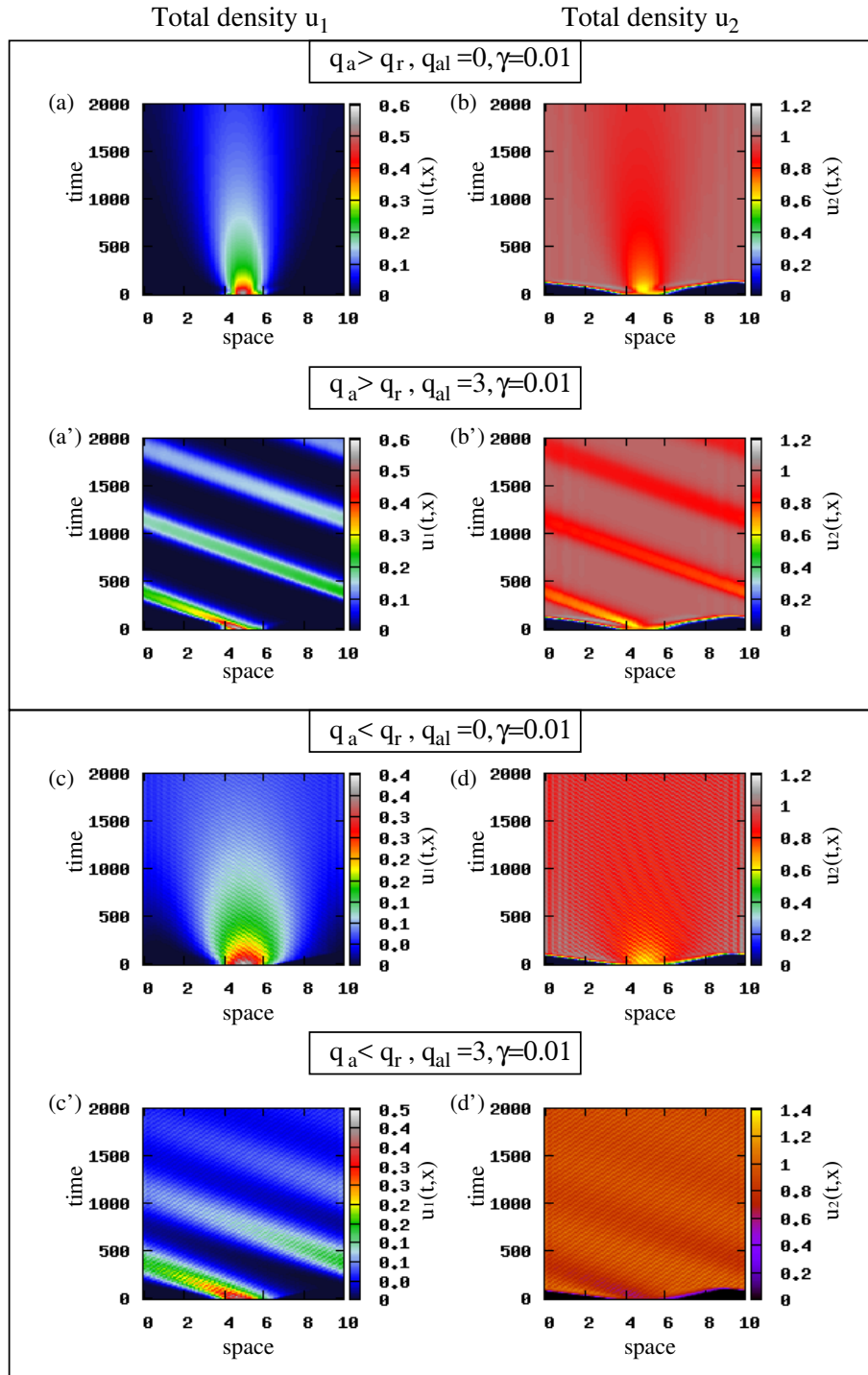Total density u_1 Total density u_2

Figure 4.7: Patterns exhibited by the hyperbolic model (4.1) showing the cancer cell density for $\gamma = 0.01$. The initial conditions for the two cancer cell populations consist of a rectangular pulse (see (4.48)). (a), (b) Total density of u_1 and u_2 for $q_a = 1.2, q_r = 0.1$ and $q_{al} = 0$; (a'), (b') Total density of u_1 and u_2 for $q_a = 1.2, q_r = 0.1$ and $q_{al} = 3$; (c), (d) Total density of u_1 and u_2 for $q_a = 1.2, q_r = 2.5$ and $q_{al} = 0$; (c'), (d') Total density of u_1 and u_2 for $q_a = 1.2, q_r = 2.5$ and $q_{al} = 3$. The rest of model parameters are given in Table 4.2.
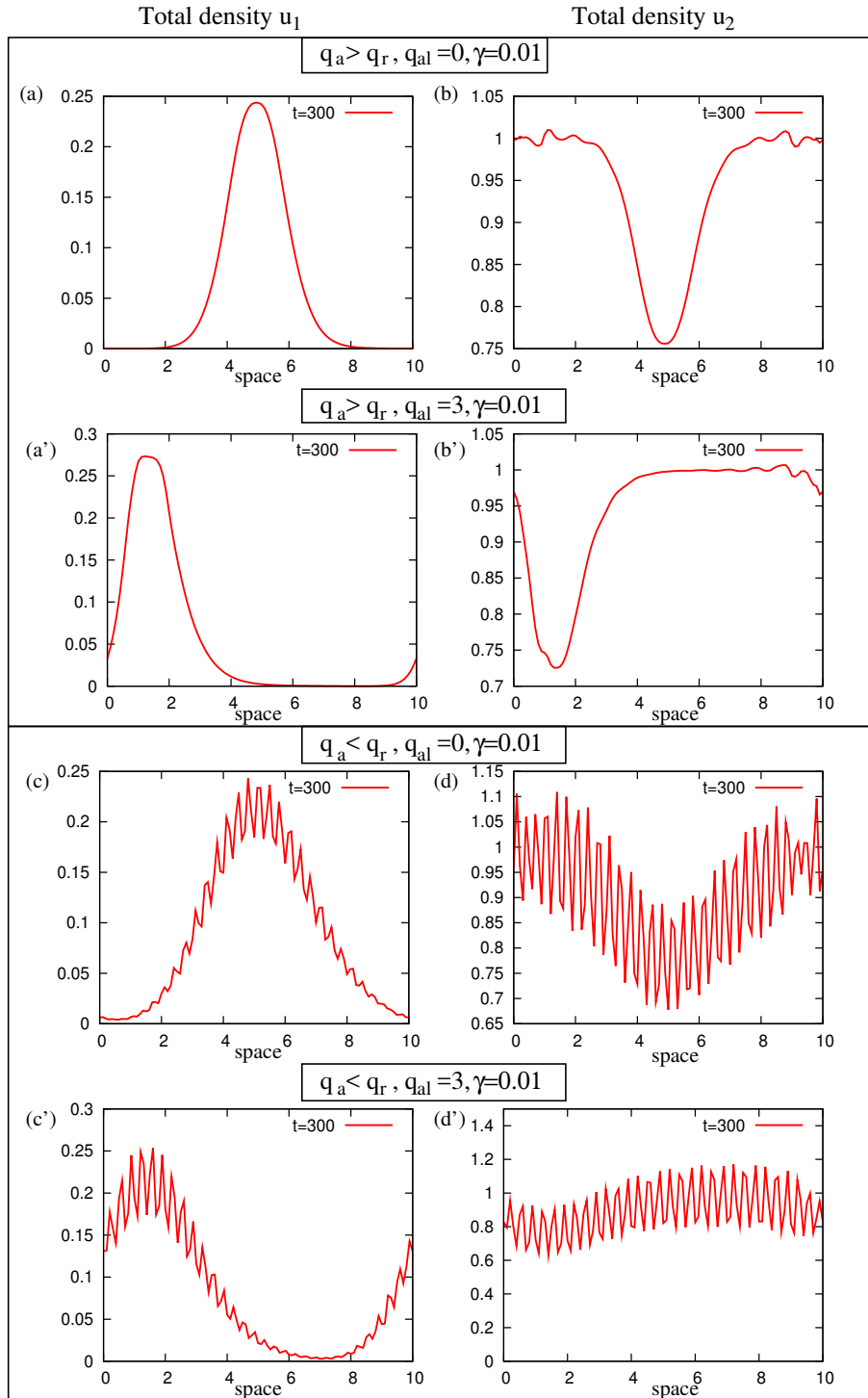
Figure 4.8: Time snapshot of the spatial distribution of u_1 and u_2 cancer cells corresponding to the patterns in Fig. 4.7, for $t = 300$. (a), (b) Spatial distribution of u_1 and u_2 for $q_a = 1.2, q_r = 0.1$ and $q_{al} = 0$; (a'), (b') Spatial distribution of u_1 and u_2 for $q_a = 1.2, q_r = 0.1$ and $q_{al} = 3$; (c), (d) Spatial distribution of u_1 and u_2 for $q_a = 1.2, q_r = 2.5$ and $q_{al} = 0$; (c'), (d') Spatial distribution of u_1 and u_2 for $q_a = 1.2, q_r = 2.5$ and $q_{al} = 3$. The rest of model parameters are given in Table 4.2.

128

4.5.2 Pattern formation for the limiting parabolic model

In this section we run simulations for the limiting parabolic model given by (4.25). As in the hyperbolic model (4.1), we choose the initial conditions for the cancer cell populations to be small random perturbations of the spatially homogeneous steady states $(0,0)$ and $(0,1)$ (see Section 4.4.2)

$$u_i(0,x) \;\; = \;\; u_i^* + rand(0, 10^{-4}), \; i = 1, 2, \tag{4.49}$$

or small random perturbations of rectangular-shaped aggregations located in the middle of the domain

$$u_i(0,x) = \begin{cases} 0.2 + rand(0, 10^{-4}), & x \in (L/2 - 1, L/2 + 1) \\ 0, & \text{everywhere else} \end{cases} \tag{4.50}$$

First we wish to investigate again the effect of attraction and repulsion on the collective movement of cancer cells and compare the patterns with those obtained by the hyperbolic model (see Fig. 4.5). To this end, we see in Fig. 4.9 that for the very large speed and large turning behaviour cells tend to move in a stationary manner, forming stationary pulses. For $q_a > q_r$ (Fig. 4.9(a)-(b)) cancer cell populations exhibits large stationary pulses, with the cells being concentrated in the spatial region where the pulse forms due to the strong attractive forces. In contrast, when repulsive forces are greater than attractive forces, i.e., $q_a < q_r$ (Fig. 4.9(a')-(b')), the cells form large number of small stationary pulses. Similar results (not shown here) were obtained for the initial conditions (4.49) with $\left(u_1^*, u_2^*\right) = (0, 1)$.

Reducing now the speed, as we did for the hyperbolic model, we notice that the patterns displayed in Fig. 4.10 are similar to those obtained for the hyperbolic model presented in Figs. 4.7(a),(b) and 4.7(c),(d), with the parabolic model forming again

Figure 4.9: Patterns exhibited by the parabolic model (4.25). The initial conditions for the two cancer cell populations are described by small random perturbations of the steady state $(0,0)$ (see (4.49)). (a), (b) Total density of u_1 and u_2 for $q_a = 1.2, q_r = 0.1$ and $q_{al} = 0$; (a'), (b') Total density of u_1 and u_2 for $q_a = 1.2, q_r = 2.5$ and $q_{al} = 0$. The rest of model parameters are given in Table 4.2.
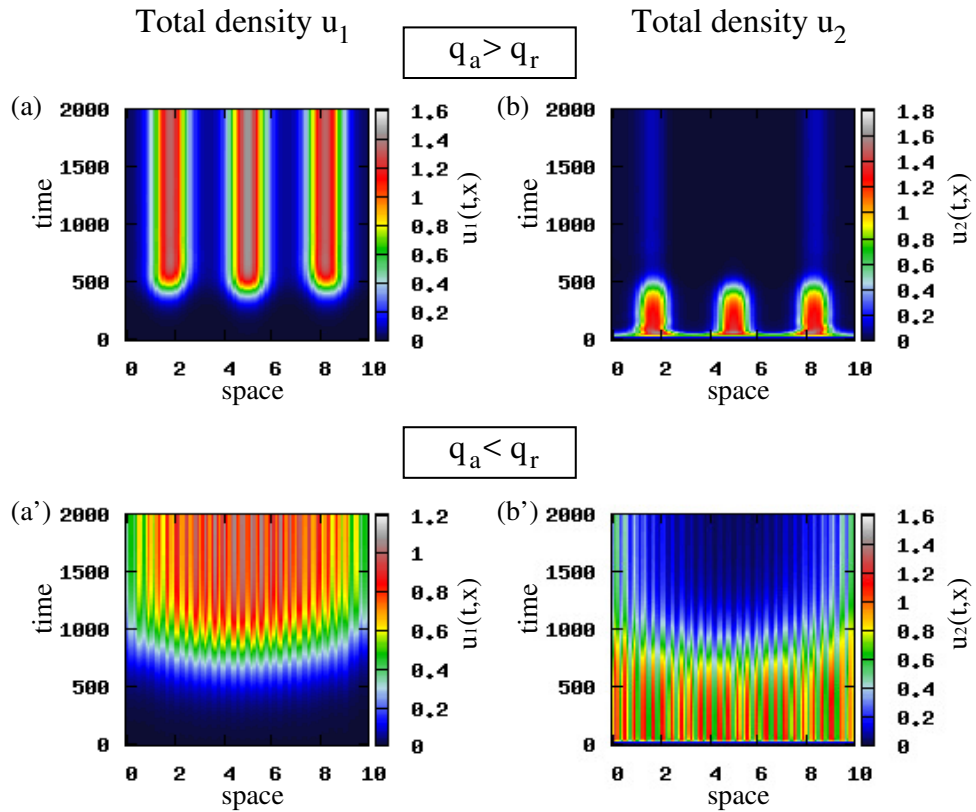
small stationary pulses.

The other fact that is being confirmed by the numerical results of the parabolic model is the clonal competition depending on the speed of cancer cells.

From the numerical simulations of both models, we deduce that the hyperbolic model exhibits mainly standing or rotating waves, in contrast to the parabolic model that exhibits a more stationary behaviour. We should mention also that the limiting parabolic model was deduced after assuming large speed and turning rates, which leads to the

reduced sensitivity to the environment and thus to the formation of stationary aggregations.
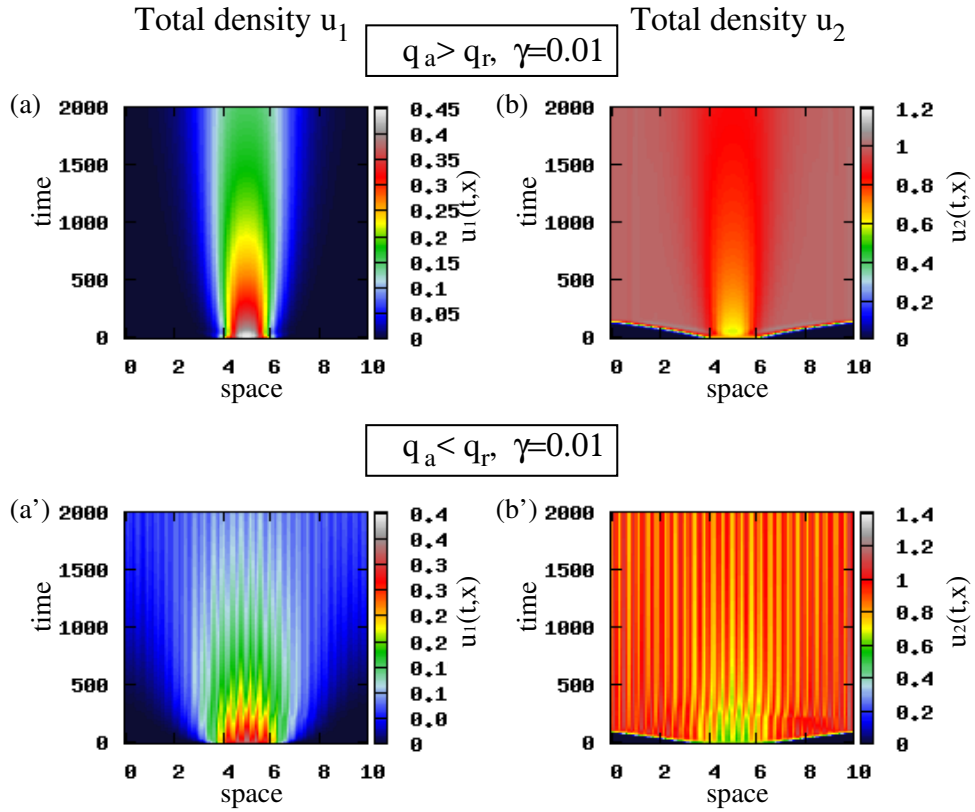
Figure 4.10: Patterns exhibited by the parabolic model (4.25) showing the cancer cell density for $\gamma = 0.01$. The initial conditions for the two cancer cell populations consist of a rectangular pulse (see (4.50)). (a), (b) Total density of u_1 and u_2 for $q_a = 1.2, q_r = 0.1$ and $q_{al} = 0$; (a'), (b') Total density of u_1 and u_2 for $q_a = 1.2, q_r = 2.5$ and $q_{al} = 0$. The rest of model parameters are given in Table 4.2.

4.5.3 Summary of model variables and parameters

As in the previous chapters, we present here two tables with the model variables and parameters. In Table 4.1 we list the model variables with their units. In Table 4.2 we list the parameters of our model and their corresponding units and non-dimensional values used in the simulations. For a detailed discussion on the estimation of the rest parameters see Section 2.4.1.

Table 4.1: A list of model variables with their units. Since we are in 1D, length and volume coincide and we express the variables in terms of domain length.

Variable	Description	Dimensional Units
u_1^+	Right-moving early stage cancer cell density	$cell/length$
u_1^-	Left-moving early stage cancer cell density	$cell/length$
u_1	Total early stage cancer cell density	$cell/length$
u_2^+	Right-moving late stage cancer cell density	$cell/length$
u_2^-	Left-moving late stage cancer cell density	$cell/length$
u_2	Total late stage cancer cell density	$cell/length$

Table 4.2: A list of model parameters with their units and their non-dimensional values, which we used during numerical simulations.

Param.	Description	Dimensional Units	Non-dim. value ($\tilde{p}$)	Reference
R_s	Sensing radius	$length$	1	Armstrong et al. (2006)
γ	Constant base-line speed of cancer cells	$length/time$	0.1	Estimated
q_a	Magnitude of attraction	$length^2/cell$	1.2	Estimated
q_r	Magnitude of repulsion	$length^2/cell$	0.1	Estimated
q_{al}	Magnitude of alignment	$length^2/cell$	0.5	Estimated
s_a	Attraction range	$length$	1	Estimated
s_r	Repulsion range	$length$	0.25	Estimated
s_{al}	Alignment range	$length$	0.5	Estimated
m_a	Width of attraction kernel	$length$	1/8	Estimated
m_r	Width of repulsion kernel	$length$	0.25/8	Estimated
m_{al}	Width of alignment kernel	$length$	0.5/8	Estimated

Continued on next page

Table 4.2 – *Continued from previous page*

Param.	Description	Dimensional Units	Non-dim. value ($\tilde{p}$)	Reference
M	Mutation rate	$1/time$	0.0001	Calabrese and Shibata (2010); Mareel et al. (1991)
λ_1^r	Base-line random turning rate of cancer cell population u_1	$1/time$	0.2	Estimated
λ_2^r	Base-line random turning rate of cancer cell population u_2	$1/time$	0.4	Estimated
λ_1^b	Biased turning rate of cancer cell population u_1	$1/time$	0.8	Estimated
λ_2^b	Biased turning rate of cancer cell population u_2	$1/time$	1	Estimated
r_1	Growth rate of u_1	$1/time$	0.1	Morani et al. (2014)
r_2	Growth rate of u_2	$1/time$	0.2	Morani et al. (2014)

4.6 Conclusion and discussion

In this chapter, we introduced a one-dimensional nonlocal hyperbolic model describing the interactions between heterogeneous cancer cells. In contrast to the models presented in the previous chapters, here we developed a model where nonlocal turning rates are included and incorporate all three social interactions: attraction, repulsion, and alignment, that play a crucial role in cell movement and aggregation. We assumed that a cell changes its movement direction only after weighing the information received from left and right, speeding up and slowing down to catch up with the surrounding cells, or to avoid collisions. The mutation terms and the proliferation terms are similar with those proposed in the first model in Chapter 2, taking into account the movement of cells in opposite directions. We should emphasize that the cancer cells can detect cells that are in front and behind them.

Then we connected our nonlocal hyperbolic model with a nonlocal parabolic model to study the aggregation formation, since parabolic models have been used mainly in the study of the formation and movement of cell aggregations. This connection was made by assuming that both the speed and the turning rates approach infinity.

Linear stability analysis of both the hyperbolic and the parabolic model was applied to examine the possibility of aggregation to form. The results showed that aggregation can arise from spatial perturbations of the steady states. We should mention here that for the hyperbolic model the dispersion relation had non-zero imaginary part (hence it is possible to have Hopf bifurcations, in addition to real bifurcations), while for the parabolic model the dispersion relation had zero imaginary part (hence aggregation could arise only via real bifurcations). Finally, we ran simulations for the hyperbolic and the related parabolic model and compared the results. The models exhibited a wide range of patterns with the hyperbolic model being more rich in patterns, showing mainly a travelling behaviour, compared to the parabolic model that exhibits mainly

stationary movement. These numerical results (for the nonlinear models) are consistent with the linear results obtained via stability analysis, emphasizing the more complex behaviour of the hyperbolic model.

Chapter 5

Conclusion and future directions

We conclude this thesis with a brief summary of the major points and some possible directions of future work. Of course, this is by no means exhaustive, and we refer the reader to the appropriate chapters for a more detailed account.

5.1 Conclusion and discussion

The breaking and forming of adhesive bonds, a process critical in cancer invasion and metastasis, can be influenced by the mutation of cancer cells and other crucial molecules, with TGF-β being one of the most significant. Cells adhere to each other and to the extracellular matrix (ECM) through protein molecules on the surface of the cells, called cell receptors, e.g., integrins. In this thesis we derived three new nonlocal models describing the interactions between heterogeneous cancer cells with different levels of mutation.

The first model, introduced and studied in Chapter 2, focussed mainly on the effect of

the mutation level on the cancer invasion. Precisely, we developed a nonlocal mathematical model describing cancer cell invasion and movement as a result of integrin-controlled cell-cell adhesion and cell-matrix adhesion, for two cancer cell populations with different levels of mutation. The model consists of a nonlinear parabolic-hyperbolic coupled system describing the cell dynamics, as well as ordinary differential equations describing the extracellular matrix (ECM) degradation and the production and decay of integrins. The rate at which cancer cells mutate seemed to play a critical role in our model. We used this model to investigate the role of cancer mutation on the possibility of cancer clonal competition with alternating dominance, or even competitive exclusion. Moreover, to verify if the linear stability results for the 1D model (2.21) were valid also in 2D, we applied linear stability analysis also for the two dimensional case. We showed that for similar kernels, we obtained similar dispersion relations with no imaginary parts (and hence no Hopf bifurcations). Therefore, we expect that the 2D model (2.39) would exhibit stationary pulses similar to the ones exhibited by the 1D model (2.21). We discussed different possible cell aggregation patterns, as well as travelling wave patterns. In regard to the travelling waves, we investigated the effect of cancer mutation rate on the speed of cancer invasion.

In Chapter 3 we developed a second nonlocal model describing cancer cell invasion and movement as a result of integrin-controlled cell-cell adhesion and cell-matrix adhesion, and transforming growth factor-beta (TGF-β) effect on cell proliferation and adhesion, for two cancer cell populations with different levels of mutation. The model consists of partial integro-differential equations describing the dynamics of two cancer cell populations, coupled with ordinary differential equations describing the ECM degradation and the production and decay of integrins, and with a parabolic PDE governing the evolution of TGF-β concentration. We proved the global existence of weak solutions to the model. We then used our model to explore numerically the role of TGF-β in cell aggregation and movement.

In Chapter 4 we presented a new system of first order nonlinear hyperbolic partial differential equations describing the dynamics of two polarised cancer cell populations. The speed of the cancer cells depends on the attractive and repulsive forces between the cells, while the turning rates depend also on the alignment interactions. We took a formal parabolic limit to reduce this hyperbolic model to a nonlinear parabolic model for cancer invasion. Then, we applied linear stability analysis to both the hyperbolic and parabolic models to investigate the possibility of aggregation form. We discussed different patterns and we compared the numerical results for the hyperbolic model with those obtained for the parabolic model. The results for large speeds and large turning rates showed an interesting behaviour, with cells forming stationary pulses (aggregations), in contrast to the behaviour of the hyperbolic model where cells exhibited mainly rotating and standing waves.

In conclusion, the work presented in this thesis has aimed to study analytically and numerically the heterogeneous cancer cell movement and aggregation, under interactions with several molecules, to obtain a better understanding of the dynamics exhibited by this class of nonlocal models. The dynamics of cancer cells has been described mainly by complex nonlocal nonlinear parabolic-hyperbolic coupled systems. The results obtained by this thesis are significant, however there are many open related topics that need to be studied in the future in order to fully validate the results, including biological evidence to support these findings.

5.2   Future directions

The analytical and numerical investigation opened multiple new questions regarding the existence of solution, the pattern formation and the further extension of the models presented, which would be very interesting to study. In the following we present some

of these topics.

- In Chapters 2 and 4 we focused on one-dimensional models. However, real life cell dynamics occurs in two or three dimensions. In the future, we plan to extend these models to higher spatial dimensions, studying the existence of solution and extending also the numerical simulations to two and three spatial dimensions. This is the first topic that it will be studied in the future, and it will provide results that are more biologically realistic and comparable with experiments.

- The complexity of the second model incorporating TGF-β dynamics (3.10) leads to the proof of existence of weak solutions. In future we will investigate also the uniqueness and regularity of such solutions.

- Numerical simulations for models (2.21) and (3.10) revealed travelling-wave patterns. In this thesis we have merely 'scratched the surface' of the travelling waves theory. The major future plan is to provide the proof of the existence of travelling wave solutions. Moreover, it will be interesting to study the effect of adhesive forces, as well as the TGF-β effect, on the speed of travelling wave propagation, as it was revealed numerically.

- In Section 4.3 we connected the nonlocal hyperbolic equations (4.1) to the nonlocal parabolic equations (4.25) by scaling the speed and the turning rates. In future, it would be interesting to consider also hydrodynamic scaling.

- The linear stability analysis revealed that it is possible to have unstable modes with complex parts. Moreover, the numerical results for model (4.1) showed that it is possible to have rotating waves (corresponding to moving cell aggregations). In the future, we plan to investigate analytically the existence of possible Hopf bifurcations (from spatially homogeneous or heterogeneous steady states). Moreover, it will be interesting also to investigate analytically the possibility of

heteroclinic connections between stationary and travelling aggregations exhibited by model (4.1), as suggested by figure 4.6.

- The model presented in Chapter 4 focussed mainly on the interactions between cells, excluding the important role of ECM and integrins on cellular adhesion, movement and aggregation. A straightforward direction is to include ECM and integrin density in this model that incorporates alignment.

- Finally, as the intra/extra-cellular activities are random, another modelling technique to consider in the future is to use an element of randomness for our models and thus by using stochastic processes to extend our deterministic models to stochastic models.

Bibliography

Aabo, K., Vindeløv, L., and Spang-Thomsen, M. (1994). Interaction between three subpopulations of Ehrlich carcinoma in mixed solid tumours in nude mice: evidence of contact domination. *Brit. J. Cancer*, 70(1):91–96.

Ambrosi, D. and Preziosi, L. (2002). On the closure of mass balance models for tumor growth. *Math. Models Methods Appl. Sci.*, 12(5):737–754.

Andasari, V. and Chaplain, M. A. J. (2012). Intracellular modelling of cell-matrix adhesion during cancer cell invasion. *Math. Model. Nat. Phenom.*, 7(01):29–48.

Andasari, V., Gerisch, A., Lolas, G., South, A. P., and Chaplain, M. A. J. (2011). Mathematical modeling of cancer cell invasion of tissue: biological insight from mathematical analysis and computational simulation. *J. Math. Biol.*, 63(1):141–171.

Anderson, A. R. A., Chaplain, M. A. J., Newman, E. L., Steele, R. J. C., and Thompson, A. M. (2000). Mathematical modelling of tumour invasion and metastasis. *J. Theor. Med.*, 2(2):129–154.

Armstrong, N. J., Painter, K. J., and Sherratt, J. A. (2006). A continuum approach to modelling cell-cell adhesion. *J. Theor. Biol.*, 243(1):98–113.

Ascolani, G. and Liò, P. (2014). Modeling TGF-β in early stages of cancer tissue dynamics. *PLoS One*, 9(2):e88533.

Basheer, I. A. and Hajmeer, M. (2000). Artificial neural networks: fundamentals, computing, design, and application. *J. Microbiol. Meth.*, 43(1):3–31.

Beckmann, M. W., Niederacher, D., Schnürch, H.-G., Gusterson, B. A., and Bender, H. G. (1997). Multistep carcinogenesis of breast cancer and tumour heterogeneity. *J. Mol. Med,*, 75(6):429–439.

Bellomo, N., Bellouquid, A., and Chouhad, N. (2016). From a multiscale derivation of nonlinear cross-diffusion models to Keller-Segel models in a Navier-Stokes fluid. *Math. Models Methods Appl. Sci.*, 26(11):2041–2069.

Bellomo, N., Li, N., and Maini, P. K. (2008). On the foundations of cancer modelling: selected topics, speculations, and perspectives. *Math. Models Methods Appl. Sci.*, 18(4):593–646.

Benedetto, S., Pulito, R., Crich, S. G., Tarone, G., Aime, S., Silengo, L., and Hamm, J. (2006). Quantification of the expression level of integrin receptor $\alpha v \beta 3$ in cell lines and MR imaging with antibody-coated iron oxide particles. *Magn. Reson. Med.*, 56(4):711–716.

Benson, D. L., Sherratt, J. A., and Maini, P. K. (1993). Diffusion driven instability in an inhomogeneous domain. *Bull. Math. Biol.*, 55(2):365–384.

Bitsouni, V., Chaplain, M. A. J., and Eftimie, R. (2017). Mathematical modelling of cancer invasion: The multiple roles of TGF-β pathway on tumour proliferation and cell adhesion. *Math. Models Methods Appl. Sci.*, 27(10):1929–1962.

Bitsouni, V. and Eftimie, R. (2017). A nonlocal model for cell polarisation in heterogeneous cancer cell populations. *Submitted*.

Bitsouni, V., Trucu, D., Chaplain, M. A. J., and Eftimie, R. (2016). Aggregation and travelling wave dynamics in a two-population model of cancer cell growth and invasion. *Submitted*.

Buono, P.-L. and Eftimie, R. (2015). Symmetries and pattern formation in hyperbolic versus parabolic models of self-organised aggregation. *J. Math. Biol.*, 71(4):847–881.

Byrne, H. and Chaplain, M. (1996). Modelling the role of cell-cell adhesion in the growth and development of carcinomas. *Mathematical and Computer Modelling*, 24(12):1–17.

Byrne, H. and Preziosi, L. (2003). Modelling solid tumour growth using the theory of mixtures. *Math. Med. Biol.*, 20(4):341–366.

Calabrese, P. and Shibata, D. (2010). A simple algebraic cancer equation: calculating how cancers may arise with normal mutation rates. *BMC Cancer*, 10(1):3.

Calvo, F. and Sahai, E. (2011). Cell communication networks in cancer invasion. *Curr. Opin. Cell Biol.*, 23(5):621–629.

Canizo, J., Carrillo, J., and Rosado, J. (2010). Collective behavior of animals: Swarming and complex patterns. *Arbor*, 186:1035–1049.

Carrillo de la Plata, J. A., Eftimie, R., and Hoffmann, F. (2015). Non-local kinetic and macroscopic models for self-organised animal aggregations. *Kinetic and Related Models*, 8(3):413–441.

Cavagna, A., Cimarelli, A., Giardina, I., Parisi, G., Santagati, R., Stefanini, F., and Tavarone, R. (2010). From empirical data to inter-individual interactions: unveiling the rules of collective animal behavior. *Math. Models Methods Appl. Sci.*, 20(supp01):1491–1510.

Chaplain, M. A. J., Lachowicz, M., Szymańska, Z., and Wrzosek, D. (2011). Mathematical modelling of cancer invasion: The importance of cell-cell adhesion and cell-matrix adhesion. *Math. Models Methods Appl. Sci.*, 21(4):719–743.

143

Chaplain, M. A. J. and Lolas, G. (2006). Mathematical modelling of cancer invasion of tissue: dynamic heterogeneity. *Netw. Heterog. Media*, 1(3):399–439.

Chapman, A., del Ama, L. F., Ferguson, J., Kamarashev, J., Wellbrock, C., and Hurlstone, A. (2014). Heterogeneous tumor subpopulations cooperate to drive invasion. *Cell Reports*, 8(3):688–695.

Cholewa, J. W. and Dlotko, T. (2000). *Global attractors in abstract parabolic problems*, volume 278. Cambridge University Press.

Cillo, C., Dick, J. E., Ling, V., and Hill, R. P. (1987). Generation of drug-resistant variants in metastatic B16 mouse melanoma cell lines. *Cancer Research*, 47(10):2604–2608.

Cristini, V., Li, X., Lowengrub, J. S., and Wise, S. M. (2009). Nonlinear simulations of solid tumor growth using a mixture model: invasion and branching. *J. Math. Biol.*, 58(4-5):723–763.

Cunningham, D. and You, Z. (2015). In vitro and in vivo model systems used in prostate cancer research. *J. Biol. Meth.*, 2(1):e17,1–14.

Cutler, S. M. and García, A. J. (2003). Engineering cell adhesive surfaces that direct integrin $\alpha_5\beta_1$ binding using a recombinant fragment of fibronectin. *Biomaterials*, 24(10):1759–1770.

Davis, T. L., Rabinovitz, I., Futscher, B. W., Schnölzer, M., Burger, F., Liu, Y., Kulesz-Martin, M., and Cress, A. E. (2001). Identification of a novel structural variant of the $\alpha6$ integrin. *J. Biol. Chem.*, 276(28):26099–26106.

Deakin, N. E. and Chaplain, M. A. J. (2013). Mathematical modeling of cancer invasion: the role of membrane-bound matrix metalloproteinases. *Frontiers in oncology*, 3.

Delcommenne, M. and Streuli, C. H. (1995). Control of integrin expression by extracellular matrix. *J. Biol. Chem.*, 270(45):26794–26801.

Deman, J. J., Vakaet, L. C., and Bruyneel, E. A. (1976). Cell size and mutual cell adhesion. II. Evidence for a relation between cell size, long-range electrostatic repulsion and intercellular adhesiveness during density-regulated growth in suspension. *J. Membr. Biol.*, 26(1):205–215.

Domschke, P., Trucu, D., Gerisch, A., and Chaplain, M. A. J. (2014). Mathematical modelling of cancer invasion: Implications of cell adhesion variability for tumour infiltrative growth patterns. *J. Theor. Biol.*, 361:41–60.

Dyson, R., Green, J., Whiteley, J., and Byrne, H. (2016). An investigation of the influence of extracellular matrix anisotropy and cell-matrix interactions on tissue architecture. *J. Math. Biol.*, 72:1775–1809.

Edelstein-Keshet, L. and Ermentrout, G. (1990). Models for contact-mediated pattern formation: cells that form parallel arrays. *J. Theor. Biol.*, 29:33–58.

Eftimie, R., de Vries, G., Lewis, M. A., and Lutscher, F. (2007). Modeling group formation and activity patterns in self-organizing collectives of individuals. *Bull. Math. Biol.*, 69(5):1537–1565.

Egan, J. B., Shi, C.-X., Tembe, W., Christoforides, A., Kurdoglu, A., Sinari, S., Middha, S., Asmann, Y., Schmidt, J., Braggio, E., et al. (2012). Whole-genome sequencing of multiple myeloma from diagnosis to plasma cell leukemia reveals genomic initiating events, evolution, and clonal tides. *Blood*, 120(5):1060–1066.

Enderling, H., Anderson, A. R., Chaplain, M. A. J., Munro, A. J., and Vaidya, J. S. (2006). Mathematical modelling of radiotherapy strategies for early breast cancer. *J. Theor. Biol.*, 241(1):158–171.

Enderling, H., Chaplain, M. A. J., and Hahnfeldt, P. (2010). Quantitative modeling of tumor dynamics and radiotherapy. *Acta Biotheor.*, 58(4):341–353.

Engwer, C., Hillen, T., Knappitsch, M., and Surulescu, C. (2015). Glioma follow white matter tracts: a multiscale dti-based model. *J. Math. Biol.*, 71(3):551–582.

Evans, L. C. (2010). *Partial differential equations (Graduate Studies in Mathematics; v. 19).* American Mathematical Society.

Fan, J. and Zhao, K. (2014). A note on a 3D haptotaxis model of cancer invasion. *Applied Mathematics Research Express*, 2014(1):74–86.

Fetecau, R. C. (2011). Collective behavior of biological aggregations in two dimensions: a nonlocal kinetic model. *Math. Models Methods Appl. Sci.*, 21(07):1539–1569.

Fetecau, R. C. and Eftimie, R. (2010). An investigation of a nonlocal hyperbolic model for self-organization of biological groups. *J. Math. Biol.*, 61(4):545–579.

Fisher, R., Pusztai, L., and Swanton, C. (2013). Cancer heterogeneity: implications for targeted therapeutics. *Brit. J. Cancer*, 108(3):479–485.

Friedl, P. and Wolf, K. (2003). Tumour-cell invasion and migration: diversity and escape mechanisms. *Nature Reviews Cancer*, 3(5):362–374.

Gallant, N. D., Michael, K. E., and García, A. J. (2005). Cell adhesion strengthening: contributions of adhesive area, integrin binding, and focal adhesion assembly. *Mol. Biol. Cell*, 16(9):4329–4340.

Gautrais, J., Ginelli, F., Fournier, R., Blanco, S., Soria, M., Chaté, H., and Theraulaz, G. (2012). Deciphering interactions in moving animal groups. *PLoS Comput. Biol.*, 8(9):e1002678.

Geiger, B. (1991). Long-range morphogenetic signals and cell adhesion. *BioEssays*, 13(12):665–666.

Gerisch, A. and Chaplain, M. A. J. (2008). Mathematical modelling of cancer cell invasion of tissue: local and non-local models and the effect of adhesion. *J. Theor. Biol.*, 250(4):684–704.

Gerish, A. and Painter, K. J. (2010). Chapter 12: Mathematical modelling of cell adhesion and its applications to developmental biology and cancer invasion. In *Cell mechanics: from single scale-based models to multiscale modelling*. Chapman & Hall/CRC.

Goswami, S., Sahai, E., Wyckoff, J. B., Cammer, M., Cox, D., Pixley, F. J., Stanley, E. R., Segall, J. E., and Condeelis, J. S. (2005). Macrophages promote the invasion of breast carcinoma cells via a colony-stimulating factor-1/epidermal growth factor paracrine loop. *Cancer Research*, 65(12):5278–5283.

Greaves, M. and Maley, C. (2012). Clonal evolution in cancer. *Nature*, 481(7381):306–313.

Green, J. E. F., Waters, S. L., Whiteley, J. P., Edelstein-Keshet, L., Shakesheff, K. M., and Byrne, H. M. (2010). Non-local models for the formation of hepatocyte-stellate cell aggregates. *J. Theor. Biol.*, 267(1):106–120.

Hadeler, K. (1999). *Reaction transport systems in biological modelling*. Springer.

Haga, H., Irahara, C., Kobayashi, R., Nakagaki, T., and Kawabata, K. (2005). Collective movement of epithelial cells on a collagen gel substrate. *Biophys. J.*, 88(3):2250–2256.

Hagemann, T., Wilson, J., Kulbe, H., Li, N. F., Leinster, D. A., Charles, K., Klemm, F., Pukrop, T., Binder, C., and Balkwill, F. R. (2005). Macrophages induce invasiveness of epithelial cancer cells via NF-κB and JNK. *J. Immunol.*, 175(2):1197–1205.

Hanahan, D. and Weinberg, R. A. (2000). The hallmarks of cancer. *Cell*, 100(1):57–70.

Henry, D. (1981). *Geometric theory of semilinear parabolic systems*, volume 840. Springer-Verlag.

Hill, R. P., Chambers, A. F., and Ling, V. (1984). Dynamic heterogeneity: rapid generation of metastatic variants in mouse B16 melanoma cells. *Science*, 224:998–1001.

Hillen, T., Rohde, C., and Lutscher, F. (2001). Existence of weak solutions for a hyperbolic model of chemosensitive movement. *J. Math. Anal. Appl.*, 260(1):173–199.

Huang, S. and Chakrabarty, S. (1994). Regulation of fibronectin and laminin receptor expression, fibronectin and laminin secretion in human colon cancer cells by transforming growth factor-β1. *Int. J. Cancer*, 57(5):742–746.

Huth, A. and Wissel, C. (1992). The simulation of the movement of fish schools. *J. Theor. Biol.*, 156(3):365–385.

Kaminska, B., Wesolowska, A., and Danilkiewicz, M. (2005). TGF beta signalling and its role in tumour pathogenesis. *Acta Biochim. Pol.*, 52(2):329.

Kang, E. and Lee, J. (2015). Global solutions to chemotaxis-haptotaxis tumor invasion system with tissue re-establishment. *J. Chungcheong Math. Soc.*, 28(1):161–172.

Keats, J. J., Chesi, M., Egan, J. B., Garbitt, V. M., Palmer, S. E., Braggio, E., Van Wier, S., Blackburn, P. R., Baker, A. S., Dispenzieri, A., et al. (2012). Clonal competition with alternating dominance in multiple myeloma. *Blood*, 120(5):1067–1076.

Khalique, L., Ayhan, A., Weale, M. E., Jacobs, I. J., Ramus, S. J., and Gayther, S. A. (2007). Genetic intra-tumour heterogeneity in epithelial ovarian cancer and its implications for molecular diagnosis of tumours. *J. Pathol.*, 211(3):286–295.

Khan, S. A., Joyce, J., and Tsuda, T. (2012). Quantification of active and total transforming growth factor-β levels in serum and solid organ tissues by bioassay. *BMC Res. Notes*, 5(1):1.

Kidera, Y., Tsubaki, M., Yamazoe, Y., Shoji, K., Nakamura, H., Ogaki, M., Satou, T., Itoh, T., Isozaki, M., Kaneko, J., et al. (2010). Reduction of lung metastasis, cell invasion, and adhesion in mouse melanoma by statin-induced blockade of the Rho/Rho-associated coiled-coil-containing protein kinase pathway. *J. Exp. Clin. Cancer Research*, 29(1):127.

Kim, Y. and Othmer, H. G. (2013). A hybrid model of tumor-stromal interactions in breast cancer. *Bull. Math. Biol.*, 75(8):1304–1350.

Knútsdóttir, H., Pálsson, E., and Edelstein-Keshet, L. (2014). Mathematical model of macrophage-facilitated breast cancer cells invasion. *J. Theor. Biol.*, 357:184–199.

Kunz, H. and Hemelrijk, C. K. (2003). Artificial fish schools: collective effects of school size, body size, and body form. *Artificial Life*, 9(3):237–253.

Laird, A. K. (1964). Dynamics of tumor growth. *Brit. J. Cancer*, 18(3):490–502.

Leith, J. T., Michelson, S., and Glicksman, A. S. (1989). Competitive exclusion of clonal subpopulations in heterogeneous tumours after stromal injury. *Brit. J. Cancer*, 59(1):22–27.

LeVeque, R. J. (2007). *Finite difference methods for ordinary and partial differential equations: steady-state and time-dependent problems*, volume 98. Siam.

Lin, E. Y., Li, J.-F., Gnatovskiy, L., Deng, Y., Zhu, L., Grzesik, D. A., Qian, H., Xue, X.-n., and Pollard, J. W. (2006). Macrophages regulate the angiogenic switch in a mouse model of breast cancer. *Cancer Research*, 66(23):11238–11246.

Ling, S., Hu, Z., Yang, Z., Yang, F., Li, Y., Lin, P., Chen, K., Dong, L., Cao, L., Tao, Y., et al. (2015). Extremely high genetic diversity in a single tumor points to prevalence of non-Darwinian cell evolution. *Proceedings of the National Academy of Sciences*, 112(47):E6496–E6505.

Liu, J., He, X., Qi, Y., Tian, X., Monkley, S. J., Critchley, D. R., Corbett, S. A., Lowry, S. F., Graham, A. M., and Li, S. (2011). Talin1 regulates integrin turnover to promote embryonic epithelial morphogenesis. *Mol. Cell Biol.*, 31(16):3366–3377.

Lobert, V. H., Brech, A., Pedersen, N. M., Wesche, J., Oppelt, A., Malerød, L., and Stenmark, H. (2010). Ubiquitination of $\alpha 5 \beta 1$ integrin controls fibroblast migration through lysosomal degradation of fibronectin-integrin complexes. *Dev. Cell*, 19(1):148–159.

Loeb, K. R. and Loeb, L. A. (2000). Significance of multiple mutations in cancer. *Carcinogenesis*, 21(3):379–385.

Lukeman, R., Li, Y.-X., and Edelstein-Keshet, L. (2010). Inferring individual rules from collective behavior. *PNAS*, 107(28):12576–12580.

Lutscher, F. (2002). Modeling alignment and movement of animals and cells. *J. Math. Biol.*, 45(3):234–260.

Maheshwari, G., Brown, G., Lauffenburger, D. A., Wells, A., and Griffith, L. G. (2000). Cell adhesion and motility depend on nanoscale RGD clustering. *J. Cell Sci*, 113(10):1677–1686.

Mamuya, F. A. and Duncan, M. K. (2012). aV integrins and TGF-β-induced EMT: a circle of regulation. *J. Cell Mol. Med.*, 16(3):445–455.

Mareel, M. M., De Baetselier, P., and Van Roy, F. M. (1991). *Mechanisms of invasion and metastasis*. CRC press.

Markowitz, S., Wang, J., Myeroff, L., Parsons, R., Sun, L., Lutterbaugh, J., Fan, R. S., et al. (1995). Inactivation of the type a TGF-β receptor in colon cancer cells with microsatellite instability. *Science*, 268(5215):1336–1338.

Martelotto, L. G., Ng, C. K., Piscuoglio, S., Weigelt, B., and Reis-Filho, J. S. (2014). Breast cancer intra-tumor heterogeneity. *Breast Cancer Research*, 16(3):210.

Marusyk, A., Almendro, V., and Polyak, K. (2012). Intra-tumour heterogeneity: a looking glass for cancer? *Nature Reviews Cancer*, 12:323–334.

Marusyk, A. and Polyak, K. (2010). Tumor heterogeneity: causes and consequences. *Biochim. Biophys. Acta*, 1805(1):105.

Mayor, R. and Carmona-Fontaine, C. (2010). Keeping in touch with contact inhibition of locomotion. *Trends Cell Biol.*, 20(6):319–328.

Medlock, J. and Kot, M. (2003). Spreading disease: integro-differential equations old and new. *Math. Biosci.*, 184(2):201–222.

Michael, K. E., Dumbauld, D. W., Burns, K. L., Hanks, S. K., and García, A. J. (2009). Focal adhesion kinase modulates cell adhesion strengthening via integrin activation. *Mol. Biol. Cell*, 20(9):2508–2519.

Michelson, S. and Leith, J. (1991). Autocrine and paracrine growth factors in tumor growth: a mathematical model. *Bull. Math. Biol.*, 53(4):639–656.

Miyazono, K. (2009). Transforming growth factor-β signaling in epithelial-mesenchymal transition and progression of cancer. *P. Jpn. Acad., B-Phys.*, 85(8):314–323.

Mogilner, A. and Edelstein-Keshet, L. (1995). Selecting a common direction: I. How orientational order can arise from simple contact responses between interacting cells. *J. Math. Biol.*, 33(6):619–660.

Mogilner, A. and Edelstein-Keshet, L. (1996). Spatio-angular order in populations of self-aligning objects: formation of oriented patches. *Physica D: Nonlinear Phenomena*, 89(3-4):346–367.

Mogilner, A. and Edelstein-Keshet, L. (1999). A non-local model for a swarm. *J. Math. Biol.*, 38(6):534–570.

Mogilner, A., Edelstein-Keshet, L., and Ermentrout, G. B. (1996). Selecting a common direction: II. Peak-like solutions representing total alignment of cell clusters. *J. Math. Biol.*, 34(8):811–842.

Mollison, D. (1991). Dependence of epidemic and population velocities on basic parameters. *Math. Biosci.*, 107(2):255–287.

Morani, F., Phadngam, S., Follo, C., Titone, R., Thongrakard, V., Galetto, A., Alabiso, O., and Isidoro, C. (2014). PTEN deficiency and mutant p53 confer glucose-addiction to thyroid cancer cells: impact of glucose depletion on cell proliferation, cell survival, autophagy and cell migration. *Genes Cancer*, 5(7-8):226–39.

Moustakas, A. and Heldin, C.-H. (2007). Signaling networks guiding epithelial-mesenchymal transitions during embryogenesis and cancer progression. *Cancer Science*, 98(10):1512–1520.

Nawshad, A., LaGamba, D., Polad, A., and Hay, E. D. (2005). Transforming growth factor-β signaling during epithelial-mesenchymal transformation: implications for embryogenesis and tumor metastasis. *Cells Tissues Organs*, 179(1-2):11–23.

Nessyahu, H. and Tadmor, E. (1990). Non-oscillatory central differencing for hyperbolic conservation laws. *J. Comput. Phys.*, 87(2):408–463.

Nicholson, G. L. (1984). Cell surface molecules and tumor metastasis. Regulation of metastatic phenotypic diversity. *Exp. Cell Res.*, 150(1):3–22.

Nicholson, G. L. (1987). Tumor cell instability, diversification and progression to the metastatic phenotype: from oncogene to oncofetal expression. *Cancer Research*, 47(6):1473–1487.

Nowell, P. C. (1976). The clonal evolution of tumor cell populations. *Science*, 194(4260):23–28.

Omelchenko, T., Vasiliev, J. M., Gelfand, I., Feder, H., and Bonder, E. (2003). Rho-dependent formation of epithelial "leader" cells during wound healing. *Proc. Natl. Acad. Sci. USA*, 100(19):10788–10793.

Outada, N., Vauchelet, N., Akrid, T., and Khaladi, M. (2016). From kinetic theory of multicellular systems to hyperbolic tissue equations: Asymptotic limits and computing. *Math. Models Methods Appl. Sci.*, 26(14):2709–2734.

Painter, K., Bloomfield, J., Sherratt, J., and Gerisch, A. (2015). A nonlocal model for contact attraction and repulsion in heterogeneous cell populations. *Bull. Math. Biol.*, 77(6):1132–1165.

Painter, K. J. (2009). Continuous models for cell migration in tissues and applications to cell sorting via differential chemotaxis. *Bull. Math. Biol.*, 71:1117–1147.

Painter, K. J., Armstrong, N. J., and Sherratt, J. A. (2010). The impact of adhesion on cellular invasion processes in cancer and development. *J. Theor. Biol.*, 264(3):1057–1067.

Press, W. H., Teukolsky, S. A., Vetterling, W. T., and Flannery, B. P. (2007). *Numerical recipes: The art of scientific computing, 3rd edition*. Cambridge university press.

Principe, D. R., Doll, J. A., Bauer, J., Jung, B., Munshi, H. G., Bartholin, L., Pasche, B., Lee, C., and Grippo, P. J. (2014). TGF-β: duality of function between tumor prevention and carcinogenesis. *J. Natl. Cancer I.*, 106(2):djt369.

Reffay, M., Petitjean, L., Coscoy, S., Grasland-Mongrain, E., Amblard, F., Buguin, A., and Silberzan, P. (2011). Orientation and polarity in collectively migrating cell structures: Statics and dynamics. *Biophys. J.*, 100(11):2566–2575.

Rørth, P. (2009). Collective cell migration. *Annu. Rev. Cell Dev. Biol.*, 25:407–429.

Rørth, P. (2012). Fellow travellers: emergent properties of collective cell migration. *EMBO Rep.*, 13(11):984–991.

Runst, T. and Sickel, W. (1996). *Sobolev spaces of fractional order, Nemytskij operators, and nonlinear partial differential equations*, volume 3. Walter de Gruyter.

Schakenraad, J. M., Busscher, H. J., Wildevuur, C. R. H., and Arends, J. (1986). The influence of substratum surface free energy on growth and spreading of human fibroblasts in the presence and absence of serum proteins. *J. Biomed. Mater. Res.*, 20(6):773–784.

Schuh, A., Becq, J., Humphray, S., Alexa, A., Burns, A., Clifford, R., Feller, S. M., Grocock, R., Henderson, S., Khrebtukova, I., et al. (2012). Monitoring chronic lymphocytic leukemia progression by whole genome sequencing reveals heterogeneous clonal evolution patterns. *Blood*, 120(20):4191–4196.

Shah, N. P., Nicoll, J. M., Nagar, B., Gorre, M. E., Paquette, R. L., Kuriyan, J., and Sawyers, C. L. (2002). Multiple BCR-ABL kinase domain mutations confer polyclonal resistance to the tyrosine kinase inhibitor imatinib (STI571) in chronic phase and blast crisis chronic myeloid leukemia. *Cancer Cell*, 2(2):117–125.

Sherratt, J. A., Gourley, S. A., Armstrong, N. J., and Painter, K. J. (2009). Boundedness of solutions of a non-local reaction-diffusion model for adhesion in cell aggregation and cancer invasion. *Eur. J. Appl. Math.*, 20(01):123–144.

Shiao, S.-Y. P. K. and Ou, C.-N. (2007). Validation of oxygen saturation monitors in neonates. *Am. J. Crit. Care*, 16(02):168–178.

154

Stackpole, C. W. (1983). Generation of phenotypic diversity in the B16 mouse melanoma relative to spontaneous metastasis. *Cancer Research*, 43:3057–3065.

Szymańska, Z., Rodrigo, C. M., Lachowicz, M., and Chaplain, M. A. J. (2009). Mathematical modelling of cancer invasion of tissue: the role and effect of nonlocal interactions. *Math. Models Methods Appl. Sci.*, 19(02):257–281.

Tao, Y. (2011). Global existence for a haptotaxis model of cancer invasion with tissue remodeling. *Nonlinear Anal. Real World Appl.*, 12(1):418–435.

Tao, Y. and Winkler, M. (2014). Energy-type estimates and global solvability in a two-dimensional chemotaxis-haptotaxis model with remodeling of non-diffusible attractant. *J. Differential Equations*, 257(3):784–815.

Topaz, C. M., Bertozzi, A. L., and Lewis, M. A. (2006). A nonlocal continuum model for biological aggregation. *Bull. Math. Biol.*, 68(7):1601–1623.

Turner, S., Sherratt, J. A., and Cameron, D. (2004). Tamoxifen treatment failure in cancer and the nonlinear dynamics of TGFβ. *J. Theor. Biol.*, 229(1):101–111.

Van Schepdael, A., Carlier, A., and Geris, L. (2016). *Sensitivity analysis by design of experiments*. Springer.

Venkatraman, L., Chia, S.-M., Narmada, B. C., White, J. K., Bhowmick, S. S., Dewey, C. F., So, P. T., Tucker-Kellogg, L., and Yu, H. (2012). Plasmin triggers a switch-like decrease in thrombospondin-dependent activation of TGF-β1. *Biophys. J.*, 103(5):1060–1068.

Vicente-Manzanares, M. and Sánchez-Madrid, F. (2000). Cell polarization: a comparative cell biology and immunological view. *Clin. Dev. Immunol.*, 7(2-4):51–65.

Wang, H., Radjendirane, V., Wary, K. K., and Chakrabarty, S. (2004). Transforming

growth factor β regulates cell-cell adhesion through extracellular matrix remodeling and activation of focal adhesion kinase in human colon carcinoma moser cells. *Oncogene*, 23(32):5558–5561.

Wang, S. E., Hinow, P., Bryce, N., Weaver, A. M., Estrada, L., Arteaga, C. L., and Webb, G. F. (2009). A mathematical model quantifies proliferation and motility effects of TGF-β on cancer cells. *Comput. Math. Methods Med.*, 10(1):71–83.

Weitzman, J. B., Chen, A., and Hemler, M. E. (1995). Investigation of the role of $\beta 1$ integrins in cell-cell adhesion. *J. Cell Science*, 108(11):3635–3644.

Wojciechowska, S. and Patton, E. E. (2015). Going forward together: cooperative invasion in melanoma. *Pigm. Cell Melanoma R.*, 28(1):6–7.

Wu, M.-S., Lin, J.-T., Hsu, P.-N., Lin, C.-Y., Hsieh, Y.-T., Chiu, Y.-H., Hsueh, P.-R., and Liao, K.-W. (2007). Preferential induction of Transforming Growth Factor-β production in gastric epithelial cells and monocytes by Helicobacter pylori soluble proteins. *J. Infect. Dis.*, 196(9):1386–1393.